PARTITIONING OF Mn AND Co BETWEEN
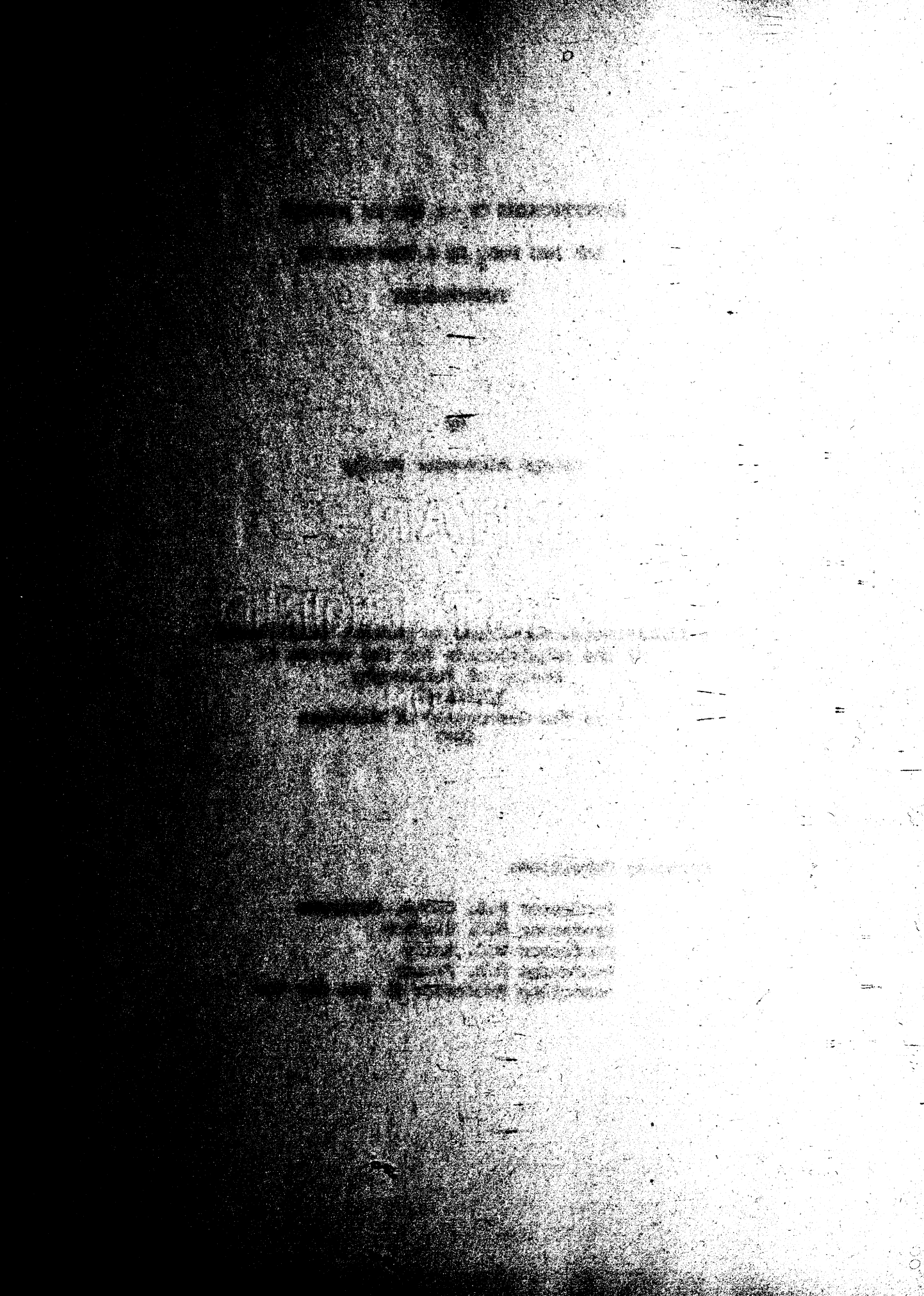
ZnS AND FeS_2 AS A FUNCTION OF

TEMPERATURE

by

George Alexander Reilly

A dissertation submitted in partial fulfillment
of the requirements for the degree of
Doctor of Philosophy
(Geology)
in The University of Michigan
1977

Doctoral Committee:

        Professor P.L. Cloke, Chairman
        Professor W.C. Bigelow
        Professor W.C. Kelly
        Professor D.R. Peacor
        Associate Professor R. Van der Voo

ACKNOWLEDGMENTS

TABLE OF CONTENTS

Page

LIST OF TABLES

LIST OF ILLUSTRATIONS

LIST OF APPENDICES

INTRODUCTION

In numerous studies (Fleischer, 1955), attempts have been made to interpret conditions of ore formation (e.g., T, P, f_{S_2}) from the distribution of trace elements in single sulphide phases. Unfortunately, the concentration of a trace element in any one sulphide mineral is dependent not only on temperature and pressure, but also on the chemical characteristics of the hydrothermal solutions from which the mineral formed. Such solutions, however, are generally not available for study, except in the form of fluid inclusions.

It has been shown (Holland, 1956; McIntire, 1963; Kretz, 1961) that the distribution or partitioning of an element between two coexisting minerals, formed in chemical equilibrium, is dependent only on temperature and pressure, provided that the element forms ideal solid solutions in both minerals over the range of concentrations considered. If non-ideal solid solution obtains in one or both of the minerals, the partitioning of the element bears no simple relationship to temperature and pressure. However, if sufficient information is available about the character of such non-ideal behaviour, compensation may be made for this added effect. Recent experimental studies (Bethke and Barton, 1971; Halbig, 1969) indicate that the effect of pressure on partitioning between co-existing sulphides is minimal. On the other hand, Bethke and Barton (1971) and others have demonstrated that the distributions of certain

1

elements among a variety of sulphides may constitute very useful geothermometers.

The association of sphalerite and pyrite is common and ubiquitous in ore deposits. Experimental studies by Barton and Toulmin (1966) and others show that equilibrium assemblages of sphalerite and pyrite can be formed over a wide range of temperatures (Fig. 1). Mn and Co are common constituents, normally at the minor to trace level, of both sphalerite and pyrite in ore deposits (Fleischer, 1955). Their concentration levels in both sphalerite and pyrite, coexisting in ore deposits and apparently formed in equilibrium, are often high enough to be accurately measured by standard analytical techniques (e.g., Troshin, 1965; Doe, 1962; Arnold et al, 1962). In this study, an attempt has been made to define experimentally the partitioning of Mn and Co between sphalerite and pyrite over a geologically meaningful range of temperatures, and to assess the potential of this partitioning in geothermometry.

Theory of Partitioning

The thermodynamic basis for the partitioning of a component between coexisting mineral phases formed in equilibrium has been outlined in considerable detail by Ramberg (1952), Kretz (1961) and McIntire (1963). Consider some element i which forms solid solutions in two mineral phases, A and B, deposited in chemical equilibrium at a specific temperature and pressure. The condition defining this relationship is:

$$\mu_i^A = \mu_i^B \qquad (1)$$

Figure 1: T - X projection of a portion of the ZnS-FeS-S system at 1 bar. Modified after Scott and Barnes (1972).
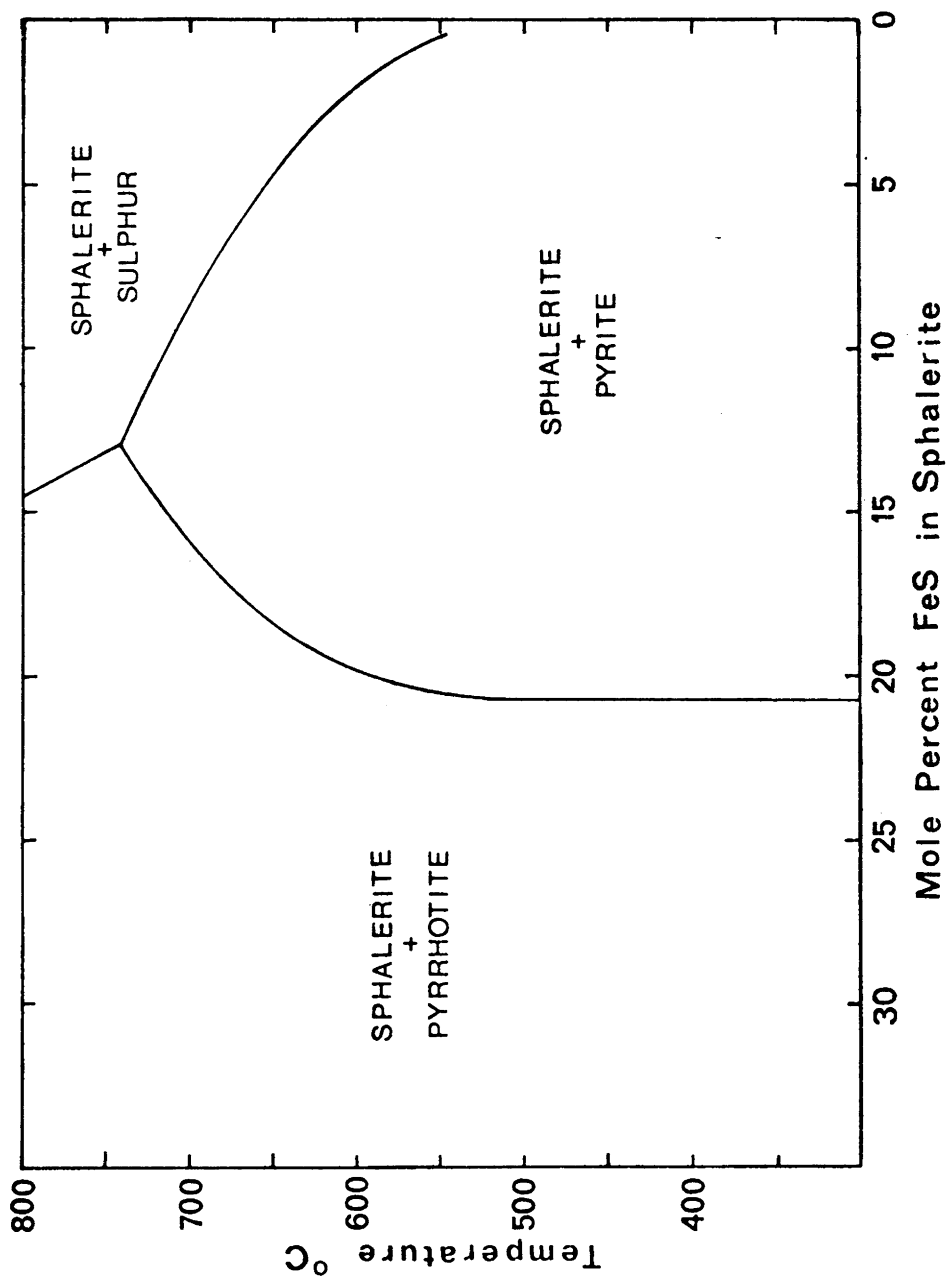
where μ_i^A and μ_i^B are the chemical potentials of i in phase A and B

respectively. In general, the relationship between chemical potential

and the concentration of element i in phases A and B is:

$$\mu_i^A = \mu_i^{*A} + RT\ln f_i^A X_i^A$$

and

$$\mu_i^B = \mu_i^{*B} + RT\ln f_i^B X_i^B$$

where $\mu_i^* =$ the chemical potential of the element i in some standard

  state

$f_i =$ the activity coefficient for element i

$X_i =$ the mole fraction of element i

R = gas constant

T = absolute temperature

A superscript, A or B, indicates the phase involved.

It could now be assumed that the solid solutions of i in the phases

A and B are ideal in character, such that $f_i^A = f_i^B = 1$ (Raoult's Law).

That is, the activity coefficients for i are independent of the

concentration of any element in both phases (Denbigh, 1971, p.270).

Alternatively, it could be assumed that below some concentration level

of i in each of the phases A and B, ideal solid solution obtains. The

activity coefficients f_i^A and f_i^B would then be constants, independent,

in those concentration ranges, of composition, but not necessarily

equal to one another, nor equal to 1 (Henry's Law). The basic condition

is that $f_i^A/f_i^B =$ constant, such that the activities and mole fractions

of i are directly related to one another by simple proportionality

constants. It is important to note that this discussion applies not

only to trace elements, but also to major and minor constituents, since
the level of dilution below which the condition of ideal solid solution
exists varies from system to system and is not easily predicted
on an a priori basis. Under conditions of ideal solid solution:

$$\mu_i^A = \mu_i^{*A} + RT\ln X_i^A$$

and

$$\mu_i^B = \mu_i^{*B} + RT\ln X_i^B$$

Then, from (1):

$$\mu_i^{*A} + RT\ln X_i^A = \mu_i^{*B} + RT\ln X_i^B$$

Therefore, by rearranging:

$$\ln\frac{X_i^A}{X_i^B} = \frac{\mu_i^{*B} - \mu_i^{*A}}{RT}$$

or

$$\ln K = \frac{\mu_i^{*B} - \mu_i^{*A}}{RT} \qquad (2)$$

where

$$K = \frac{X_i^A}{X_i^B}$$

This is a statement of the Nernst distribution law. Since $(\mu_i^{*B} - \mu_i^{*A})$
is independent of the concentration of i (but is dependent on T and P),
K, the partition coefficient, is independent of the individual
values of X_i^A and X_i^B, and is solely a function of temperature and
pressure under conditions where each solid solution is ideal. A plot
of X_i^A versus X_i^B would result in a straight line through the origin,
whose slope would be a function of T and P.

6

The dependence of K on temperature and pressure is found by differentiating (2). At constant pressure:

$$\left(\frac{\delta \ln K}{\delta T}\right)_P = \frac{\bar{H}_i^A - \bar{H}_i^B}{RT^2} = \frac{\Delta \bar{H}_i}{RT^2} \qquad (3)$$

where $\bar{H}_i$ = partial molar enthalpy for i

$\Delta \bar{H}_i$ = molar enthalpy of reaction for i.

This is the basic relationship between the partition coefficient, K, and T. Similarly, by differentiating (2) at constant temperature, the relationship between K and P is:

$$\left(\frac{\delta \ln K}{\delta P}\right)_T = \frac{\bar{V}_i^B - \bar{V}_i^A}{RT} = \frac{\Delta \bar{V}_i}{RT} \qquad (4)$$

where $\bar{V}_i$ = partial molar volume for i

$\Delta \bar{V}_i$ = molar volume of reaction for i.

Thus, the partition coefficient, K, is only a function of the temperature and pressure at which phases A and B formed in chemical equilibrium. It is not dependent on the chemical character- istics of the solution from which they were formed. This is a very fortuitous situation in the study of ore deposits since such solutions are not normally available for analysis. It has been found that the influence of pressure on the partition coefficient is quite small in sulphide systems (Bethke and Barton, 1971). Lack of correction for variations in P does not lead to large errors in the estimation of T. Therefore, the effect of P has not been dealt with in this study.

The working form of equation (3) is found by integration

(assuming $\Delta \bar{H}_i$ is independent of temperature) and is:

$$\log K = \frac{-\Delta \bar{H}_i}{2.303R} \left(^1/_T\right) + C$$

A plot of log K versus 1/T should be a straight line with slope equal to $-\Delta \bar{H}_i/2.303R$.

By experimentally determining K for element i over a range of temperatures, the basis for determining the temperature of formation of phases A and B in natural assemblages can be established. It is theoretically possible to develop a host of geothermometers by doing experimental work on suitable mineral pairs and appropriate substituting ions. Alternatively, the concordance of such temperature estimates with each other and concordance with other independent geothermometers (e.g., fluid inclusions) can be used to define conditions of chemical equilibrium in natural assemblages.

It should be emphasized that the use of partition coefficients in the geothermometry of natural assemblages is subject to certain restrictions (McIntire, 1963; Ghosh-Dastidar et al, 1970) which are:

(1) the substituting element i follows either Raoult's Law or Henry's Law in both phases A and B, at least below certain levels of dilution. The solubilities of element i are not affected by variations in concentration of other elements present in the two phases. However, correction for effects of this type can be carried out if they are well defined;

(2) the mineral phases were formed in chemical equilibrium;

(3) the distribution of element i in phases A and B has not

been affected by post-depositional events (e.g.,

metamorphism);

(4) the atoms of element i substitute for atoms in phases

A and B in their normal structural sites (i.e.,

substitution does not take place into interstitial

sites in the host), and the substituting and host

atoms are of the same charge.

Previous Experimental Studies

The first experimental studies of partitioning between

coexisting sulphides were carried out by Bethke and associates

(Bethke et al, 1958; Bethke and Barton, 1959; Bethke, personal

communication, 1967; Bethke and Barton, 1971). They investigated

the distribution of Cd, Mn and Se between sphalerite or wurtzite

and galena over the temperature range from 600° to 800°C, and the

distribution of Se between galena and chalcopyrite from 390° to

595°C. Mixtures between end members and/or binary solid solutions

were reacted dry in evacuated silica glass tubes. The compositions

of the resulting phases were analyzed by X-ray diffraction techniques

using unit cell versus composition relationships. Cd and Mn were

found to be strongly fractionated toward sphalerite or wurtzite

relative to galena, and the fractionation sequence of Se was found

to be: galena > chalcopyrite > sphalerite. Ideal solid solution

relationships apparently obtain in the systems which they considered,

at least over the concentration ranges normally found in nature.

Pressure effects, calculated from molar volume data, were found
to range from +1°C/kilobar at 600°C to -16°C/kilobar at 600°C in
these systems, and were judged to be negligible.

Yund and Giletti (1964) investigated the partitioning of Zn
between pyrite and galena at trace element levels. They synthesized
the phases in evacuated silica glass tubes using FeS, Pb or PbS
and S as the starting components. Zn^{65} was introduced as a radioactive
tracer at two temperatures, 600°C and 700°C. Two experiments were
performed at each temperature to test for equilibrium. In one, Zn^{65}
was initially present in FeS; in the second, it was initially
present in Pb (or PbS). Zn was found to concentrate in galena, with a
partition coefficient (Zn in PbS/Zn in FeS_2) ranging from 52 to 303.
Equilibrium conditions were apparently obtained.

H. D. Wright and several students at the Pennsylvania State
University have approached the problem of partitioning in coexisting
sulphides by using hydrothermal synthesis and radioactive tracer
analytical techniques. They performed a long series of experiments
to determine the solubility of a large number of elements, including
U, Ag, Sb, Cu, As, Ga, In, Tl, Hg, and Se in galena and sphalerite
over a temperature range of about 300° to 600°C (Halbig, 1965;
Barnard, 1965; Wright, Barnard and Halbig, 1965; Hutta and Barnard,
1963; Hutta and Wright, 1964). Halbig (Halbig and Wright, 1969;
Halbig, 1969) determined the partitioning of Se between sphalerite
and galena by performing hydrothermal runs over a temperature
range of 300° to 650°C, and dry silica tube runs at temperatures
above 700°C at one atmosphere pressure. The relationship between

log K and 1/T(°K) was found to be linear for Se. However, Halbig's

results are at variance with those of Bethke and Barton (1971).

Halbig also determined the effect of pressure on the partition

coefficient to be small.

Partitioning Studies on Natural Sulphide Assemblages

The only detailed and systematic study of the distribution

of trace elements between coexisting minerals from sulphide deposits

was carried out by Ghosh-Dastidar (Ghosh-Dastidar, Pajari and

Trembath, 1970; Ghosh-Dastidar, 1969). The distribution of Co, Ni,

Ti, Zn, Bi, Mn, V, Ga, Ge, In, Cd, Tl, Pb, Sn, Cu, Au, Te and As

was determined by spectrochemical methods, in pyrite, pyrrhotite,

chalcopyrite, sphalerite and magnetite from six sulphide occurrences

in the Canadian Appalachian area, namely: (a) the Gull Pond and

Rambler deposits of Newfoundland, and (b) four vein deposits (Oliver,

Cameron, South Oliver and Letite) of the Mascarene Peninsula, New

Brunswick. Plotting the concentrations of individual trace elements

in mineral pairs resulted in distribution patterns ranging from

linear through curvilinear to scattered. The majority of the

distribution patterns were found to be curvilinear and scattered

in character, indicating serious departures from the simple

distribution law. Even in cases where the distribution patterns

were linear, complexities (possibly due to differences in temperatures

of formation of the various deposits) and inconsistencies were

noted. The partition coefficient was observed to be dependent

on the element concentrations in either of the phases and/or
the presence of other trace elements in the phases in a majority
of the scattered and curvilinear distribution patterns, indicating
the non-applicability of Henry's Law. Ghosh-Dastidar concluded that
the presence of induced point imperfections may have been the
effective cause of the deviation from Henry's Law in many cases.

The importance of Ghosh-Dastidar's study is to point out
the possible complexities involved in the application of experimental
studies on the partitioning of elements between coexisting sulphides
in natural assemblages. Deviations from ideal solution behaviour
may in fact be very common even for trace constituents, and the
interaction of trace elements must be assessed in order to establish
a useful body of experimental data. Similar deviations from ideality
have been noted, by Halbig and Wright (1969), by Kretz (1959, 1960,
1961), and by Hall et al, (1971).

Crystallographic and Chemical Considerations

Solubilities of Mn and Co in ZnS and FeS_2:

Kroger (1938; 1939) found that the maximum solubility of
MnS in ZnS is about 52 mole per cent at 1180°C and 46 mole per cent
at 900°C. More recently, Bethke and Barton (1971) determined that a
miscibility gap appears at about 50 mole per cent MnS between
manganese-bearing wurtzite and alabandite (MnS). Skinner (1961)
pointed out that wurtzite is stabilized relative to sphalerite
by high concentrations of MnS. The amount of MnS required to stabilize

wurtzite decreases with increasing FeS content in ZnS. Bethke and Barton (1971) found that the limit of sphalerite stability is about 7 mole per cent MnS at 600°C in an iron free phase. The solubility of Mn in FeS_2 is known to be low despite the fact that MnS_2 (hauerite) is isostructural with pyrite. Fleischer (1955) gives the maximum concentration of Mn in pyrite from natural occurrences as 1%.

Both experimental studies and studies on natural occurrences (Klemm, 1962, 1965; Straumanis et al, 1964; Springer et al, 1964; Riley, 1965, 1968) show that CoS_2 and FeS_2 may form a complete solid solution series. Hall (1961) determined the maximum solubility of CoS in ZnS to be 33 mole per cent at 850°C.

The high solubility of FeS (up to 60 mole per cent) in ZnS (Barton and Toulmin, 1966) is well known and constitutes a complicating factor in these experiments. It is possible that variations of FeS in ZnS may have an effect on the concentration of MnS and CoS in ZnS, and thus would also affect partitioning coefficients. This point is discussed fully in a later section. The solubility of Zn in FeS_2 is very low and can be neglected.

Substitutional Sites in ZnS and FeS_2:

Zn^{+2} is in four-fold (tetrahedral) coordination in both sphalerite (cubic) and wurtzite (hexagonal). It has been normally assumed, because of the high solubility of Mn, Fe and Co in ZnS, that Mn^{+2}, Fe^{+2} and Co^{+2} substitute for Zn^{+2} at tetrahedral sites in ZnS. However, ZnS also contains octahedrally coordinated

interstitial sites which are not usually occupied. Czamanske and Goff (1973) suggest that occupancy of these sites by metal ions is energetically unfavourable because they are tetrahedrally coordinated in sphalerite and octahedrally coordinated in wurtzite by near-neighbour metal ions. Manning (1967) suggested, on the basis of absorption spectra for sphalerite containing 6.15 weight per cent Fe, that Fe is distributed in sphalerite as Fe^{+2} in tetrahedral sites (substitutional) and as Fe^{+3} in octahedral sites (interstitial). He estimated the ratio of Fe^{+2}/ Fe^{+3} in the sphalerites studies to be about 10. His findings led to the idea that the Fe^{+2}/Fe^{+3} ratio in sphalerite might be useful in determining the oxidation-reduction potential of hydrothermal solutions (paleo-E_h''). Mössbauer spectroscopy on iron rich sphalerites, by Marfunin and Mkrtchyan (1967) and Scott (1971), showed that iron in sphalerite occurs as Fe^{+2} and is randomly distributed over tetrahedral (substitutional) sites. This conclusion is supported by Cabri's (1969) density measurements of synthetic iron-bearing sphalerites.

Octahedral coordination of Co^{+2} in pyrite is confirmed because of the complete solution between CoS_2 and FeS_2, the isostructural character of CoS_2 (cattierite) and FeS_2 (pyrite), and similar physical properties of the two compounds (Hulliger, 1968). It also seems to be a safe assumption that small amounts of Mn^{+2} are octahedrally coordinated in substitutional sites in pyrite because MnS_2 (hauerite) is isostructural with FeS_2 (pyrite).

Application of Crystal Field Theory:

A review of the ionic radii and electronegativities (Table 1), for Mn^{+2}, Co^{+2}, Fe^{+2} and Zn^{+2}, indicates that the relative solubilities of Mn^{+2}, Co^{+2}, and Fe^{+2} in ZnS, and of Mn^{+2} and Co^{+2} in FeS_2 cannot be explained by applying the now classical rules of Goldschmidt and Ringwood. In recent years, geochemists (Burns, 1970; Czamanske and Goff, 1973; Nickel, 1968, 1970) have used a more sophisticated approach, crystal field theory, to explain the differences in geochemical behaviour between transition-metal ions with similar oxidation states and ionic sizes.

Elements of the first transition series have varying numbers of electrons distributed in two groups of 3d orbitals, which are: (1) $t_{2g}(d_{xy}$, d_{yz} and $d_{xz})$; (2) e_g (d_{z^2} and $d_{x^2-y^2}$). Each of the 3d orbitals may contain up to 2 spinpaired electrons. t_{2g} electrons may be thought of as forming lobes about a transition-metal ion which point between cartesian axes. Similarly, e_g orbitals form lobes about the transition metal ion which point along cartesian axes. In an unperturbed state, these orbitals are degenerate (have the same energy). However, anions (ligands) arranged symmetrically about the transition-metal ion, may cause the orbitals to "split" due to repulsive, electrostatic interaction of the outer electrons of the cation and the ligands. That is, the relative energies of the t_{2g} and e_g orbitals are dependent on the type, position and symmetry of the coordinating ligands relative to the cation. In addition, the character of this interaction is influenced by the distribution of electrons in the 3d orbitals of the cation (number of electrons, their symmetry, number of spin paired and

Table 1:   Ionic Radii And Electronegativities

Ion	Ionic Radii (Å)[1]		Electronegativity[2]
	Tetrahedral	Octahedral	
Mn^{+2}	0.77	0.75(ls)	1.4
		0.91(hs)	
Co^{+2}	0.65(hs)	0.73(ls)	1.7
		0.83(hs)	
Fe^{+2}	0.71(hs)	0.69(ls)	1.7
		0.86(hs)	
Zn^{+2}	0.68	0.83	1.5

(1)   After Whittaker and Muntus (1970). (hs) = high spin configuration

of electrons. (ls) = low spin.

(2)   After Fyfe (1964).

unpaired electrons, number of vacant orbitals). In other words, for

a certain type of ligand (e.g., S^{-2}), the most stable configuration

(e.g., octahedral or tetrahedral) of the ligands about the cation is

determined by the energy difference between the t_{2g} and e_g orbitals and by

the distribution of electrons in the five orbitals of the cation. The

crystal field stabilization energy (CFSE) measures the combined effect

of these two factors and is a direct measure of the relative stabilities

of different ligand symmetries (Table 2).

Mn^{+2} and Zn^{+2} contain 5 and 10 3d electrons respectively. These

electrons are spherically distributed about the ions so that S^{2-} ligands

are not stabilized in either an octahedral or a tetrahedral configuration

(Table 2). The coordination of these two cations is determined by their

ionic radius ratios relative to S^{2-}. The tetrahedral coordination of

Zn^{+2} in sphalerite and wurtzite, and the occurrence of Mn^{+2} in both MnS

(wurtzite structure) and MnS_2 (octahedral coordination) is neatly

explained in this way. Substitution of Mn^{+2} in ZnS causes strain in

the ZnS structure because of its larger ionic radius (Table 1). This

explains the limited solid solution of Mn in ZnS and also the stabilization

of the wurtzite structure relative to the sphalerite structure by Mn.

The CFSE's (Table 2) of both Fe^{+2} and Co^{+2} indicate a small

preference to coordinate octahedrally with S^{2-} ligands. However, this

does not explain the marked tendency of these two ions to form strongly

covalent disulphides. The magnetic properties and bond lengths of FeS_2

and CoS_2 show that Fe^{+2} and Co^{+2} occur in these compounds in low spin

configuration (spin pairing in t_{2g}), with t_{2g} electrons available for

17

Table 2: Data Relating to Crystal-Field Approach

Ion	No of 3d Electrons	No. of Unpaired Electrons		CFSE (oxide) Kcal mole^{-1}		Δ(oxide) Kcal mole^{-1}
		High Spin	Low Spin	Octahedral	Tetrahedral	
Mn^{+2}	5	5	1	0	0	0
Fe^{+2}	6	4	2	11.9	7.9	4.0
Co^{+2}	7	3	3	22.2	14.8	7.4
Zn^{+2}	10	0	0	0	0	0

After Burns (1970), Table 6.2

Note: CFSE = crystal field stabilization energy for oxide structures

Δ = octahedral-site preference energy for oxide structures

The CFSE's quoted here apply in strict sense only to oxide structures. However, their relative magnitudes are also applicable to sulphide structures (Burns, 1970, p.130).

extensive π bond formation with S^{2-} (Burns, 1970, p.192). The close similarity of the bonding properties of Co^{+2} and Fe^{+2} explains the complete solid solution between CoS_2 and FeS_2. Magnetic studies on MnS_2 indicate that Mn^{+2} has a high spin configuration. π bond formation is minimal in MnS_2 and its bonding is predominantly ionic (Burns, 1970, p. 190). The marked difference in the facility on Mn^{+2} and Fe^{+2} to form π bonds explains the low solubility of Mn in FeS_2.

The ionic radii (Table 1) of Co^{+2} and Fe^{+2} are close to that of Zn^{+2}. Also, the octahedral-site preference energy of both ions is small (Table 2). Therefore, extensive substitution of Co^{+2} and Fe^{+2} into tetrahedral sites in ZnS is allowed (Czamanske and Goff, 1973).

It has been found that bonding in ZnS is 80% ionic and 20% covalent in character (Title, 1965). This suggests that a discussion based on molecular orbital theory (Burns, 1970) would probably not change the conclusions very much.

Prediction of Partition Coefficients

An outline of the thermodynamic basis and importance of partition coefficients has already been given. A quantitative estimate of partition coefficients, and their variation with temperature and pressure, could be made using this thermodynamic schema. However, in this case, sufficient thermodynamic data are not available. A combination of crystal field theory and molecular orbital theory can be used for the rough prediction of partitioning in sulphides. Again,

quantitative estimates are, at present, impossible. There is, then, no feasible alternative to the experimental determination of partitioning coefficients.

EXPERIMENTAL PROCEDURES

Fused Salt Techniques

Boorman (1966, 1967) and Schröcke (1958) demonstrated that
the reaction rates for zinc and iron sulphides are considerably
increased by the addition of suitable eutectic salt mixtures. In
a study of the $ZnS-FeS-FeS_2$ system, Boorman employed the salt systems
KCl-LiCl (eutectic at 358°C; 41 mole per cent KCl) and NH_4Cl-LiCl
(eutectic at 267°C; 50 mole per cent NH_4 Cl) over a temperature range
of 303 to 714°C. He found that apparent equilibrium was attained
in four to seven days at temperatures from 600 to 400°C.

Fused salt techniques provide other experimental advantages
(Boorman, 1966). They allow experimentation over an extended temp-
erature range and the techniques are experimentally simpler than
hydrothermal methods of crystal growth. In addition, a large number
of metallic sulphides are at least moderately soluble in eutectic
salt mixtures such as KCl-LiCl and NH_4Cl-LiCl (Delarue, 1960, 1962).
The salt systems mentioned above are chemically inert relative to
the ZnS-FeS system, and the salt components are not soluble in the
various mineral phases of the ZnS-FeS system to any significant extent.
In short, they have a merely catalytic effect.

All experimental runs of this study were carried out using
fused salt techniques. A KCl-LiCl eutectic mixture was employed

for runs at temperatures of 403, 420, 475, 525, 575, 625 and 675°C.
A NH_4Cl-LiCl eutectic mixture was employed for runs at a temperature
of 305°C. The length of the runs varied from 5 to 47 days.

It should be noted that the solubilities of the various
sulphides of the study, particularly MnS and CoS_2, in the fused
eutectic salts, as well as the chemical character of such solutions,
are unknown (Delarue, 1962). A considerable number of preliminary
runs were performed in order to determine the amounts of MnS or CoS_2
which had to be added to the sulphide charges in order to produce ZnS
and FeS_2 with detectable amounts of Mn or Co in both phases over
a reasonably large concentration range.

Reagents

Pyrite was synthesized from polysulphide solution. A 1.0M
solution of $Na_2S.9H_2O$ was prepared to which was added 4 moles of
sublimed S. The solution was stirred overnight, and became very dark
brown, due to the formation of polysulphides (S_5^{2-} ?). The solution
was filtered to remove a small amount of undissolved S, and then was
mixed with a solution containing one mole of $FeCl_2$. A dark green
gelatinous precipitate was formed immediately. The precipitate
was heated for one day at 70°C, and for an additional day at 93 to
98°C. The precipitate settled out to a compact powder. The
solution was decanted and a 2.0 M solution of NaOH was added to

dissolve the native S precipitated at the same time as the pyrite. The solution was again decanted after stirring overnight. The pyrite was washed with distilled water followed by acetone. Subsequently, it was filtered and dried. An X-ray diffraction pattern for this material showed only diffuse peaks characteristic of pyrite. The broad form of the peaks, combined with microscopic examination of the precipitate, indicated the microcrystalline character of the pyrite.

Microcrystalline CoS_2 was synthesized in a similar fashion from a polyshulphide solution. 2.0 moles of native S were dissolved in a 1.0 M solution of $Na_2S.9H_2O$. A 1.0 M solution of $CoCl_2.6H_2O$ was mixed with the polysulphide solution to produce a gelatinous, black precipitate. The precipitate was heated at 90°C for two days to promote recrystallization. It was decanted and a 2.0 M NaOH solution was added to dissolve any excess native S. The precipitate was washed with distilled water, followed by acetone, before filtering and drying. An X-ray diffraction pattern confirmed that the precipitate was microcrystalline CoS_2.

A reagent grade, microcrystalline wurtzite (α-ZnS) was used in all runs. Its crystal structure was determined by X-ray diffraction.

The synthesis of MnS was effected by the mixing of $Na_2S.9H_2O$ and $MnCl_2.4H_2O$ solutions. A 1.2 M solution of $Na_2S.9H_2O$ was prepared and saturated with H_2S to limit hydrolysis reactions so as to maintain a maximum sulphide ion (S^{2-} + HS^-) concentration in the aqueous solution, according to the equations:

$$S^{2-} + H_2O \rightleftharpoons HS^- + OH^-$$

and

$$HS^- + H_2O \rightleftharpoons H_2S + OH^-$$
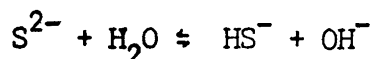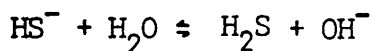
A 1.0 M $MnCl_2 \cdot 4H_2O$ solution was prepared and saturated with H_2S to reduce any Mn^{+3} ions to Mn^{+2}. The solutions were mixed slowly with the evolution of H_2S. A bright orange, curdy precipitate was instantly formed. The precipitate was heated at 70°C for two days to drive off residual H_2S and to recrystallize the precipitate. The precipitate settled in one day to a compact powder. It was decanted and washed with distilled water followed by acetone. The precipitate was then filtered and dried. X-ray diffraction methods indicated that the precipitate was β-MnS (wurtzite structure).

KCl - LiCl and NH_4Cl - LiCl eutectic salt mixtures were prepared from reagent grade materials by mixing the appropriate eutectic proportions of each component together. The mixtures were then fused, crushed and dehydrated ready for use.

Preparation And Heating Of Charges

Microcrystalline ZnS and FeS_2 were mixed thoroughly in the mole ratio of 1:1. Batches of sulphide reactant were prepared in which MnS or CoS_2 was present in amounts of from 0.2 to 40 weight per cent of the total sulphide ($ZnS + FeS_2 + MnS$ or CoS_2). An eutectic salt mixture was added to portions of these batches in a proportion varying from 1:1 to 1:4 (sulphide:eutectic salt mixture). The sulphide-eutectic salt

mixture charges were loaded in 6 mm (OD) Pyrex and Vycor tubes. The tubes were evacuated for 20 minutes with gentle heating (to eliminate residual moisture) prior to sealing.

The charges were heated in vertical tube furnaces, controlled to $\pm$ 5°C. Runs were performed at eight temperatures, namely: 675, 625, 575, 525, 475, 420, 403 and 305° C. Normally, six charges, representing a range in the amount of MnS or CoS_2 present in the charge, were heated together at each temperature. Run times varied from 5 to 47 days. At the end of each run, the tubes were air quenched. The tubes were broken and the eutectic salt mixture was dissolved away with several washings of distilled water. The remaining run products, a loose assemblage of sulphide crystals, were washed with acetone and then allowed to dry.

Run Products

Figure 2 is an example of the microcrystalline, sulphide reactant material prior to heating. The photograph illustrates that the grain size of the material is considerably less than one micron. Figure 3 shows the remarkable degree of recrystallization of the sulphides caused by heating at 575°C for a period of 21 days in a KCl-LiCl fused salt eutectic mixture.

The usually discrete, sulphide crystals were anhedral to euhedral in character, showed very little intergrowth, and were usually in the order of tens of microns in size. Difficulties were encountered with runs of 400°C and below because the grain size of the run products approached one micron in size, the limit of resolution for analysis

Figure 2: Mixture of microcrystalline, reactant wurtzite and pyrite.

Polished section. Reflected light. In oil. X360.

Figure 3: Subhedral to euhedral crystals of sphalerite and pyrite.

Reaction product of run 68 at 575°C for 21 days. Unpolished

grain mount. Reflected light. In oil. X430.

by the
in col
modifi
they c   eir
centre
Wurtzi
pyrito

(Cu -   terite
or wur   sence
of ext
ZnS in
small for single crystal X-ra   ion techniques (Scott, 1988;
Scott

Figure 2

of
salt i
(Figur   om
in suc   sions
were n   e
abnorm
inclus
peratu   a-
tures   a
heatin   nd
so thi
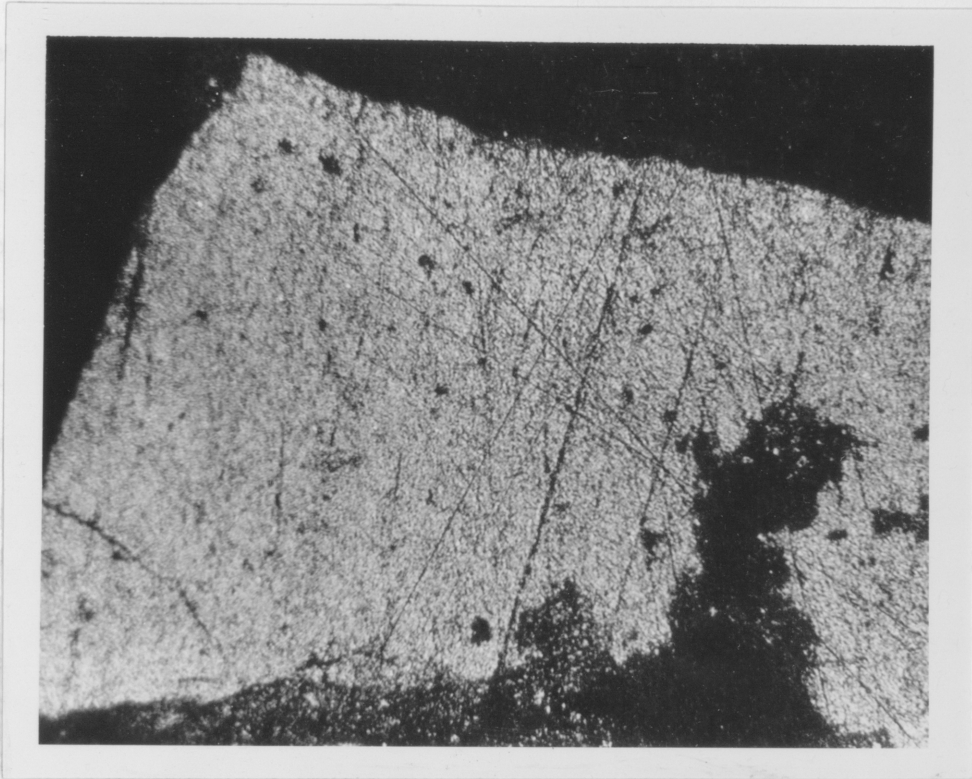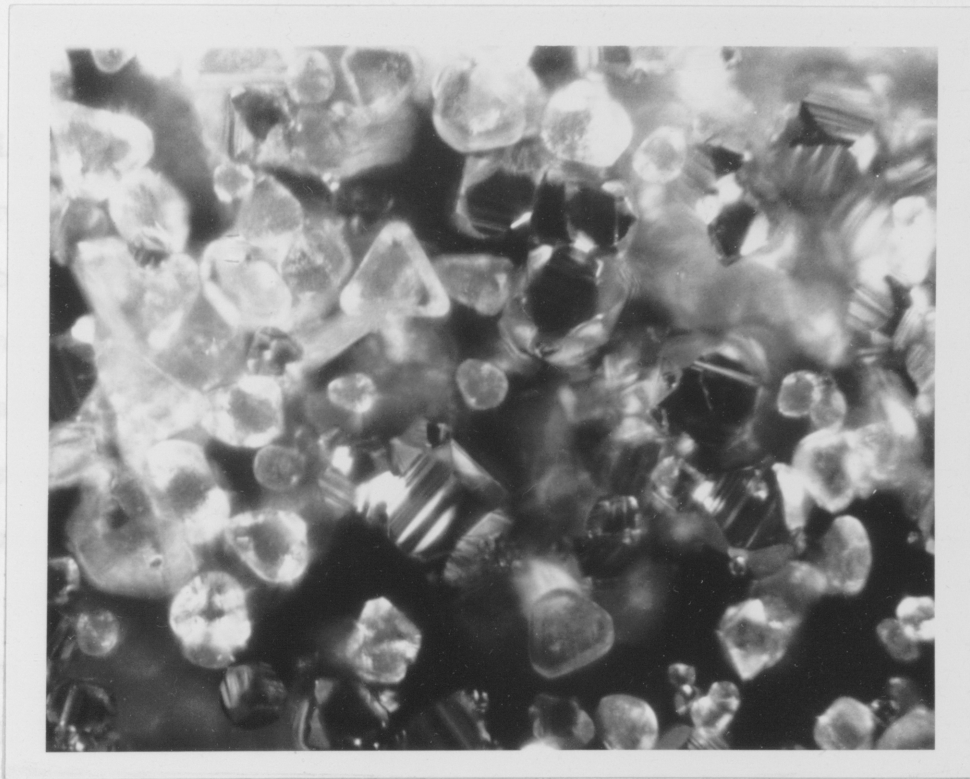
Figure 3

by the electron microprobe. Sphalerite crystals were light amber in colour and tetrahedral in form, with cubic and dodecahedral modifications. The crystals were normally clear of inclusions, but they occasionally contained fine, dusty inclusions of pyrite at their centres, and a few, larger, discrete grains of pyrite (Figure 3). Wurtzite, when present, was tabular in form. Pyrite occurred as pyritohedrons, with rare inclusions of sphalerite or wurtzite.

All run products were checked by X-ray diffractometer methods (Cu - Kα radiation), using smear mounts, for the presence of sphalerite or wurtzite (stabilized by the inclusion of MnS), and for the presence of extra phases. No attempt was made to identify polytypes of ZnS in the run products since in all cases, the grain size was too small for single crystal X-ray diffraction techniques (Scott, 1968; Scott and Barnes, 1972).

One interesting sidelight of this study was the formation of salt inclusions, complete with vacuoles, within ZnS crystals (Figure 4). They appear to be entirely analogous to fluid inclusions in such minerals as quartz and calcite (Roedder, 1967). The inclusions were not commonly present, and in fact, were observed only in some abnormally large crystals formed in one run at 575°C. The salt inclusions could theoretically, be used as a means of internal tem-- perature calibration of the runs by determining the filling tempera- tures of the salt inclusions with a heating stage. Unfortunately, a heating stage capable of reaching 575°C safely was not available and so this idea could not be checked.

Figure 4: Salt inclusions in sphalerite crystal, formed at 575°C.

Note vacuoles within inclusions. Unpolished grain mount.

Reflected light. In oil. X390.

Chemical Equilibrium
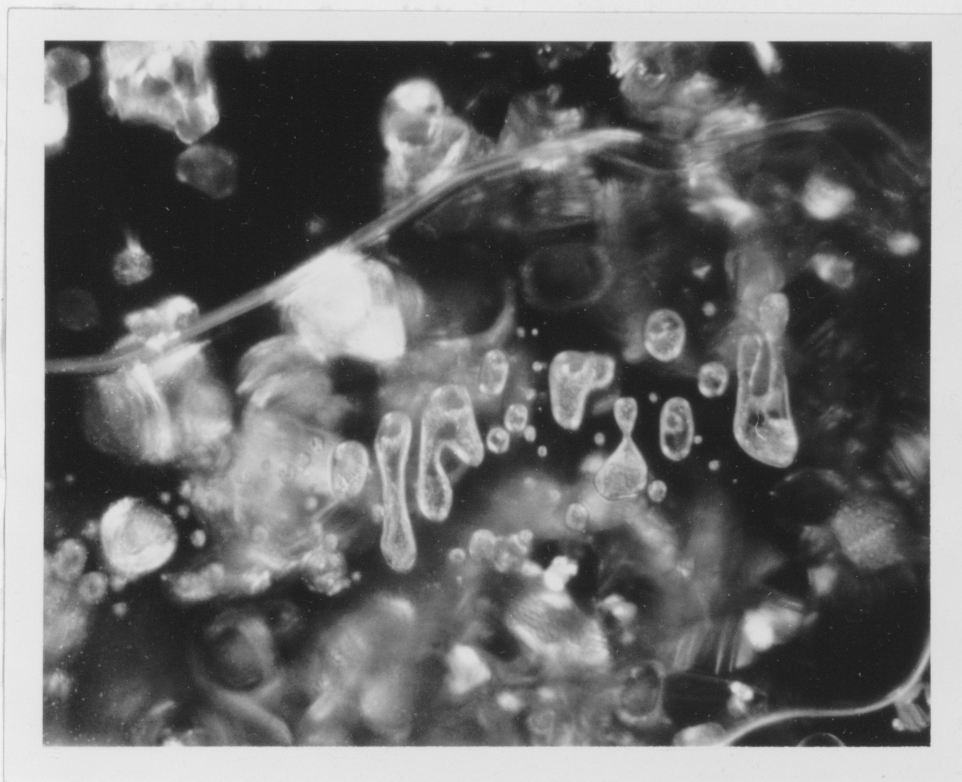
ntal

envir...

exper...   n is

by ap...   ections.

In ma...

examp...   rmometer),

since...   ry slow

(Bart...   ly

one d...   itions

have ...

                                                                     he

run products

(3) intra- and inter... ne chemical homogeneity of the

Figure 4

run products (e.g., no zonation of sphalerite).

All of these are indicative of chemical equilibrium, but only in a

permissive sense.

    The first two criteria were easily and routinely tested. Of

the three criteria, chemical homogeneity of the run products is the

most important and the most difficult to check. This criterion was

tested in two ways. Several electron microprobe scanning images

(Figures 5 and 6) were completed of the various run products. In most

cases no obvious zonation of the phases was observed. The most common

inhomogeneities detected by this method were discrete inclusions of

Chemical Equilibrium

The definition of equilibrium conditions in any experimental environment is difficult. The classical method of ensuring that experimental results represent a condition of chemical equilibrium is by approaching equilibrium from two different and independent directions. In many systems, this procedure is not technically feasible (for example, Boorman's (1967) work on the so-called sphalerite geothermometer), since the rates of reaction for runs involving unmixing may be very slow (Barton et al, 1963). In this study, reactions have been run in only one direction. However, three other criteria of equilibrium conditions have been used, namely:

(1) pronounced recrystallization of the sulphide charge;

(2) sharp peaks in the X-ray diffractometer patterns of the run products

(3) intra- and inter-crystalline chemical homogeneity of the run products (e.g., no zonation of sphalerite).

All of these are indicative of chemical equilibrium, but only in a permissive sense.

The first two criteria were easily and routinely tested. Of the three criteria, chemical homogeneity of the run products is the most important and the most difficult to check. This criterion was tested in two ways. Several electron microprobe scanning images (Figures 5 and 6) were completed of the various run products. In most cases no obvious zonation of the phases was observed. The most common inhomogeneities detected by this method were discrete inclusions of

Figure 5: Scanning electron beam images of element distributions

in sphalerite and pyrite reaction products formed at

525°C for 14 days (run 21). (A) Secondary electron image

of sphalerite crystal with adjacent pyrite crystal.

(B) Distribution of Fe. Note pyrite inclusions within

sphalerite crystal. (C) Distribution of Mn. (D) Secondary

electron image of pyrite crystal. (E) Distribution of

Mn. Mn rich phase is sphalerite. X714.
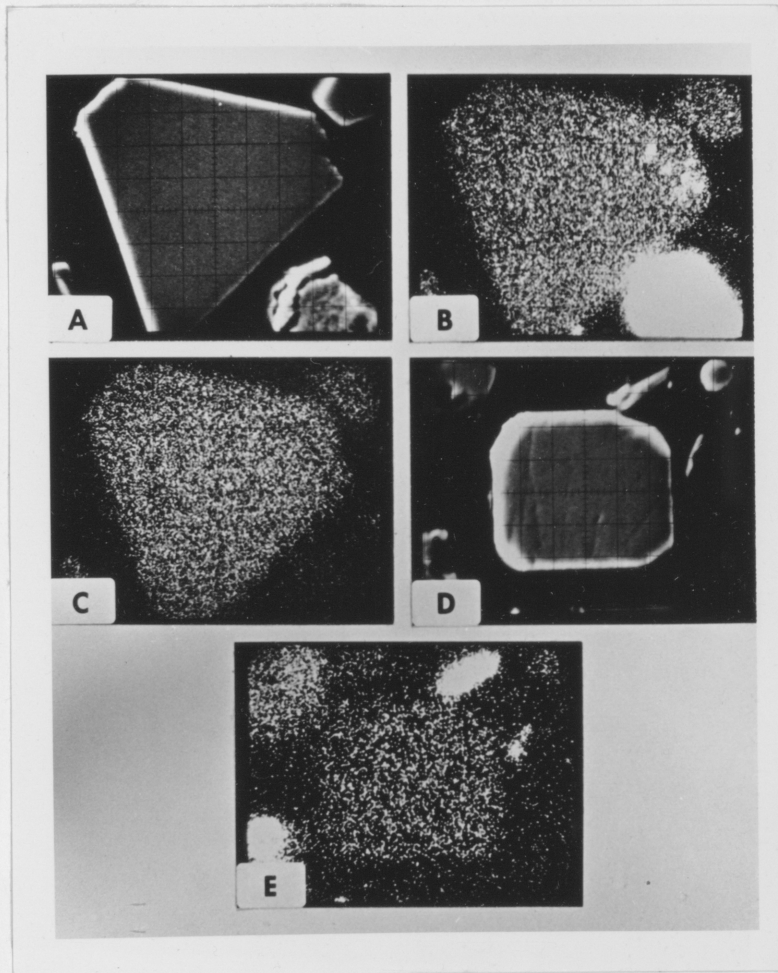
Figure 5

Figure 6: Scanning electron beam images of element distributions in sphalerite or wurtzite and pyrite reaction products from runs at 420°C for 47 days. (A) Secondary electron image of subhedral to anhedral wurtzite crystals, surrounded by slightly smaller pyrite crystals, from run 175 with MnS added. Distribution of Zn (B), Fe (C) and Mn (D) for sample (A). (E) Secondary electron image of subhedral to anhedral sphalerite crystals surrounded by much smaller pyrite crystals, from run 182 with·CoS$_2$ added. Distribution of Zn (F), Fe (G) and Co (H) for sample (E). X323.

other phases in single crystals (Figure 6). The application of

statis

homoge

Figure 6

other phases in single crystals (Figure 5). The application of
statistical methods on the analytical data to test for chemical
homogeneity of the phases in each run is discussed fully below.

ANALYTICAL METHODS

Analytical Conditions

All analyses were carried out on an Applied Research Laboratories electron microprobe X-ray analyzer (Model EMX - SM) in the Department of Materials and Metallurgical Engineering at the University of Michigan. A beam, normal to the specimen surface, focussed to a size of 1μ or less in diameter, and with a potential of 15 KeV, was employed. The X-ray take-off angle of this instrument is fixed at 52.5°. Pulses were counted for fixed times ranging from 10 to 100 seconds. Beam current was monitored by means of a sensitive microammeter, and it was kept constant at from 1.0 to $1.2\mu A$. Sample currents were found to be approximately 0.04 to $0.06\mu A$.

Pure metallic standards were used in the analysis of Mn, Co and Zn, in addition to synthetic MnS and ZnS. Pure metallic Fe and a large euhedral pyrite crystal from Gilman, Colorado were used as standards for Fe. Both the metallic and the sulphide standards gave essentially the same results.

Both the samples and standards were mounted in polyester resin and were polished with 6μ and 1μ diamond paste, and finally 0.25μ carborundum on nylon covered laps. The standards and samples were coated simultaneously with a light film of carbon to ensure conductivity.

Counts were taken on the $K\alpha$ peaks of Mn, Co, Fe and Zn. Pulse height discrimination of the peaks effected a lowering of the

background and the elimination of possible interferences by high order lines. Background counts were taken on both sides of the $K\alpha$ peaks, on both standards and samples. All sample counts were bracketed by counts on each of the standards to provide an effective drift correction.

S was not determined directly. Sulphur concentration was calculated by the stoichiometry of $(Zn, Fe, Mn, Co)S$ and $(Fe, Zn, Mn, Co)S_2$.

Correction Procedures

The raw probe data were corrected by means of two computer programs, Probe 1 and Probe 2, written in the Fortran IV language. Both programs are extensive revisions of programs developed by Frazer, Fitzgerald and Reid (1966) at the Scripps Institution of Oceanography. The first program, Probe 1, corrects probe data for background, deadtime and drift, and by comparing sample counts with the appropriate readings on standards, calculates initial probe ratios. The second program, Probe 2, corrects the data for the effects of absorption, fluorescence and atomic number.

Background Correction:

Bombardment by high energy electrons (Keil, 1967) produces both continuous radiation and characteristic X-rays. The continuous

radiation is directly proportional to the accelerating potential, the electron beam current and the average atomic number of the target. Small contributions to background are caused by cosmic rays, scattered X-rays and electrons, circuit noise and fluorescence radiation produced in the diffracting crystal. Backgrounds were measured on both sides of the Kα peaks for both standards and samples. These readings were averaged and subtracted from the appropriate counts on peaks. Accurate background readings were found to be essential for elements in low concentration.

Deadtime Correction:

Deadtime constants (τ) were determined for each element by measuring count rates on standards over a range of sample currents. Counts per second (N) were divided by sample current (i_s) and a linear function between these values (N/I_s) and sample current (i_s) was calculated by means of a least-squares technique incorporated in the Probe 2 program as a subroutine. This is the same as fitting the counts per second values with a parabola of the form $Ai_s + Bi_s^2 = 0$, where $\tau = -B/A^2$ (Frazer et al, 1966).

Deadtime constants (τ) were found to be 0.6, 2.8, 0.9 and 1.0 microseconds for CoKα, ZnKα, MnKα, and FeKα radiation, respectively. The deadtime correction was applied through the relation

$$N = N'/(1 - N'\tau)$$

where N' is the observed count rate and N is the true count rate.

Drift Correction:

All sample readings were bracketed by standard readings.
A linear drift curve was calculated by program Probe 1 and counts
on samples were corrected according to the time each count was
taken relative to the beginning of counting for each element.

Absorption Correction:

The absorption correction accounts for the loss of intensity
of characteristic X-rays by interactions with sample atoms along the
path from their point of origin to the surface of the sample (Keil,
1967). Philibert's (1963) formula for $f(\chi)$ was used to calculate
absorption correction factors:

$$f(\chi) = \frac{1+h}{(1+X/\sigma)[1+h(1+X/\sigma)]}$$

In this expression:

(1) $\qquad h = 1.2 \sum_i a_i A_i / (\sum_i a_i Z_i)^2$

$\qquad\qquad$ where a_i = the atomic fraction

$\qquad\qquad\qquad$ A_i = the atomic weight and

$\qquad\qquad\qquad$ Z_i = the atomic number of

$\qquad\qquad\qquad\qquad$ element i in

$\qquad\qquad\qquad\qquad$ a composite target.

(2) $\qquad \chi = (^\mu/_\rho)$ cosec θ

where $^\mu/_\rho = \sum_i C_i (^\mu/_\rho)_i$

and C_i = weight % of element i

$\qquad \theta$ = take-off angle of emitted radiation,

$\qquad$ in this case 52.5°. $(^\mu/_\rho)_i$ = the

$\qquad$ mass absorption coefficient of element

$\qquad$ i for the X-ray line used in the

$\qquad$ analysis.

(3) $\qquad$ Heinrich's expression for σ was used (Goldstein

and Comella, 1969, p.10) and is:

$$\sigma = \frac{4.5 \times 10^5}{E_o^{1.65} - E_c^{1.65}}$$

where E_o = the operating voltages of the

$\qquad$ electron beam in KeV

$\qquad E_c$ = the excitation potential of the

$\qquad$ analyzed element in KeV.

It should be noted that all mass absorption coefficients were calculated in the Probe 2 program using a set of equations proposed by Frazer (1967). This method calculates mass absorption coefficients which are essentially the same as those given by Heinrich (1966). An attempt was made to analyze Zn by means of an Lα line, using Frazer's equation to determine mass absorption coefficients for Zn Lα by extrapolation. The resulting analytical data were found to be seriously

in error due to a gross overcorrection for absorption.

Fluorescence Correction:

The intensity of the analytical line of one of the elements in a sample is enhanced when the wavelength of a characteristic line from one of the other elements in the sample is shorter than the absorption edge of the analyzed element. The ratio (γ) of intensity due to secondary fluorescence to the intensity of primary radiation was calculated for K - K, K - L, L - K and L - L interactions using the formula of Reed (1965). This formula is:

$$\gamma = 0.5 \; P_{ij} C_B \left(\frac{r_A - 1}{r_A}\right) W_B \frac{A'}{B'} \left(\frac{U_B - 1}{U_A - 1}\right)^{1.67} \frac{\mu_B^A}{\mu_B} \left(\frac{\ln(1+x)}{x} + \frac{\ln(1+y)}{y}\right)$$

where   A = analyzed element

   B = element causing secondary fluorescence of A

   C_B = mass concentration of element B

   r_A = absorption edge jump ratio of element A

   W_B = K or L shell fluorescence yield of element B, given by

      $W = Z^4/(a + Z^4)$, with Z = Atomic number of element B and

      $a = 1.02 \times 10^8$ for K shell

   A' and B' = atomic weights of elements A and B

   U_A = the overvoltage ratio, $^{Eo}/_{Ec}$ for element A

   U_B = the overvoltage ratio, $^{Eo}/_{Ec}$ for element B

μ_B^A = the mass absorption coefficient of element A for

radiation from element B

$\mu_{\bullet B}$ = the mass absorption coefficient of the specimen

for radiation from element B

x = $(\mu_A/\mu_B)\mathrm{cosec}\ \theta$, with μ_A = the mass absorption coefficient

of the specimen for radiation from element A

$y = \sigma/\mu_B$, with σ = the electron mass absorption coefficient

P_{ij} is a constant whose value depends upon the type of interaction (K - L, L - K, K - K, L - L) was considered. For K - K and L - L interactions, $P_{KK} = P_{LL} = 1$. For K - L and L - K interactions, $P_{KL} = 0.24$ and $P_{LK} = 4.2$.

No corrections were made for secondary fluorescence caused by K_β or L_β lines, or for secondary fluorescence due to continuous radiation. Both of these effects are usually negligible (Reed, 1965; Springer, 1967).

In this study Zn Kα caused enhancement of Mn, Co and Fe Kα lines.

Atomic Number Correction:

Electron backscattering and electron retardation depend upon the average atomic number of the target (Keil, 1967). These effects lead to analytical values which are too low for heavy elements in a light matrix and too high analytical values for light elements in a heavy matrix.

An atomic number correction was calculated by means of a method

described by Duncumb and Reed (1968). The loss of ionization efficiency

due to backscattering (R_i) was calculated for each element using a set

of polynomial equations given by Duncumb and Reed (1968). The fraction

of the total energy loss of an electron going into the ionization

of a particular shell (S_i) in a specific element (i) is given by the

equation:

$$S_i = \frac{Z_i}{A_i \ln\left[\dfrac{1.166 \times 10^3 (\frac{Eo + Ec}{2})}{J_i}\right]}$$

where   Eo = the operating voltage in keV

Ec = the excitation voltage of the X-ray line of interest

in keV

Z_i = atomic number of element i

A_i = atomic weight of element i

J_i = mean ionization potential for element i

For a multielement sample, an average R and S are calculated by:

$$\bar{R} = \sum_i C_i R_i$$

and

$$\bar{S} = \sum_i C_i S_i$$

where C_i is the weight fraction for an element in the sample. The

atomic number correction is effected by finding the ratio $\bar{R}/\bar{S}$ for the

analyzed element in the sample and in its standard, and combining these

two factors as shown below.

Combined Correction for Absorption, Fluorescence and Atomic Number:

The true concentration of an element in a sample (W_i) was calculated by:

$$W_1 = C_i \times \frac{\left(\overline{R}/\overline{S}\right)_{st}}{\left(\overline{R}/\overline{S}\right)_{sa}} \times \frac{\left(f(x)_i\right)_{st}}{\left(f(x)_i\right)_{sa}} \times \frac{\left(1 + \gamma_i\right)_{st}}{\left(1 + \gamma_i\right)_{sa}}$$

C_i is the initial estimate (probe ratio) of element i in the sample, or the most recently calculated concentration of element i. The subscripts st and sa refer to correction factors for standard and sample. The true concentration of element i was calculated by an iterative procedure in which the most recently calculated concentration of each element was used in the calculation of the correction factors. Iteration was continued until the change in concentration between consecutive iterations for all elements present in concentrations greater than 1% was less than 0.001%. The correction procedure was usually completed within three to four iterations.

Analytical Accuracy

The accuracy of the correction procedures of the computer program, Probe 2, was checked by running a test problem (Goldstein and Comella, 1969, p.48) for a silicate analyzed using K - alpha lines at 20 KeV with a take-off angle of 52.5° (Table 3). The two sets of final

Table 3:   Test Of Correction Procedures Of Program Probe 2 On

Silicate Problem From Goldstein And Comella (1969, p.48)

Element	Initial Estimate (wt.%)	Final Calculated Composition (wt%)	
		Goldstein & Comella (1969)	Program Probe 2
Ca	11.54	11.57	11.55
Mg	12.55	12.87	12.66
Si	25.13	26.1	25.80
Al	1.15	1.08	1.07
Na	0.88	0.93	0.90
Mn	0.09	0.09	0.09
Cr	0.59	0.58	0.58
Fe	2.57	2.59	2.57
Ti (known)	0.10	0.10	0.10
O	43.78	45.0	44.57
Total	98.38	100.91	99.89

Note: The compositions of the six silicate standards used in this

problem are given by Goldstein and Comella (1969, p.69).

calculated compositions show very close agreement, with program Probe 2 giving slightly lower calculated compositions for most elements, but a better analytical total (99.89% for program Probe 2 compared with 100.91% given by Goldstein and Comella).

The accuracy of the whole analytical procedure has been estimated by determining the compositions of a series of Bolivian sphalerites (Table 4) which had been analyzed by atomic absorption and X-ray diffraction techniques (Kelly and Turneaure, 1970, p.635). Grain mounts were made and three grains per mount were analyzed. Counting was done on two points in each grain to test for within-grain homogeneity. The electron microprobe data indicate that the distributions of Fe and Mn in the sphalerites are sufficiently uniform so that comparisons may be made with the atomic absorption and X-ray diffraction analyses. Both the quantitative data and semiquantitative scans indicate no marked zonation of either Fe or Mn. Considering that the electron microprobe analyses were carried out on a limited number of individual grains, whereas the atomic absorption analyses were done on bulk samples, the two methods are in good agreement for both MnS and FeS. The X-ray diffraction data for FeS are consistently higher, by as much as 7.1 mole % FeS, than the equivalent electron microprobe data. The positive error is caused by expansion of the sphalerite unit cell by Mn and Cd (Kelly and Turneaure, 1970, p.635).

Another measure of accuracy is provided by the analytical totals derived during routine analysis. Analytical totals were found to range from 95.0 to 105.7 per cent, with a mean of 100.4% and a standard deviation of 2.0% of the mean. The scatter of analytical totals increased due to the fact that S was determined stoichiometrically.

Table 4: Comparison Of Electron Microprobe, Atomic Absorption And X-ray Diffraction Data On

Some Bolivian Sphalerites (mole %)

Specimen Number	Electron Microprobe						Atomic Absorption			X-ray Diffraction
	Mean MnS	Range MnS	Mean FeS	Range FeS	Mean ZnS	Range ZnS	MnS	FeS	CdS	Apparent FeS
CQ-200	.27	.13-.51	25.6	23.6-27.3	74.2	72.2-76.2	.22	23.2	.26	27.5
CQ-609	.05	.04-.06	23.1	21.6-24.5	76.8	75.4-78.3	.04	22.9	.18	21.4
SVD-21	.08	.07-.09	23.6	22.7-24.0	76.3	75.9-77.2	.10	22.3	.45	25.8
MCC-14	.08	.04-.10	19.3	17.1-21.0	80.7	78.9-82.9	.07	14.7	.50	20.9
PZA-105	.12	.03-.50	20.5	19.7-22.1	79.4	77.4-80.2	.26	17.6	.47	25.8
PUL-113	.01	<.01-.02	.95	.47-1.47	99.0	98.5-99.5	.03	.63	.47	1.5
HRI-1	.05	.04-.06	15.7	13.6-17.5	84.2	82.4-86.4	.04	18.9	.29	18.1
HUA-132	.09	.06-.15	18.9	18.2-19.7	81.0	80.3-81.7	.08	18.9	.44	22.7
LAR-9	.06	.04-.09	8.03	7.82-8.34	91.9	91.6-92.1	.09	8.3	.23	10.7

48

Any error in the estimation of Mn, Co, Fe or Zn is magnified by the calculation of S content. The analytical totals of this study compare favourably with those found by Williams (1967, p. 490) for the electron microprobe analysis of 50 sphalerites. His analytical totals ranged from 95.6 to 104.2%, with a mean of 99.7 and a standard deviation of 2.1% of the mean. S was determined stoichiometrically by Williams.

Sensitivity

In this study, sensitivity is defined as the concentration of an element which produces a peak equal to three times the standard deviation of the background. Sensitivities have been calculated by means of a formula provided by Norrish and Chappell (1967, p. 204).

$$\text{Lower limit of detection} = \frac{6}{m} \sqrt{\frac{C_b}{T}}$$

where m = the number of counts per second obtained per unit of concentration for the element, C_b = background counts per second, and T = counting time in seconds. For typical counting rates of this study, using a 100 second counting time, the calculated sensitivities for Mn, Co, Fe, and Zn are 75, 70 95 and 520 ppm respectively.

DISCUSSION OF RESULTS

Partitioning Of Mn Between Sphalerite Or Wurtzite And Pyrite

The analytical data for all sphalerite - or wurtzite-pyrite pairs containing Mn are listed in Appendices I and II in terms of mole percent. The runs are in order of temperature from 675 to 305°C. The concentration of MnS in sphalerite or wurtzite varies from very low levels to about 42 mole percent. The concentration of FeS is fairly constant. Most analyses fall within the range of 2 to 10 mole percent FeS. There is a slight increase in FeS to 16 mole percent at 675°C. MnS_2 in pyrite is usually less than 1 mole percent. ZnS_2 in pyrite was found to be low at 1 mole percent or less, a concentration probably too low to affect the partitioning of Mn.

Homogeneity Of Run Products:

As mentioned previously, an important criterion of chemical equilibrium is homogeneity of the run products. Several electron microprobe scanning images of both sphalerite and wurtzite showed no obvious zonation of Mn and Fe in either polymorph. However, because of the common growth zoning present in sphalerite from natural occurrences (Barton et al, 1963) and because of the iron-rich "patches" in hydrothermally synthesized sphalerites found by Scott and Barnes (1972), a more accurate test of homogeneity was carried out on the sphalerite and wurtzite run products. In the analysis

of 32 of the runs, counts were taken on two distinct points in each of the crystals. One - way analysis of variance (Snedecor and Cochran, 1967, chapter 10) indicated that the within - crystal variation of both MnS and FeS is much less than the between - crystal variation at the 99% level of confidence. In general, then, both MnS and FeS are homogeneously distributed within the sphalerite and wurtzite crystals. Electron microprobe scanning images of the distribution of Mn within pyrite crystals showed no obvious zonation of the crystals. Because of the low concentration of MnS_2 in the pyrite crystals, this cannot be taken as a discriminating test.

The Mn analyses for each phase in each run were tested for between - crystal homogeneity by a statistical method (Dixon and Massey, 1957, p.276) designed to detect extreme values in a group of data. For a group of k analyses, x_1, x_2, $- - - - -$, x_k, which are ranked in order of magnitude, the statistic:

$$ r_{10} = \frac{x_2 - x_1}{x_k - x_1} $$

where $x_2 - x_1$ = the difference between the maximum or minimum
value and the next highest or lowest value

and

$x_k - x_1$ = the difference between the maximum and
minimum value

is a measure of the deviation of the minimum or maximum value from the whole group of analyses. Ratios of this type were calculated and compared with a set of critical values tabulated by Dixon and

Massey (1957, Table 8e, p.412) for the 95% confidence level for k observations. Ratios higher than the appropriate critical value were taken to indicate that the phase, in the particular run considered, contains extreme concentrations of Mn and must be considered to be heterogeneous. In cases where duplicate analyses were performed at different spots on single crystals, the duplicate analyses were averaged before this test was performed. Phases found to be heterogeneous by this method are marked in Appendices I and II. The results of the corresponding runs were not used in the determination of partition coefficients.

Consideration was given to the use of Boyd's (1969) "homogeneity index" which tests the statistical fit of the distribution of a group of X-ray counts to the Poisson distribution. That is, if the variation in counts for a particular group of crystals follows the Poisson distribution, the apparent chemical variation among the crystals is due solely to counting errors. Boyd's index has two drawbacks. It is not a sensitive test for elements at the trace element level. Secondly, it makes the a priori assumption that the only permissible component of variation in a group of analyses must be due to counting errors. This latter assumption seems restrictive and would probably lead to the rejection of potentially meaningful data.

The occurrence of heterogeneities of the type detected in the data may have several causes. Extreme values of Mn in sphalerite, wurtzite or pyrite may reflect incomplete mixing of MnS in the original sulphide charge, particularly at high concentrations of

MnS. Heterogeneities in runs at 305°C (e.g. run 200) are probably due to lack of reaction. Anomalously low concentrations in crystals from runs at other temperatures could indicate the presence of unreacted or partially reacted material. High concentrations of ZnS_2 in pyrite (greater than 1.5 mole percent) may be caused by micro-inclusions of sphalerite or wurtzite in pyrite, and should be accompanied by a corresponding increase of MnS_2 in the same pyrite crystals. This is apparently what has happened in a few of the runs (e.g. run 138, Appendix II), in spite of the fact that pains were taken to avoid all inclusions during the microprobe analyses. An error of this type would cause anomalously low partition coefficients for the runs involved. To further investigate this point, a rank correlation coefficient (Snedecor and Cochran, 1967, p.194) was calculated for the ZnS_2 and MnS_2 analyses in pyrite. The rank correlation coefficient was found to be non-significant at the 95% confidence level, indicating that contamination of this sort is not a common problem. Finally, apparent heterogeneities may result from the relatively high errors inherent in measuring MnS_2 in pyrite at low concentrations.

Distribution Of Mn Between Sphalerite Or Wurtzite And Pyrite:

The distribution of Mn in sphalerite – or wurtzite-pyrite pairs for seven different temperatures, from 675 to 403°C, is shown in Figures 7 to 13. The error bars about each point in these diagrams represent the variation of MnS in sphalerite or wurtzite
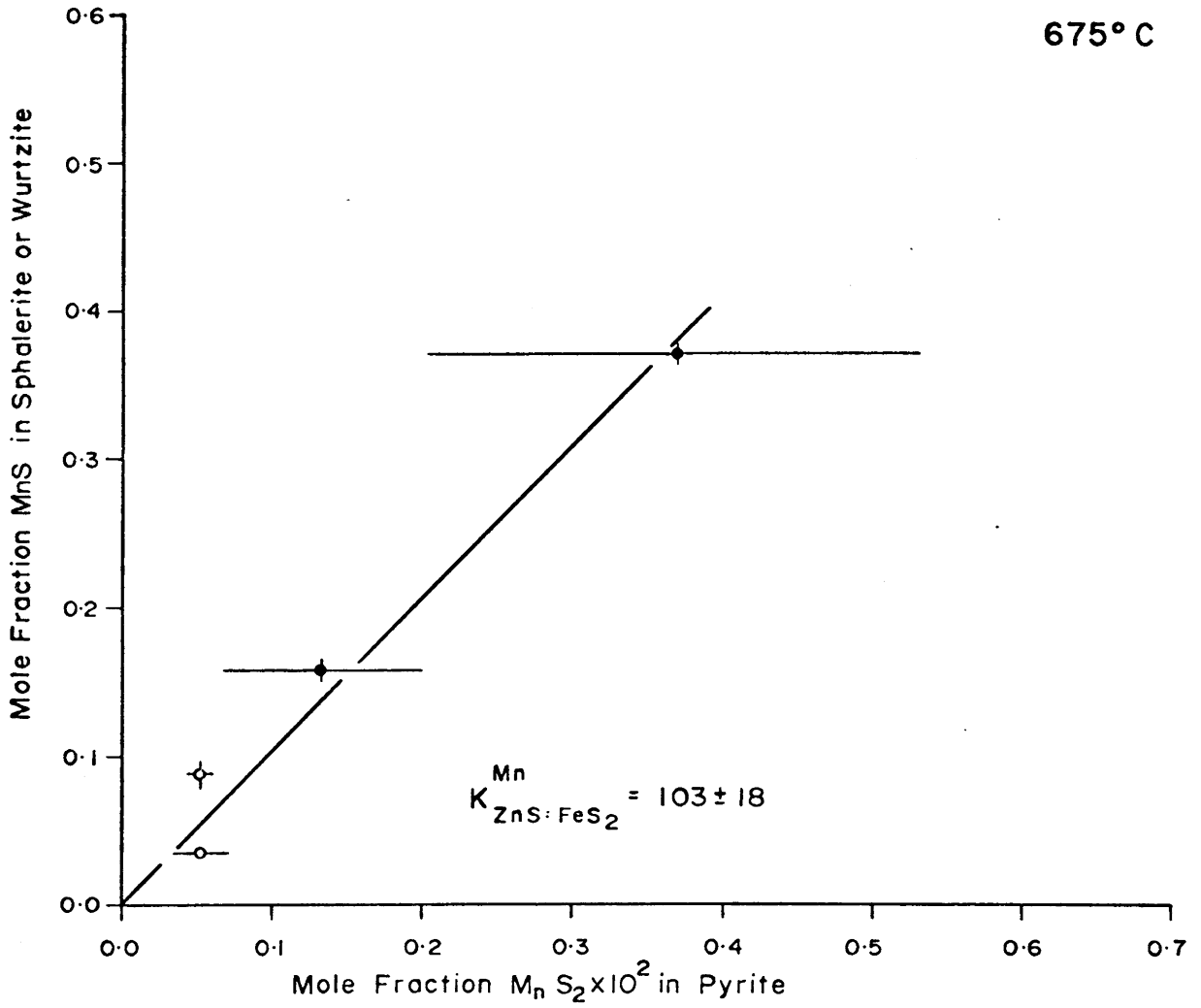
Figure 7: Partitioning of Mn between sphalerite or wurtzite and pyrite at 675°C. o = sphalerite. ● = wurtzite.
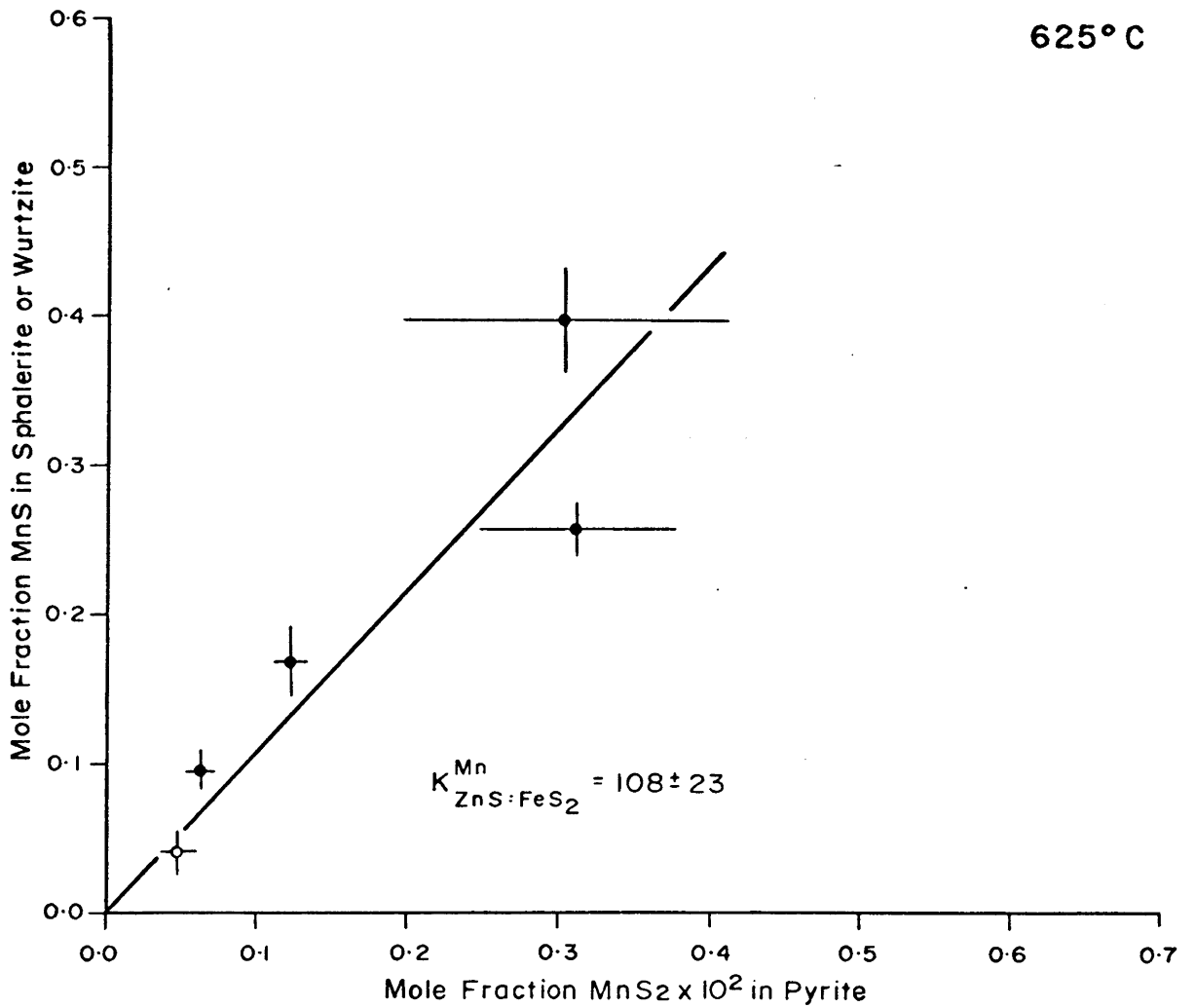
Figure 8: Partitioning of Mn between sphalerite or wurtzite and pyrite at 625°C. o = sphalerite. ● = wurtzite.
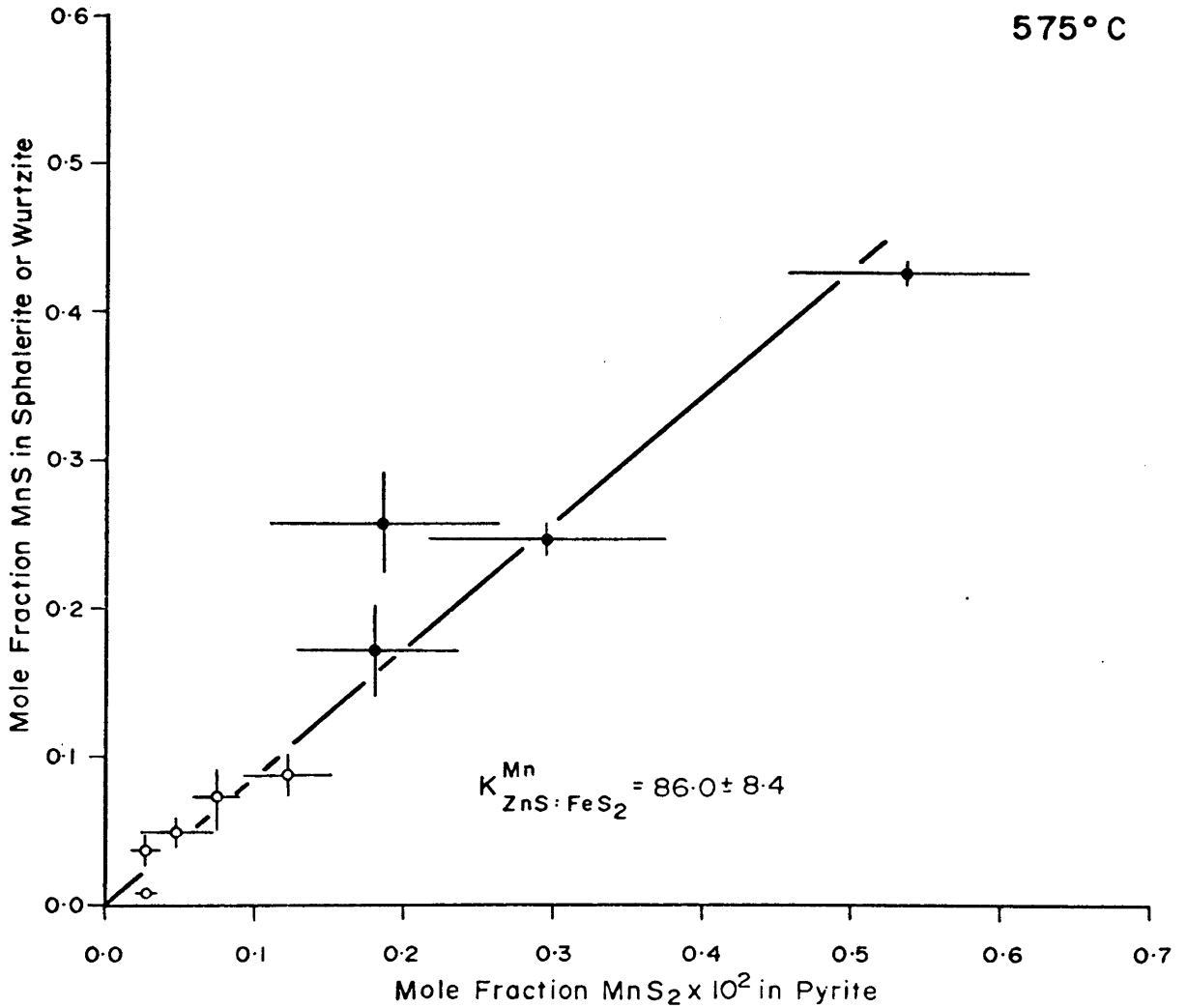
Figure 9: Partitioning of Mn between sphalerite or wurtzite and pyrite at 575°C. o = sphalerite. ● = wurtzite.
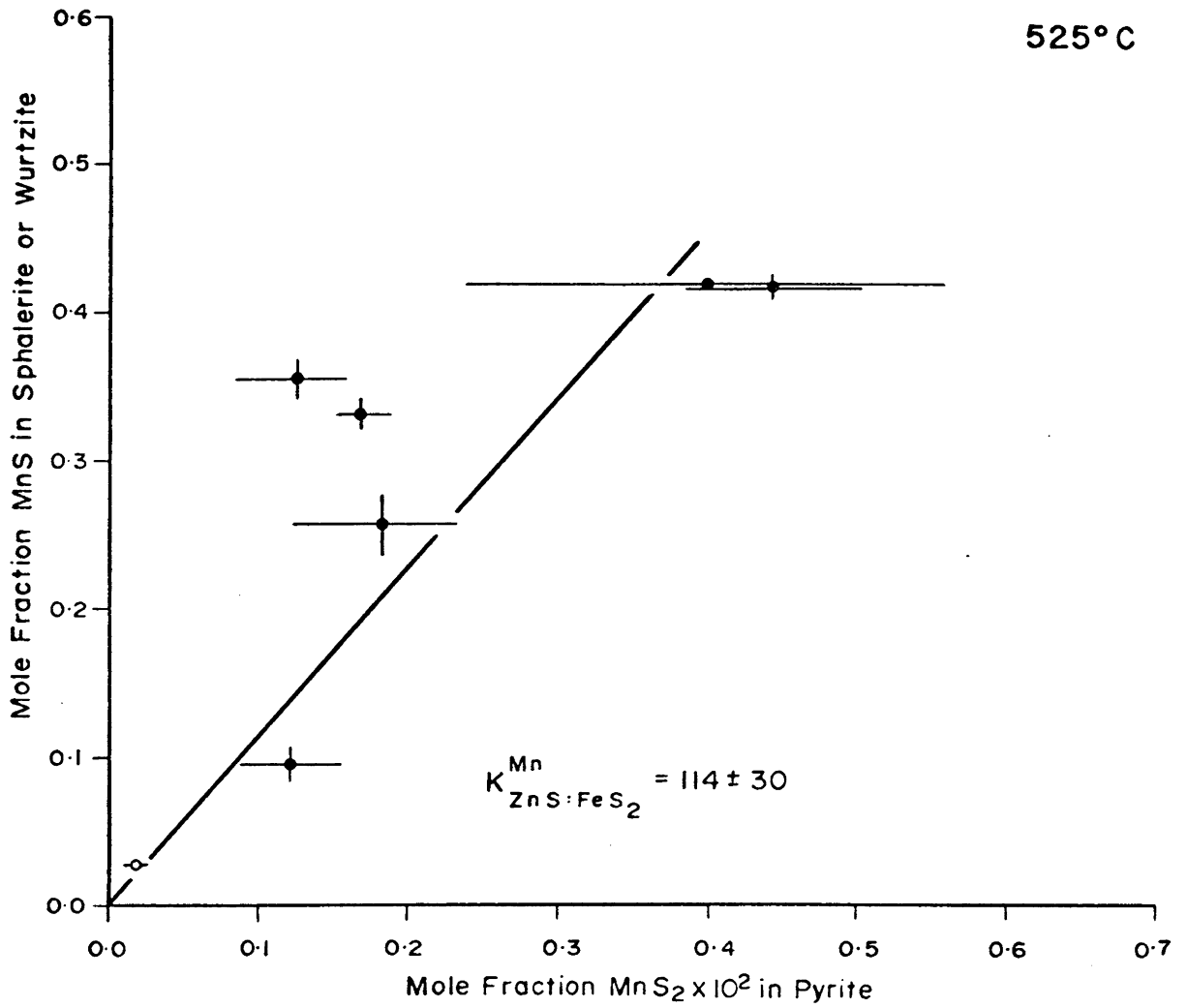
Figure 10: Partitioning of Mn between sphalerite or wurtzite and pyrite at 525°C. o = sphalerite. ● = wurtzite.
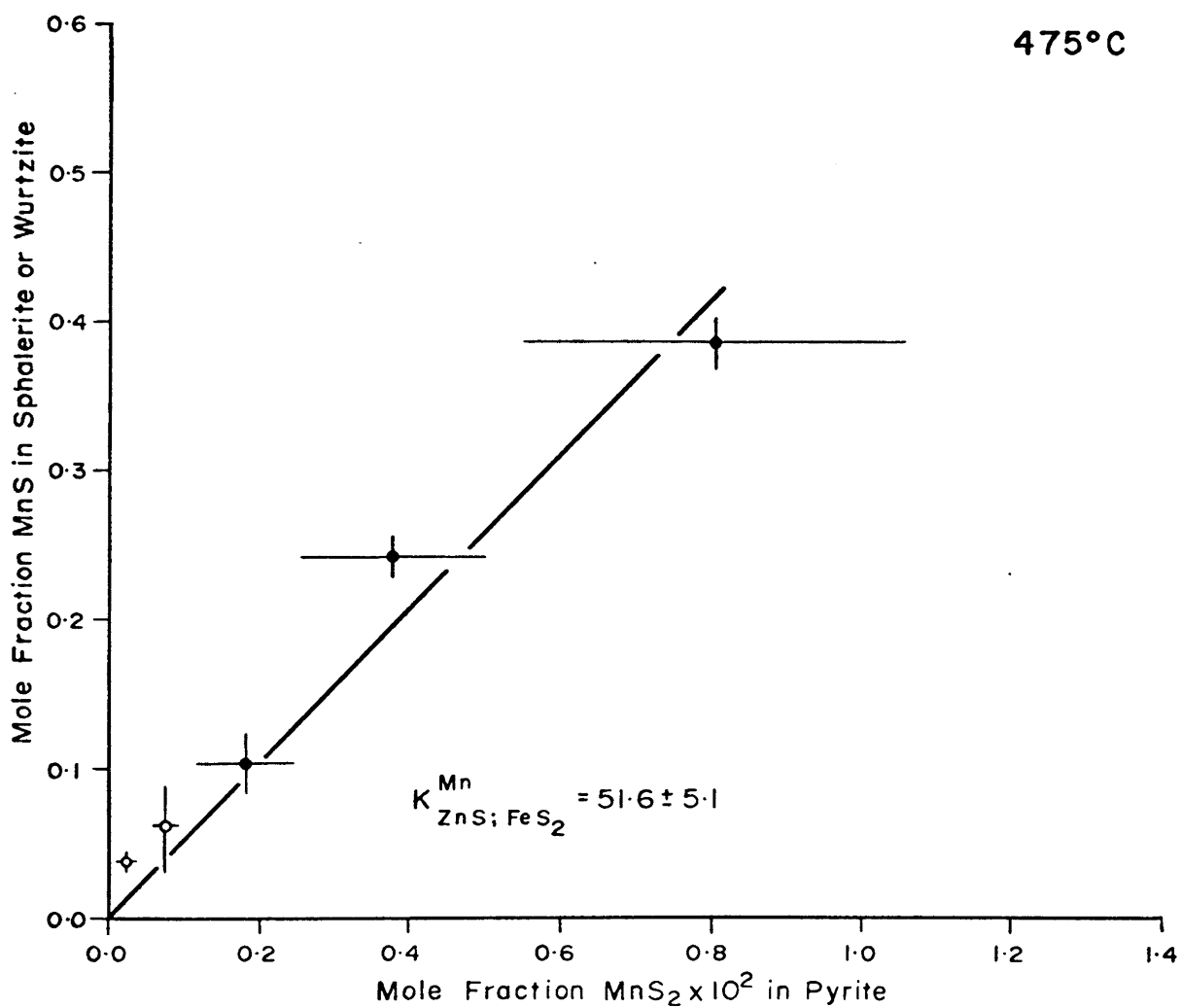
Figure 11: Partitioning of Mn between sphalerite or wurtzite and pyrite at 475°C. o = sphalerite. ● = wurtzite.
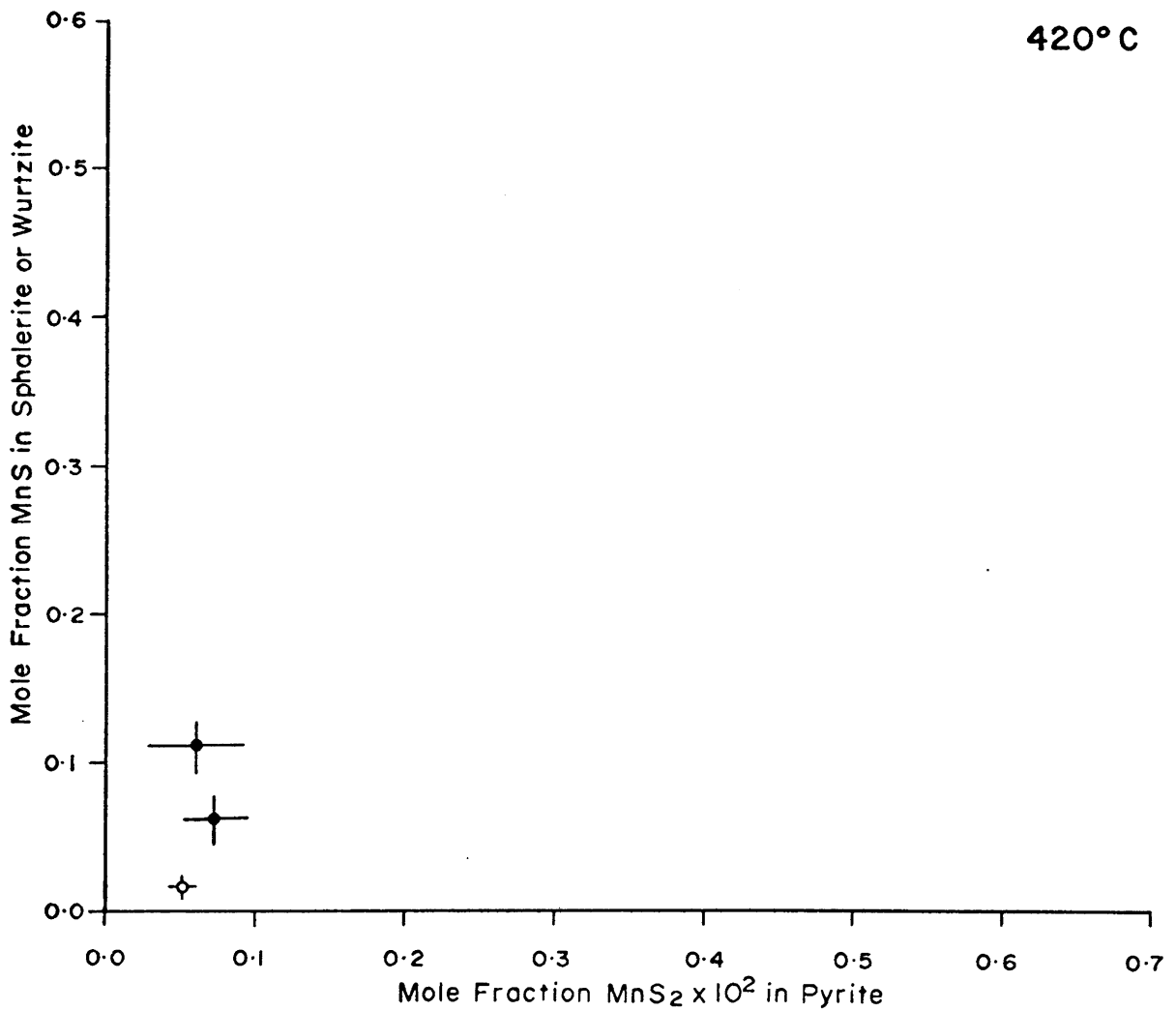
Figure 12: Partitioning of Mn between sphalerite or wurtzite and pyrite at 420°C. o = sphalerite. ● = wurtzite.
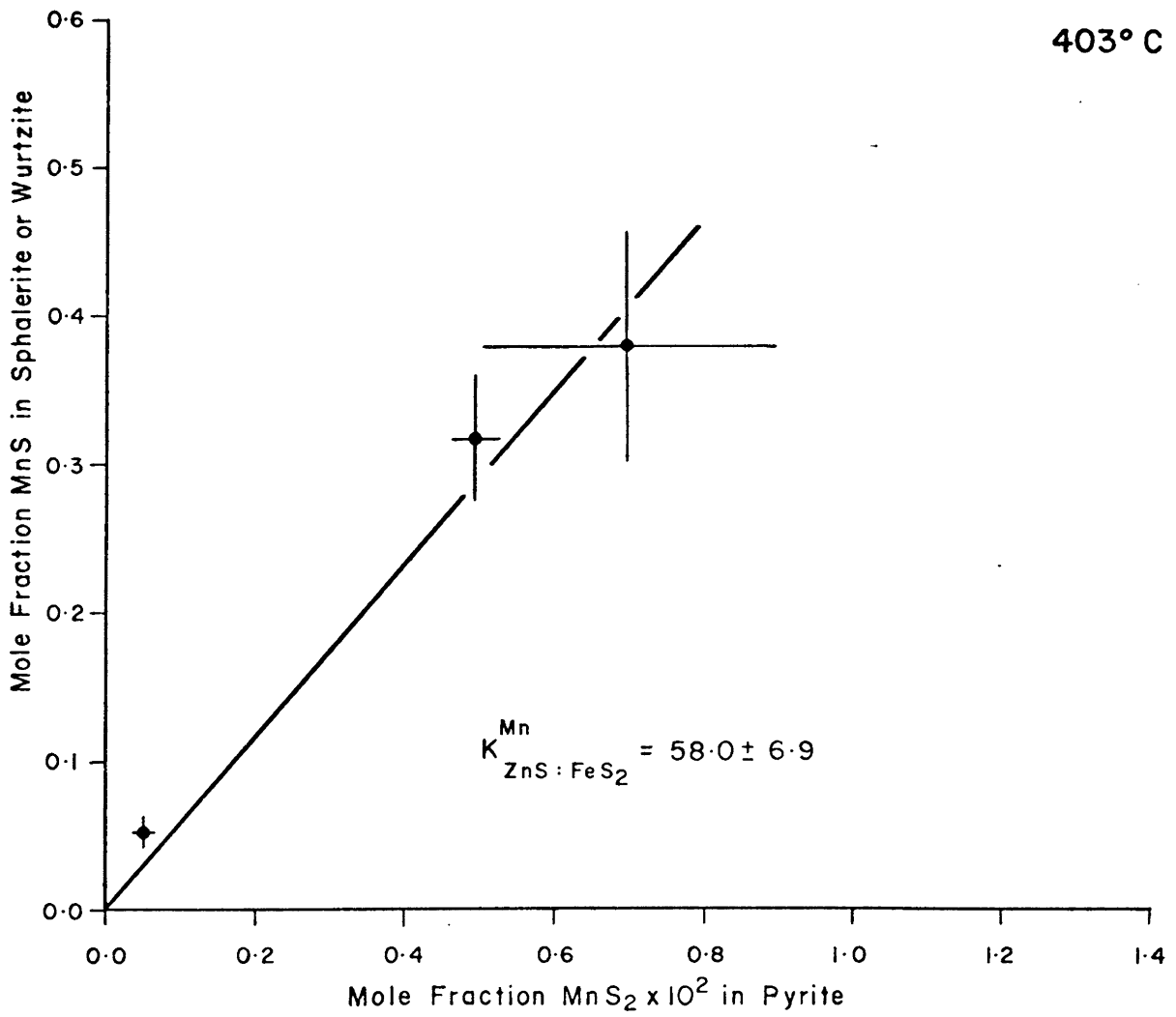
Figure 13: Partitioning of Mn between sphalerite or wurtzite and pyrite at 403°C. o = sphalerite. ● = wurtzite.

and of MnS_2 in pyrite as $\pm 1\sigma$. If no error bar is present about a point, the value of $\pm 1\sigma$ was found to be too small to plot. No diagram has been plotted for runs at 305°C because a reasonable approach to chemical equilibrium was probably not attained in any of the runs at this temperature.

A partition coefficient, $K_{ZnS:FeS_2}^{Mn}$, for each temperature has been estimated by linear regression (Krumbein and Graybill, 1965, p.240; Snedecor and Cochran, 1967, p.166), according to the model:

$$Y = bX + e$$

In this case:

$\quad$ Y = concentration of MnS in sphalerite or wurtzite

$\quad$ X = concentration of MnS_2 in pyrite

$\quad$ b = $K_{ZnS:FeS_2}^{Mn}$

$\quad$ e = a normally distributed random error in Y.

It is assumed in this model that the calculated line passes through the origin of the diagram. The slope of such a line is $K_{ZnS:FeS_2}^{Mn}$ and is an estimate of the mean value of the partition coefficients for all sphalerite - or wurtzite-pyrite pairs at a specific temperature. The calculated values of $K_{ZnS:FeS_2}^{Mn}$ are given on the appropriate distribution diagrams (Figures 7 to 11 and 13) along with the standard deviations of their estimates. No value of $K_{ZnS:FeS_2}^{Mn}$ was calculated for runs at 420°C (Figure 12) since the remaining data points do not represent a sufficiently large range of concentration of Mn.

The statistical fit of the data points in each distribution diagram (Figures 7 to 11 and 13) to a straight line passing through the origin was tested by calculating a linear correlation coefficient, r, according to a method described by Krumbein and Graybill (1965, p.240). At each temperature considered, the value of r was found to be significantly different from zero at the 95% confidence level, indicating that there is a statistically significant linear relationship between MnS in sphalerite or wurtzite and MnS_2 in pyrite and that the calculation of $K^{Mn}_{ZnS:FeS_2}$ is justified since Henry's Law is at least approximated in both phases over the range of concentrations considered.

Wurtzite is apparently stabilized relative to sphalerite by concentrations of MnS between 5 and 10 mole percent and there is very little variation with temperature of the amount of MnS required to stabilize wurtzite. This is in agreement with the work of Bethke and Barton (1971, p.149). The change from sphalerite to wurtzite is probably transitional in character due to : (1) within - run variation in the concentration of MnS in ZnS; and (2) the possible presence of polytypes which cannot be identified except by single-crystal X-ray diffraction methods. These effects may have led to the misclassification of some runs as either sphalerite or wurtzite runs.

No distinction has been made in the calculation of $K^{Mn}_{ZnS:FeS_2}$ between sphalerite-pyrite and wurtzite-pyrite pairs since there is no clustering of the sphalerite-pyrite as opposed to the wurtzite-pyrite data points in the distribution diagrams. A clustering of

this sort would mean that different straight lines could be calculated for the partitioning of Mn between sphalerite-pyrite and wurtzite-pyrite, and as a consequence, different partition coefficients ($K^{Mn}_{Sp:Py}$ and $K^{Mn}_{Wz:Py}$) would be calculated at each temperature. Bethke and Barton (1971) describe an effect similar to this for the partitioning of Cd and Mn between sphalerite-galena and wurtzite-galena. They concluded that the character of the polymorph of ZnS significantly affects partitioning behaviour, and that polytypism in natural sphalerites would significantly affect temperature estimates. This phenomenon has not been demonstrated here.

Variation Of $K^{Mn}_{ZnS:FeS_2}$ With Temperature :

A plot of log $K^{Mn}_{ZnS:FeS_2}$ versus $10^3/T(^{\circ}K)$ is given in Figure 35 in terms of mole percent. The error ($\pm 1\sigma$) in determining $K^{Mn}_{ZnS:FeS_2}$ at each of the six temperatures is shown as an error bar.

Two things are immediately apparent. The partition coefficients are in the order of 10^2, denoting a strong selective uptake of Mn in sphalerite or wurtzite relative to pyrite. Secondly, there is a slight but distinct increase of the partition coefficient with temperature. The statistical significance of the variation of log $K^{Mn}_{ZnS:FeS_2}$ versus $10^3/T(^{\circ}K)$ has been tested by linear regression. The linear equation representing the variation among these data is:

$$\log K^{Mn}_{ZnS:FeS_2} = 2.828 - \frac{735.1}{T(^{\circ}K)} \text{ (mole \%)}.$$

The corresponding linear correlation coefficient is -0.773, a value which is significant at the 90% confidence level and which

indicates a significant linear relationship between $\log K_{ZnS:FeS_2}^{Mn}$ and $10^3/T$.

Using the $\log K_{ZnS:FeS_2}^{Mn}$ versus $10^3/T$ line plotted in Figure 35 for the determination of the temperature of formation of a natural sphalerite-pyrite assemblage, assuming an analytical error of $\pm$ 10% would result in an error of $\pm$ 50°C at 500°C in the temperature estimate. This is a rather large error and it is a reflection of the low slope of the line. In addition, at expected concentrations of Mn in natural sphalerites (1000 to 2000 ppm), the concentration of Mn in coexisting pyrite would be about 10 to 20 ppm, a concentration too low for measurement with an electron microprobe. This would necessitate chemical analysis of pyrite by a more sensitive method (e.g. atomic absorption), with the attendant problems of phase separation and sample purity. It is tempting to extrapolate the line to temperatures outside the experimental range. However, there is no basis for assuming that $\overline{\Delta H}$ (partial molar enthalpy of reaction) and therefore the slope of the line is constant beyond the range of temperatures considered. In summary, these data may be useful for both rough determinations of tempera-ture of formation for natural sphalerite-pyrite assemblages and as a means of detecting and defining conditions of chemical equilibrium in such assemblages.

Interaction Of MnS and FeS In Sphalerite Or Wurtzite:

One of the major assumptions in partitioning theory is
that changes in composition of either of the phases involved does
not influence the partitioning of the element common to both
phases. FeS is a very common constituent of both sphalerite and
wurtzite and its concentration ranges up to about 60 mole percent.
It is reasonable to assume that there may be an interaction of
MnS and FeS in sphalerite or wurtzite. This is a particularly   -
important consideration in view of the strong influence of total
pressure on the FeS content of sphalerite (Scott and Barnes, 1972).
An interaction of this type would almost certainly cause the partition
coefficient for Mn to be sensitive to changes in total pressure.

To test for interaction of MnS and FeS in sphalerite or
wurtzite, mole percent FeS has been plotted against mole percent
MnS for sphalerites and wurtzites for each point analyzed in all of
the runs at each of the eight temperatures (Figures 14 to 21). A
correlation coefficient (Snedecor and Cochran, 1967, chapter 13)
was calculated between MnS and FeS for all sphalerite and wurtzite
analyses at each temperature. In no case were the correlation coeffi-
cients found to be significant at the 95% level of confidence.
No interaction of FeS and MnS is evident at any of the run tempe-
ratures. It should be noted that the amount of FeS in sphalerite
or wurtzite does not vary widely in any of the runs and the apparent
lack of interaction of FeS and MnS can be assumed only within the
range of FeS concentrations in this study.

Figure 14: Interaction of MnS and FeS in sphalerite or wurtzite at 675°C.
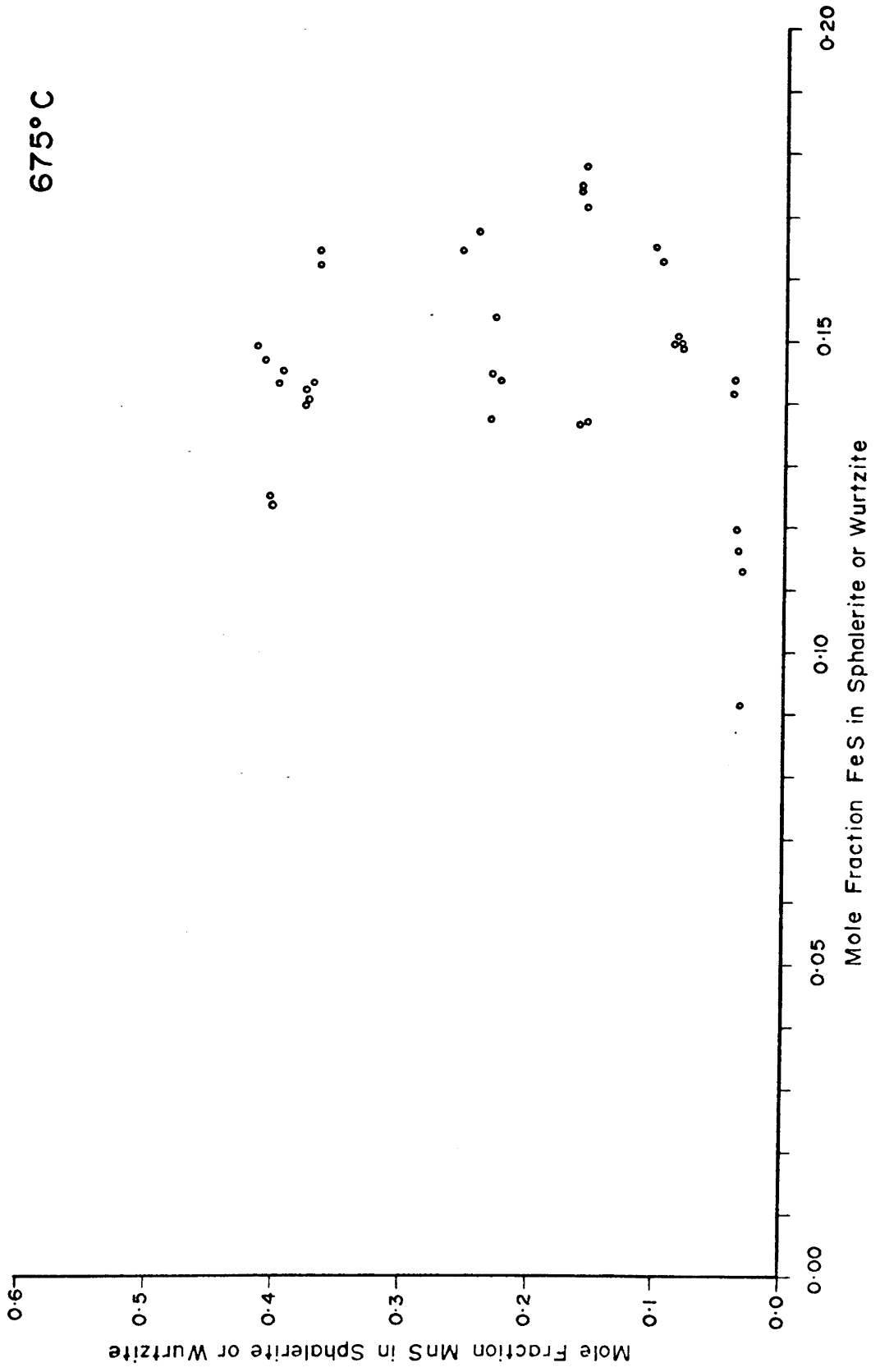
Figure 15: Interaction of MnS and FeS in sphalerite or wurtzite at 625°C.
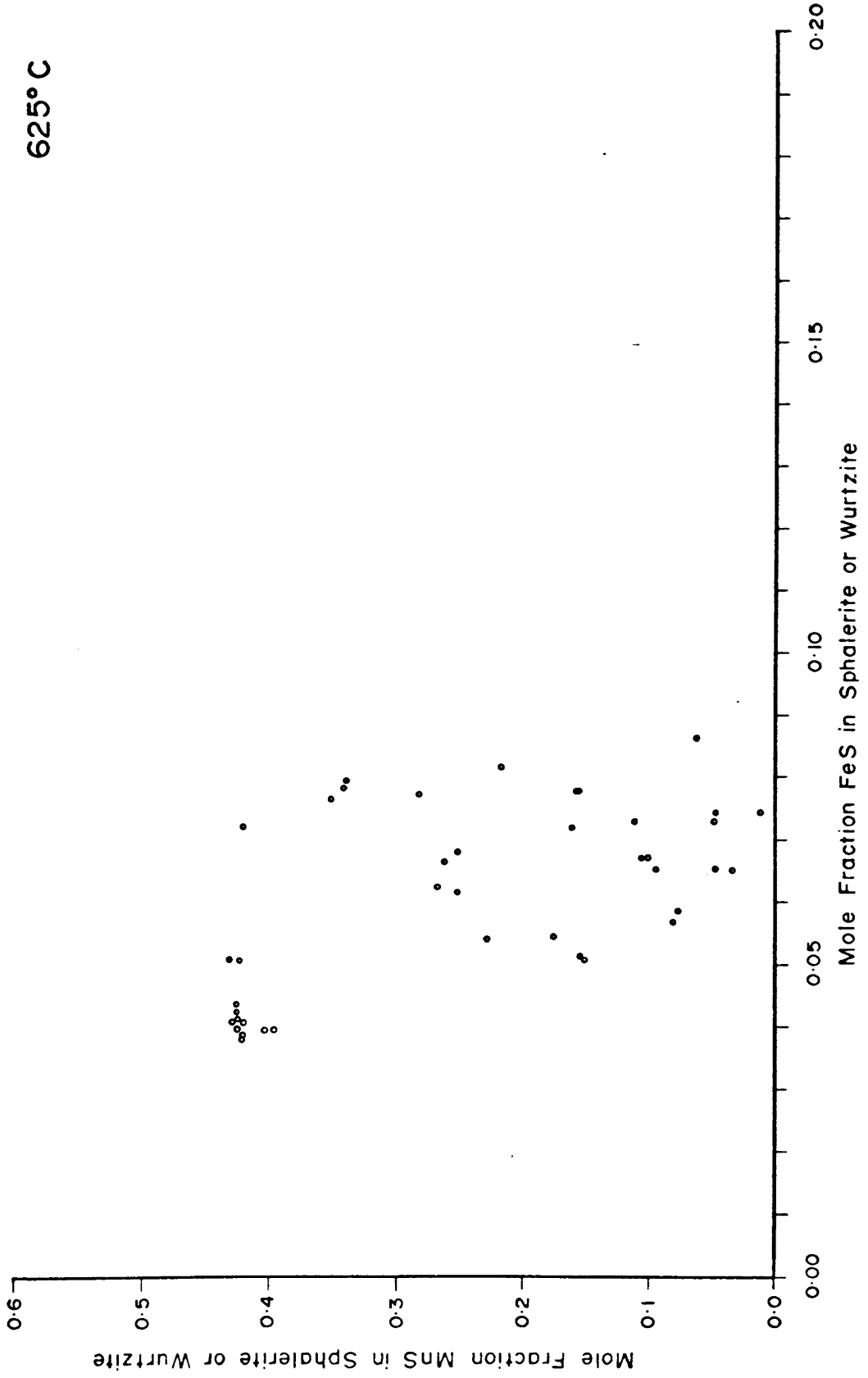
Figure 16: Interaction of MnS and FeS in sphalerite or wurtzite at 575°C.
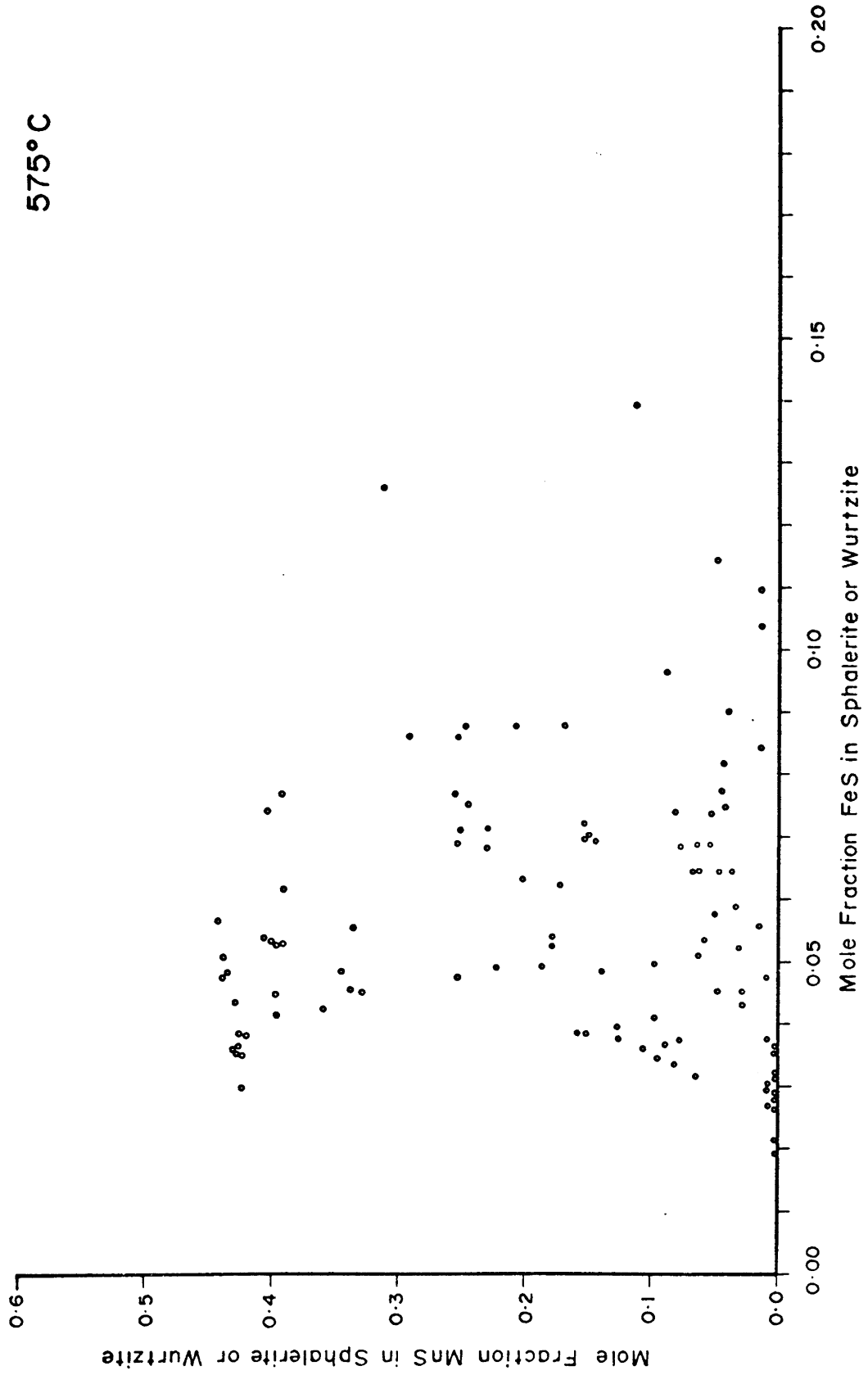
Figure 17: Interaction of MnS and FeS in sphalerite or wurtzite at 525°C.
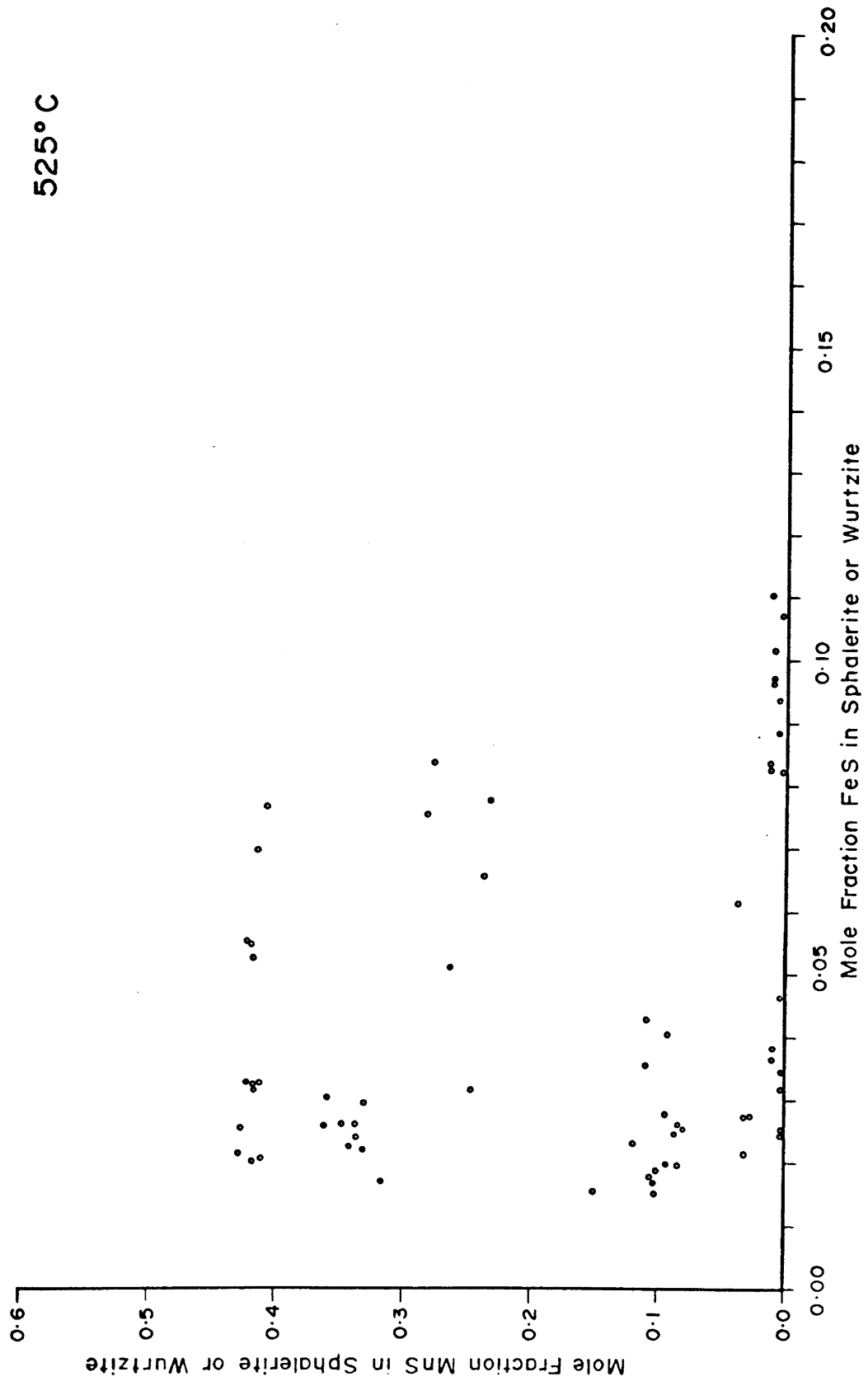
Figure 18: Interaction of MnS and FeS in sphalerite or wurtzite at 475°C.
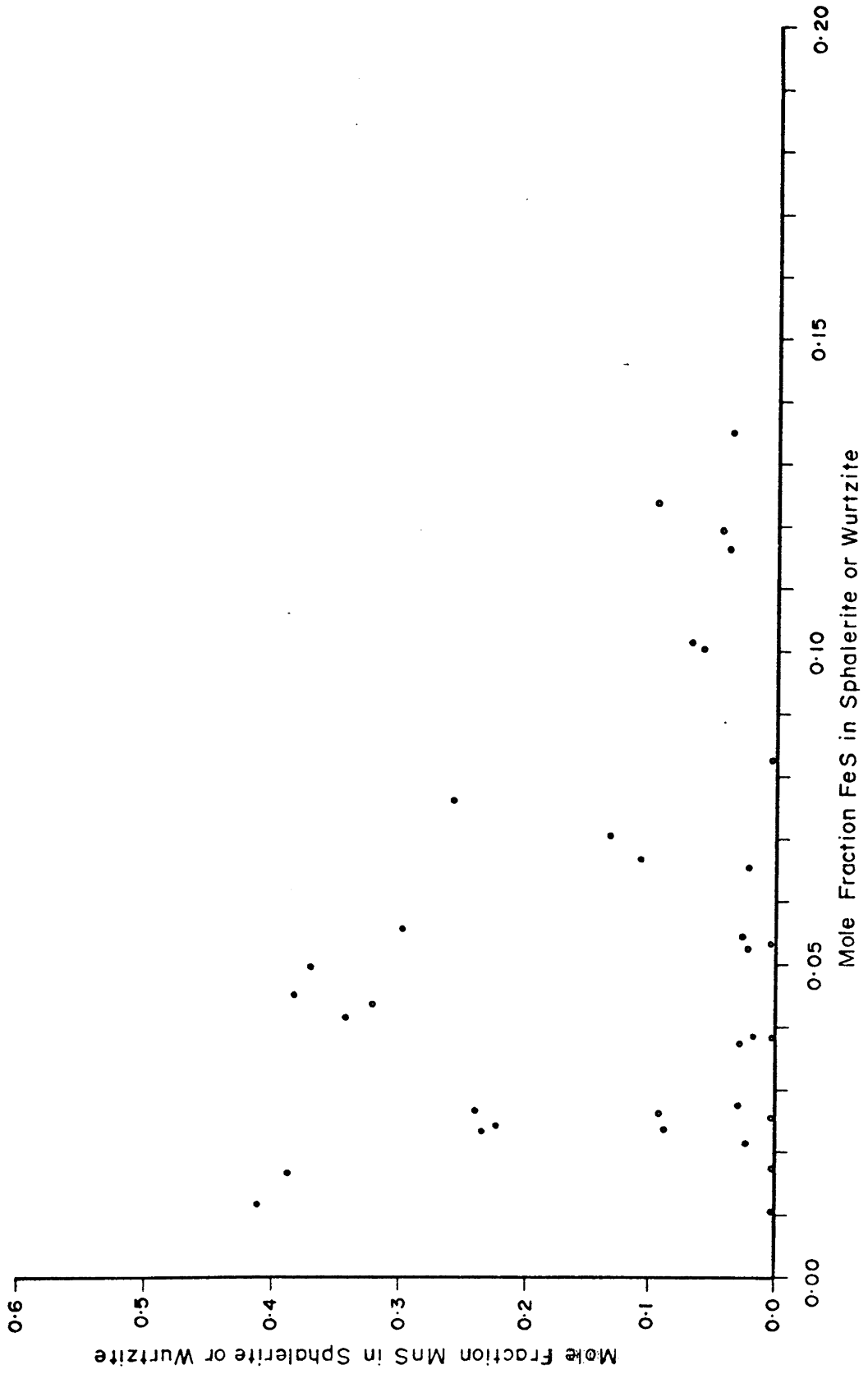
Figure 19: Interaction of MnS and FeS in sphalerite or wurtzite at 420°C.

71
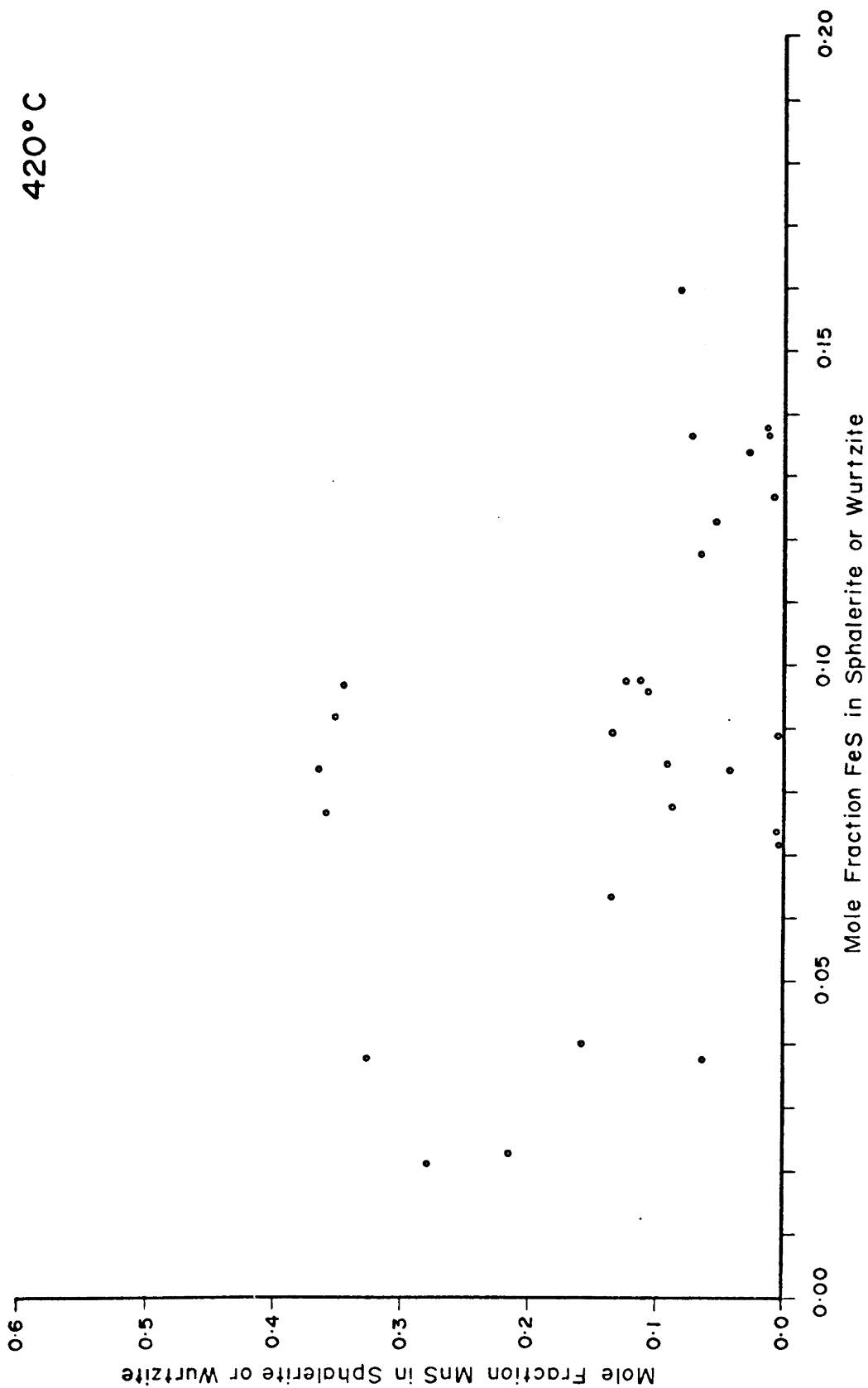
Figure 20: Interaction of MnS and FeS in sphalerite or wurtzite at 403°C.

72
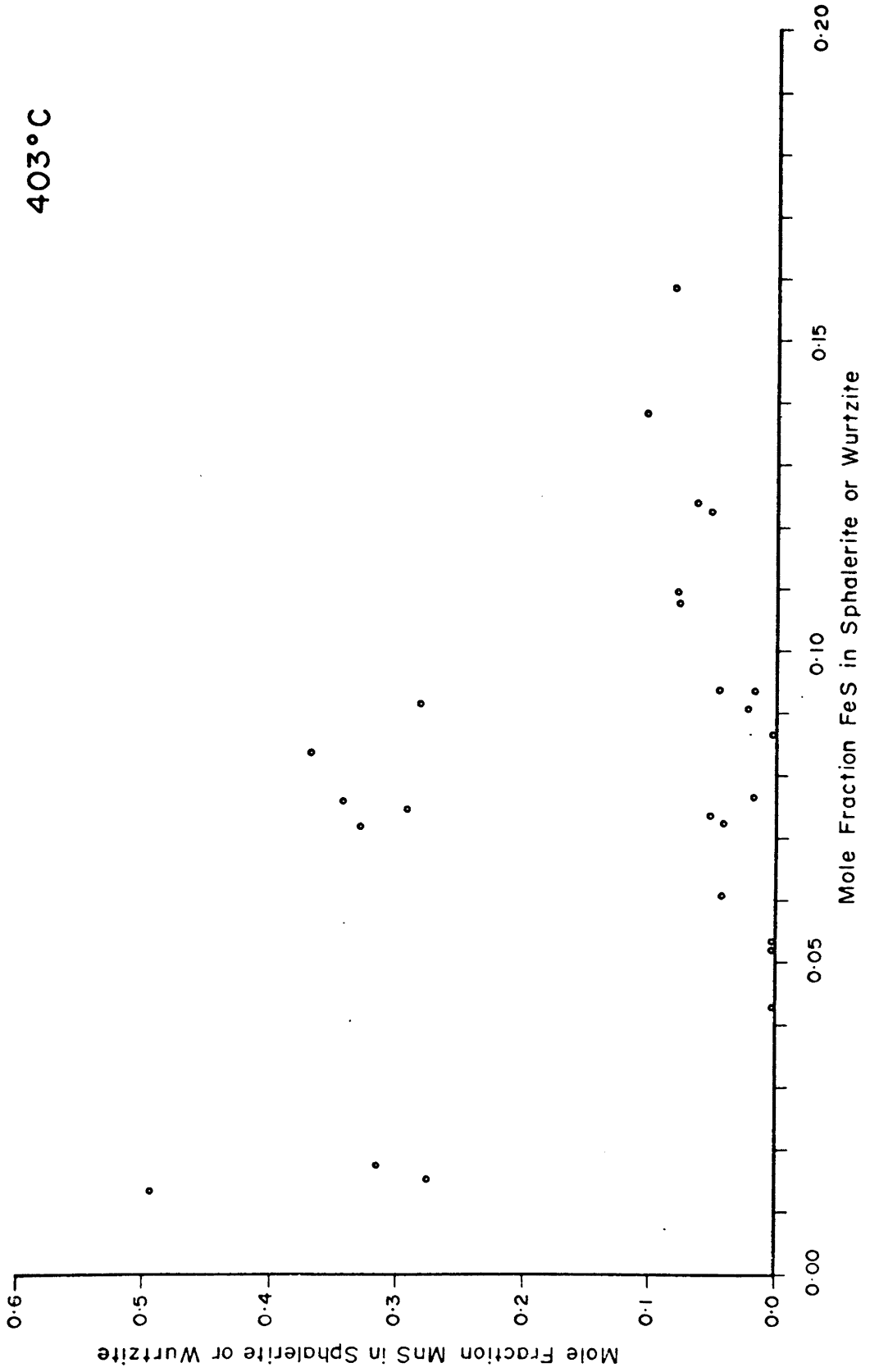
Figure 21: Interaction of MnS and FeS in sphalerite or wurtzite at 305°C.
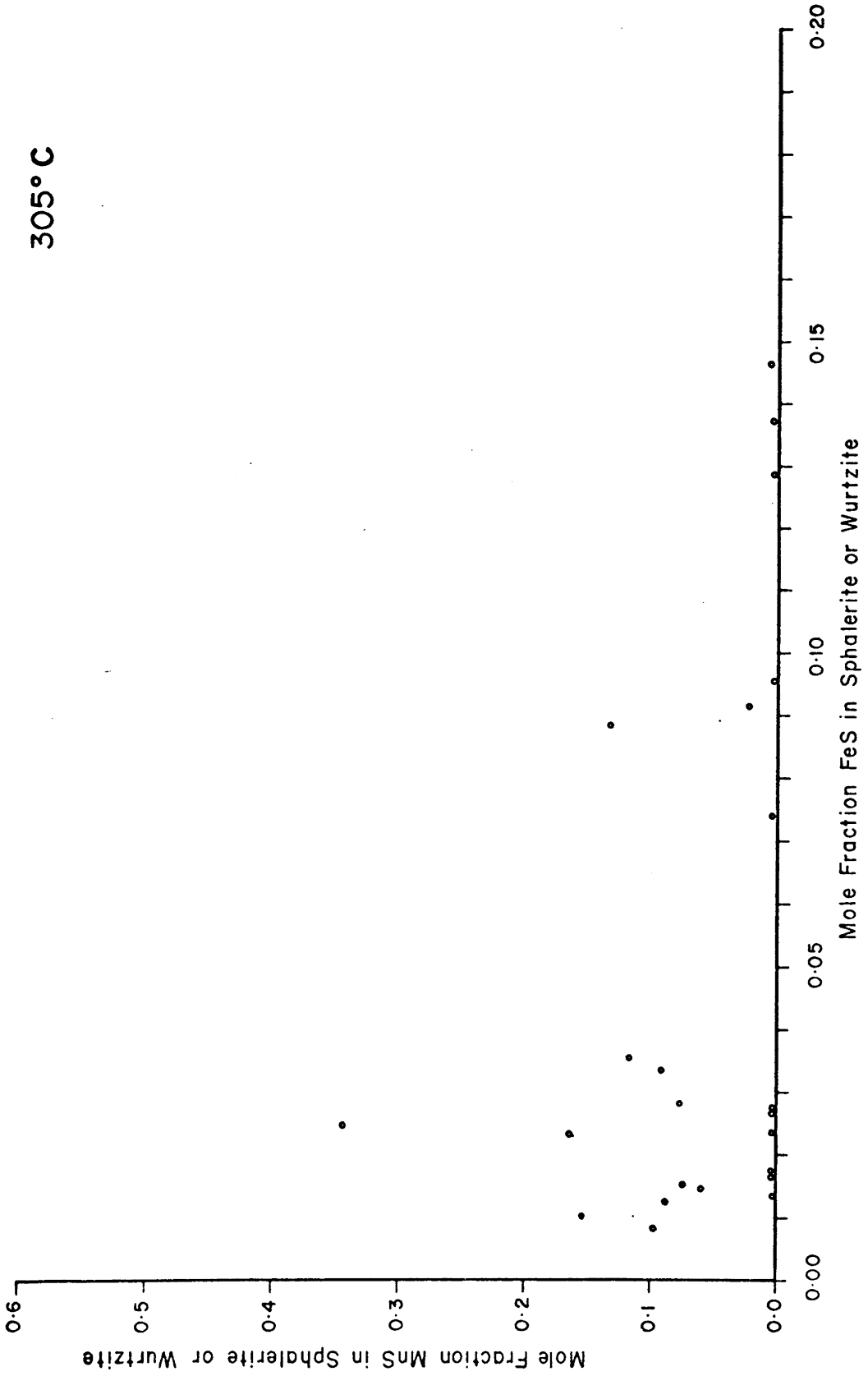
Variation Of FeS In Sphalerite Or Wurtzite:

Figure 22 shows the variation of FeS in sphalerite or wurtzite with temperature. The error bars at each point on this diagram represent twice the pooled standard deviation of FeS for all runs at each temperature. FeS in the sphalerite or wurtzite of these runs was derived from the breakdown of FeS_2, according to a reaction of the type:

$$2\,FeS_{2,ss} = 2\,FeS_{ss} + S_2$$
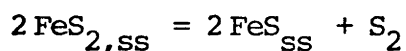
The concentration of FeS in sphalerite or wurtzite was controlled by the amount of sulphur that could be released during reaction in the closed and originally evacuated reaction tubes. For all runs, only a ZnS phase, a FeS_2 phase and sulphur vapour were present, at temperature, in addition to the molten fused salt. The concentration of FeS, at each temperature, was controlled by: (1) the amount of vapour space available in the reaction tubes relative to the size of the sulphide charge; and (2) the solubility of sulphur in the molten fused salt. The ratio of (ZnS + MnS) / FeS_2 in the sulphide charge was maintained constant at 1:1 throughout the runs.

The relatively narrow compositional range for FeS in sphalerite or wurtzite at temperatures at and below 625°C (Figure 22) is the result of uniform experimental conditions. Variations of FeS, at any one temperature, are caused by random weighing errors and changes in the vapour space relative to the sulphide charge,
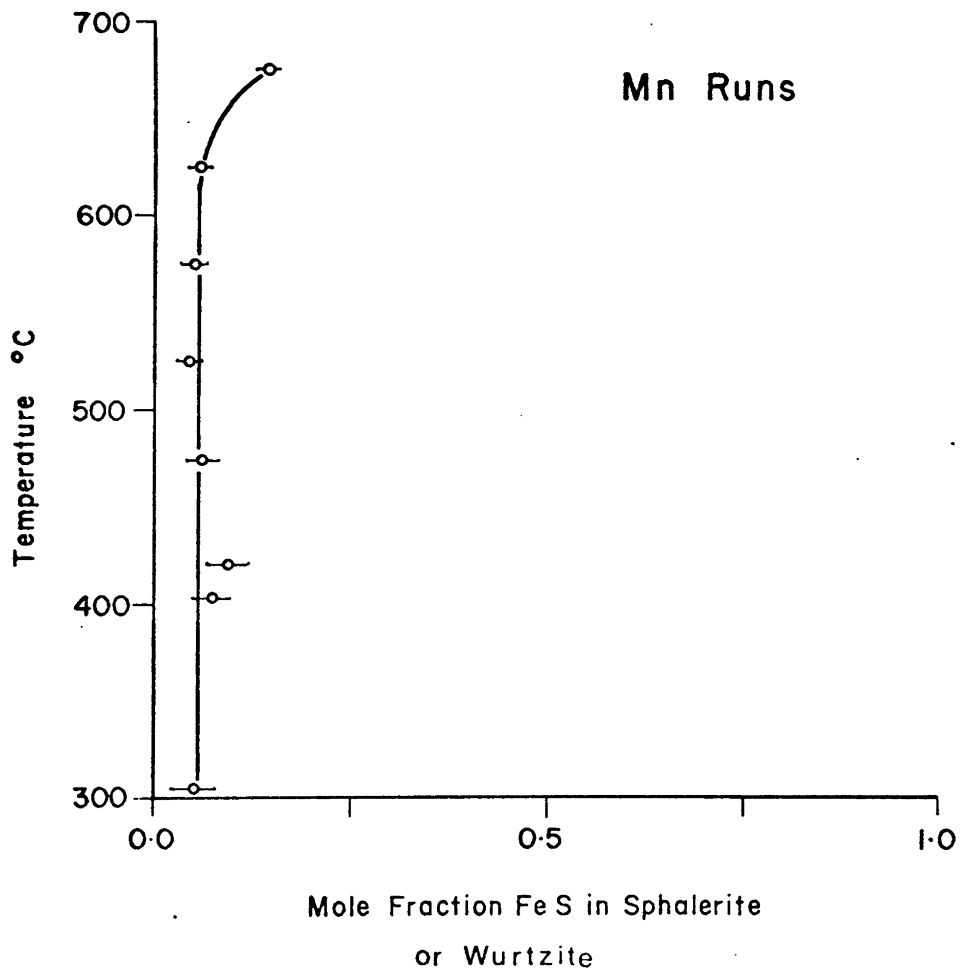
Figure 22: Variation of FeS in MnS-bearing sphalerite or wurtzite with temperature.

in addition to analytical errors. To illustrate this point, the FeS concentration in the wurtzites of runs 26 (2.6 mole % FeS) and 103 (6.4 mole % FeS) may be compared (Appendix I). The runs were carried out under almost identical conditions, except that the vapour space relative to the size of the sulphide charge was approximately double in run 103. The increase of FeS to about 16 mole percent in runs at 675°C (Figure 22) was caused by the use of a much smaller sulphide charge and a much larger vapour space than in runs at other temperatures.

For runs in which MnS in sphalerite or wurtzite is hetero-geneous, FeS tends to be homogeneous (Appendix I). This may mean that FeS equilibrates more rapidly than MnS. This observation can be compared with the work of Doe (1962) on sphalerite-pyrite assemblages from No. 2 Mine of the Balmat area, New York. Doe found that the ratio of Mn (mole %) in sphalerite relative to pyrite varies from 3 to 1100. FeS (mole %) in sphalerite, in the same suite of samples ranges from 8.1 to 13.6. Doe concluded that Mn had not equilibrated between sphalerite and pyrite, but that Fe had equilibrated.

Partitioning Of Co Between Sphalerite And Pyrite

The analytical data for all sphalerite-pyrite pairs containing Co are listed in Appendices III and IV, in terms of mole percent and in order of temperature from 675 to 305°C. The concentration of CoS in sphalerite ranges from very low values to

approximately 2.6 mole percent. The FeS content of sphalerite varies from less than 1 to about 14 mole percent. It is relatively uniform in runs at and below 625°C but there is a slight increase of FeS to 14 mole percent at 675°C, similar to that found in the previous system. Only sphalerite, and not wurtzite, was found in the experimental runs. This is in agreement with the results of Hall (1961) who determined that sphalerite is stable at concentrations of CoS up to 33 mole percent at 850°C. The concentration of CoS_2 in pyrite ranges up to 80 mole percent. The concentration of ZnS_2 in pyrite is usually less than 1 mole percent. Its concentration and limited variation in pyrite is not likely to influence the partitioning of Co.

Homogeneity Of Run Products:

The analyses of Co in both sphalerite and pyrite for each run were tested for the occurrence of extreme values by the same statistical method used for runs containing Mn (Dixon and Massey, 1957, p.276). Phases found to be heterogeneous by this method are marked in Appendices III and IV. The results of the corresponding runs were not used in the determination of partition coefficients.

The distribution of Co in sphalerite was found to be uniform by means of electron microprobe scanning images. However, this is not a definitive test because of the low concentration of Co in sphalerite. In the analysis of 24 of the runs, counts were taken on two distinct points within each of the sphalerite crystals. A

one-way analysis of variance of these data indicates that within-crystal variation of both CoS and FeS is much less than the between-crystal variation of those elements at the 99% confidence level. With few exceptions, the runs contain no extreme values for CoS in sphalerite. The sphalerite crystals appear to be quite homogeneous for CoS.

Scanning images of Co-bearing pyrites from runs at 675, 625 and 575°C showed no within-crystal heterogeneity. However, for runs at and below 525°C irregular zonation of pyrite is evident. Moreover, a crystal to crystal variation of Co, considerably more pronounced than the within-crystal zoning (Figure 6, E to H) is present. Inspection of Appendix IV for runs at and below 575°C indicates that there is wide variation of CoS_2 content among pyrite crystals in any one run.

Klemm (1965) reported a solubility gap in the CoS_2 - FeS_2 system at temperatures below 700°C. According to Klemm, the gap lies between 55 and 75 mole percent CoS_2 at 600°C, between 33 and 83 mole percent CoS_2 at 500°C, and 7 and 83 mole percent CoS_2 at 400°C. This could explain the heterogeneity of pyrite in these runs, since two varieties of the CoS_2 - FeS_2 solid solution should be present within runs below 600°C. However, CoS_2 compositions lying within Klemm's solubility gap have been found (Appendix IV) at temperatures below 575°C. Assuming Klemm's data to be correct, chemical equilibrium was not attained in the Co bearing runs below 575°C. Even if there is complete solid solution of CoS_2 and FeS_2 at these temperatures, as indicated by the study of natural bravoites (Riley, 1965; 1968),

the same conclusion must be accepted.

The pyrite crystals produced in this temperature range are subhedral to anhedral in character, and are much smaller and more numerous than the corresponding sphalerite crystals. It is possible that the pyrite crystals nucleated rapidly at many centres, preserving and reflecting original inhomogeneities in the sulphide charge. The sphalerite crystals probably grew at a slower rate, maintaining only surface equilibrium with the FeS_2 - CoS_2 fraction of the sulphide charge. The subhedral to anhedral nature of the pyrite crystals may be due to surface etching subsequent to their formation.

Distribution Of Co Between Sphalerite And Pyrite:

Figures 23 to 25 show the distribution of Co between sphalerite and pyrite at three different temperatures from 675 to 575°C. The plots are in terms of mole percent. The error bars about each point in these diagrams represents the variation of CoS in sphalerite and of CoS_2 in pyrite as $\pm$ 1σ. No diagrams have been plotted for runs below 575°C because of the gross disequilibrium evident at these temperatures.

A partition coefficient, $K^{Co}_{FeS_2:ZnS}$, has been estimated for runs at 675°C and 625°C by linear regression in the same way as in the case of runs containing Mn (Krumbein and Graybill, 1965, p.240; Snedecor and Cochran, 1967, p.166). The calculated values of $K^{Co}_{FeS_2:ZnS}$ for each temperature are given in Figures 23 and 24 along with their appropriate standard deviations of estimate. The
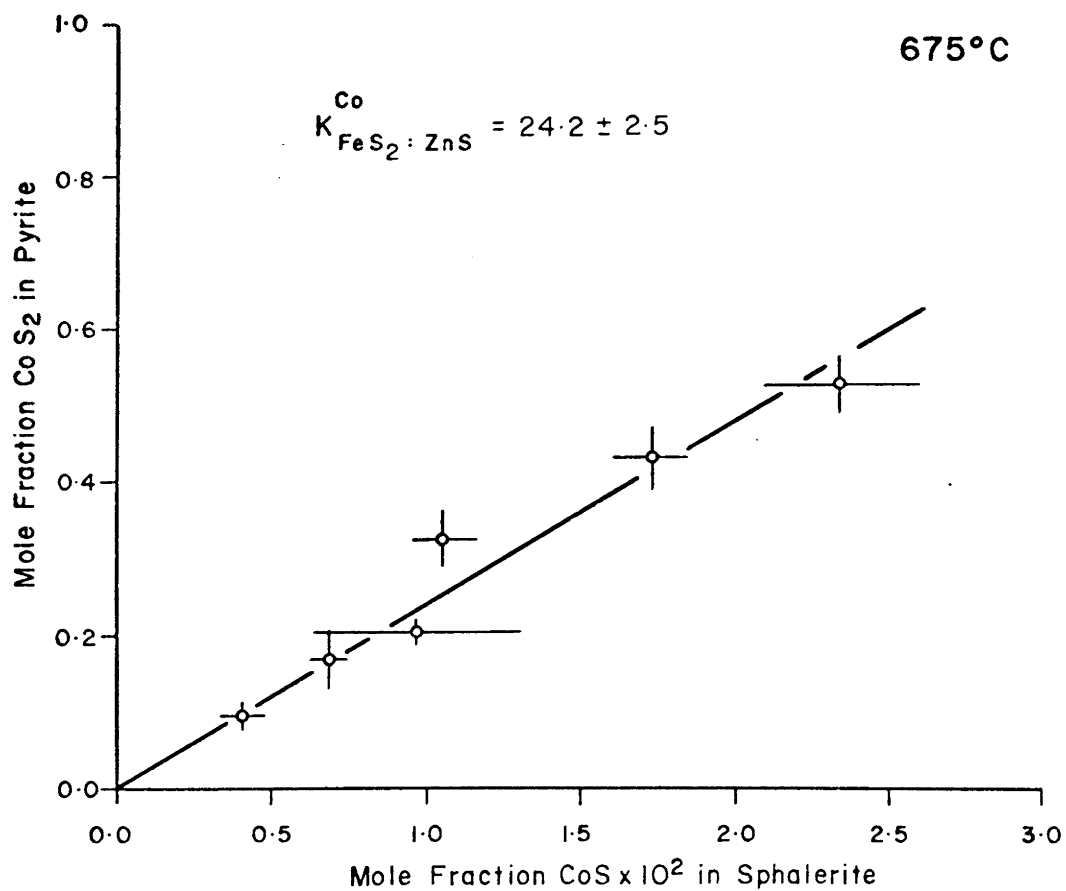
Figure 23: Partitioning of Co between sphalerite and pyrite at 675°C.
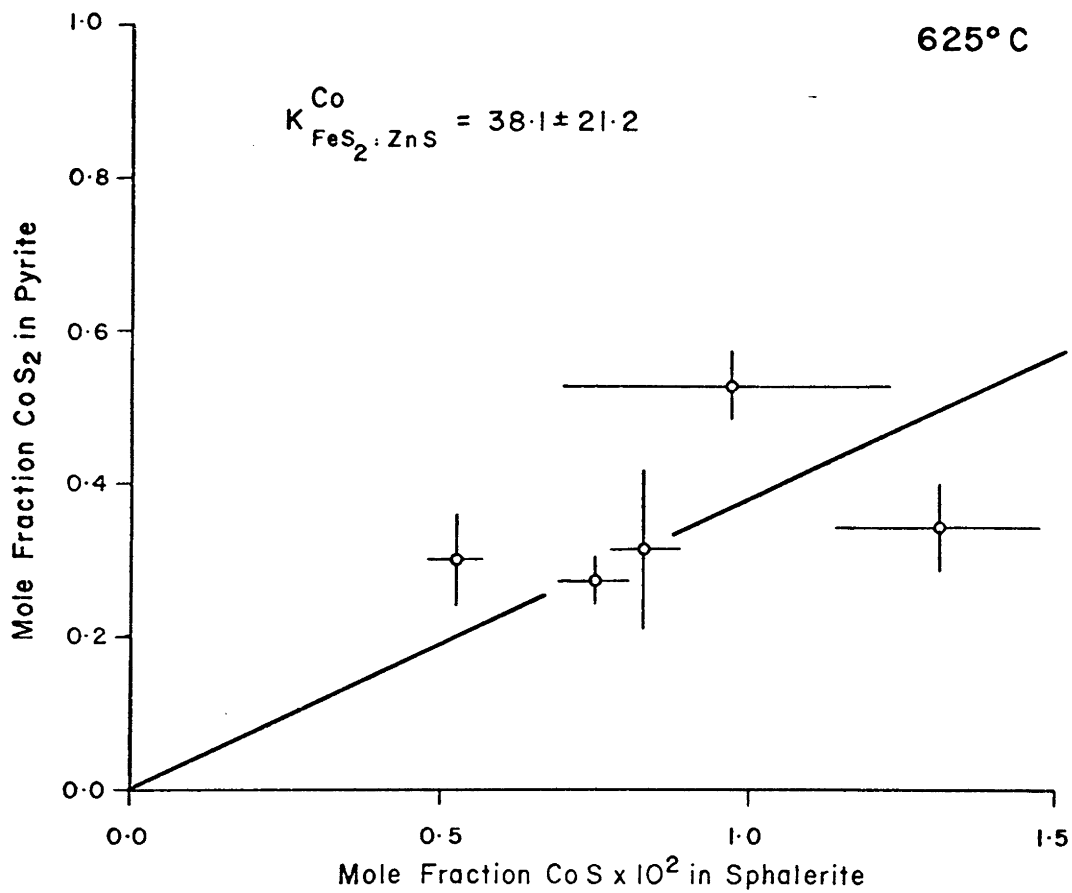
Figure 24: Partitioning of Co between sphalerite and pyrite at 625°C.
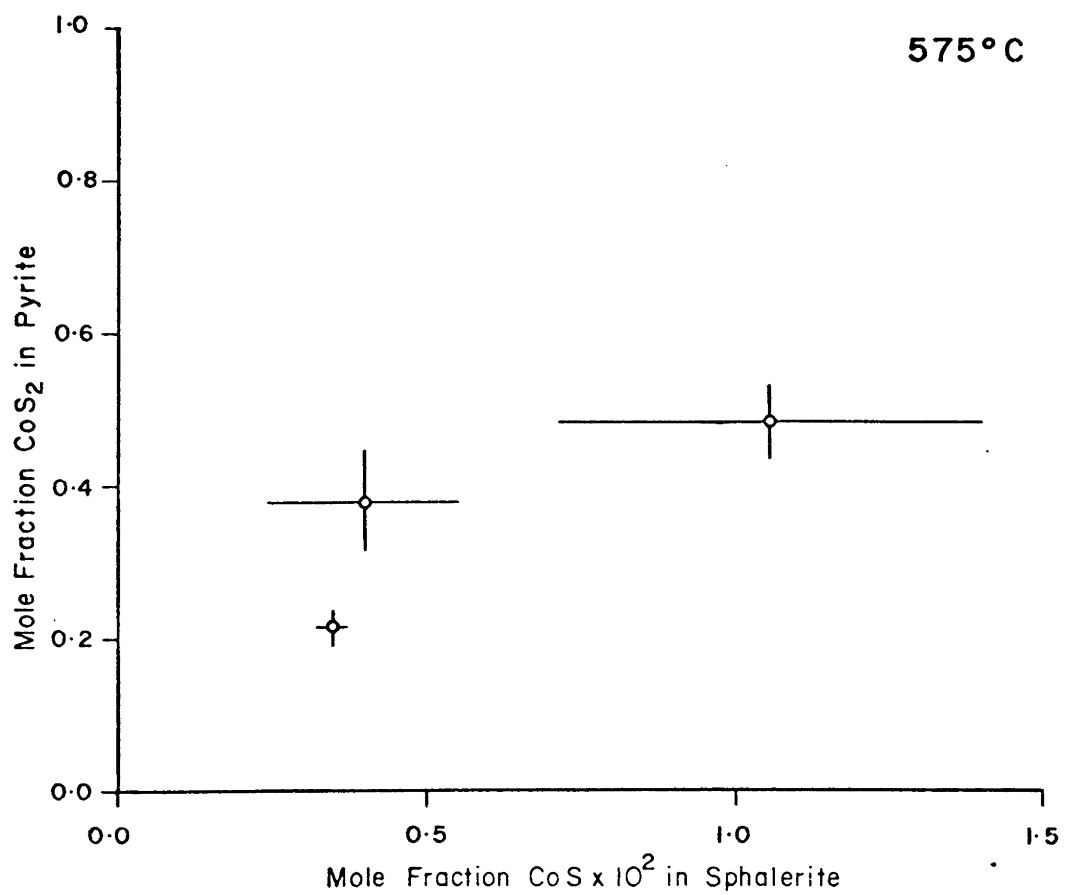
Figure 25: Partitioning of Co between sphalerite and pyrite at 575°C.

statistical fit of the data points in each distribution diagram
(Figures 23 to 25) to a straight line passing through the origin
was tested by calculating a linear correlation coefficient (Krumbein
and Graybill, 1965, p.240) for each temperature. For temperatures
of 675 and 625°C, the correlation coefficient was found to be
significantly different from zero at the 95% confidence level,
indicating that the calculation of $K^{Co}_{FeS_2:ZnS}$ is justified at those
temperatures. For runs at 575°C, a statistically significant linear
relationship does not exist between CoS in sphalerite and CoS_2 in
pyrite and a value of $K^{Co}_{FeS_2:ZnS}$ has not been calculated. Henry's
Law has been approximated in both phases only in runs at 675 and
625°C over the range of concentrations considered.

Variation Of $K^{Co}_{FeS_2:ZnS}$ With Temperature:

Two values of log $K^{Co}_{FeS_2:ZnS}$ versus $10^3/T(°K)$ are shown in
Figure 35 in terms of mole percent. The error ($\pm$ 1σ) in determining
$K^{Co}_{FeS_2:ZnS}$ at each temperature is shown as an error bar.

The value of $K^{Co}_{FeS_2:ZnS}$ at 675 and 625°C are, respectively,
24.2 $\pm$ 2.5 and 38.1 $\pm$ 21.2. There is a strong selective uptake
of Co in pyrite relative to sphalerite. Nothing definitive can be
said about the variation of log $K^{Co}_{FeS_2:ZnS}$ with $10^3/T(°K)$ since only
two valid data points exist. There could be a rapid increase of
the concentration of Co in sphalerite relative to pyrite with
increasing temperature, but this has not been firmly established.

Interaction Of CoS and FeS In Sphalerite:

Variations of FeS in sphalerite may affect the partitioning of Co between sphalerite and pyrite. Mole percent CoS in sphalerite has been plotted against mole percent FeS in sphalerite, for each point analyzed in all of the runs at each of the eight temperatures (Figures 26 to 33). A linear correlation coefficient (Snedecor and Cochran, 1967, chapter 13) was calculated between CoS and FeS for all sphalerite analyses at each temperature. Four statistically significant (at the 95% confidence level) interactions between CoS and FeS have been found, namely at 675, 525, 420 and 305°C (Figures 26, 29, 31, and 33). In each case, the corresponding correlation coefficient and the equation of the calculated regression line is given in the appropriate diagram (Figures 26, 29, 31, and 33).

The inverse relationship between CoS and FeS in sphalerite at 675°C (Figure 26) is very similar to the inverse relationship of NiS and FeS in sphalerite formed at 755°C reported by Czamanske and Goff (1973, p.260). They explained the preferential acceptance of Fe^{+2} relative to Ni^{+2} in terms of crystal field theory. Fe^{+2} has a lower octahedral site preference energy than Ni^{+2} and should be more stable in the tetrahedral sites available in sphalerite. Differences in ionic size are apparently of secondary consideration. In a similar way, the preference of sphalerite for Fe^{+2} at the expense of Co^{+2} may be due to the small octahedral site preference energy of Fe^{+2} relative to Co^{+2} (Table 2). No significant inverse

Figure 26: Interaction of CoS and FeS in sphalerite at 675°C.

675° C

Mole Fraction CoS x 10² in Sphalerite

Mole Fraction FeS in Sphalerite

$CoS = 4.876 - 0.3260 \ FeS$ (mole%)

$r = -0.7940$
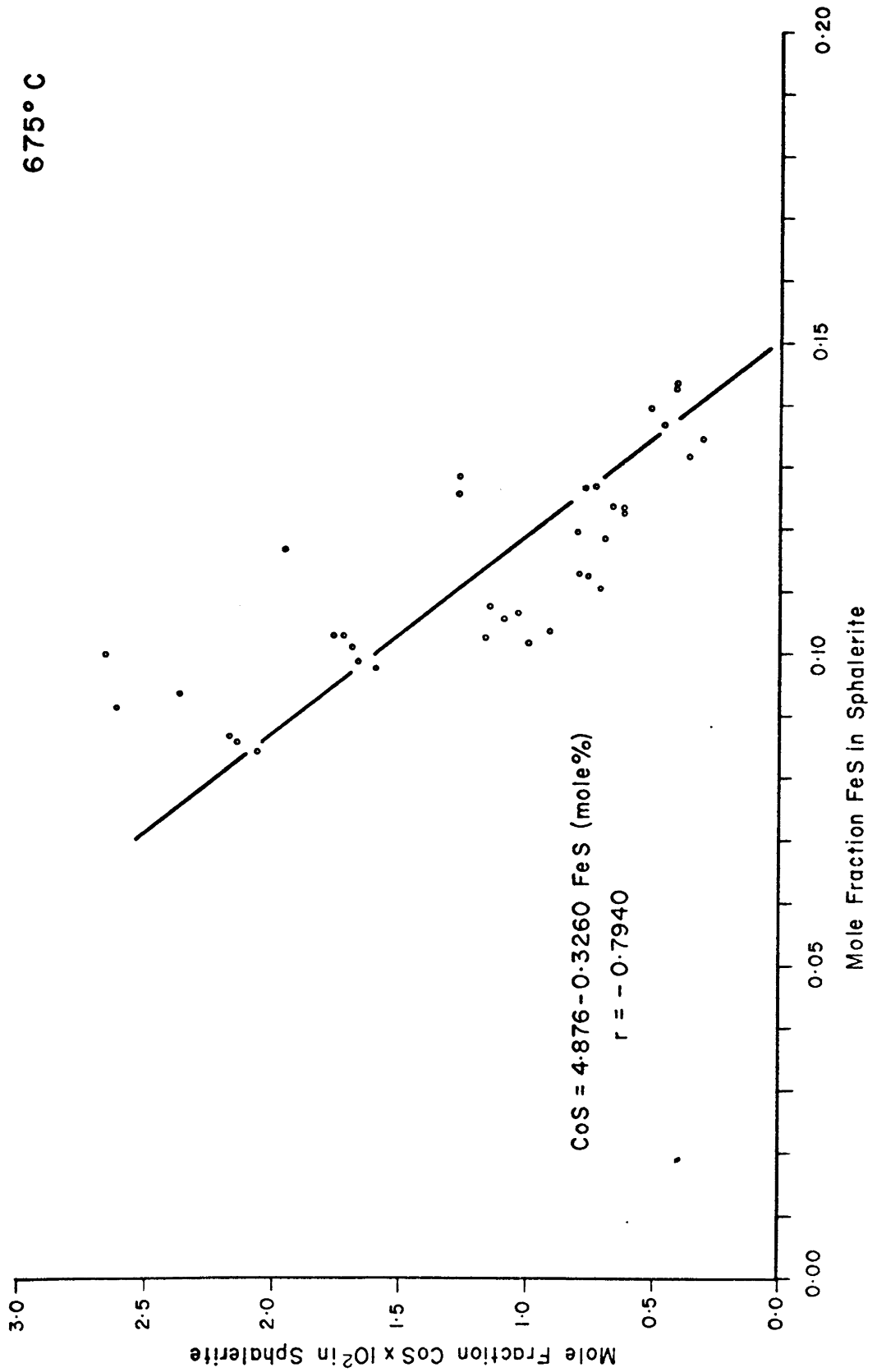
Figure 27: Interaction of CoS and FeS in sphalerite at 625°C.
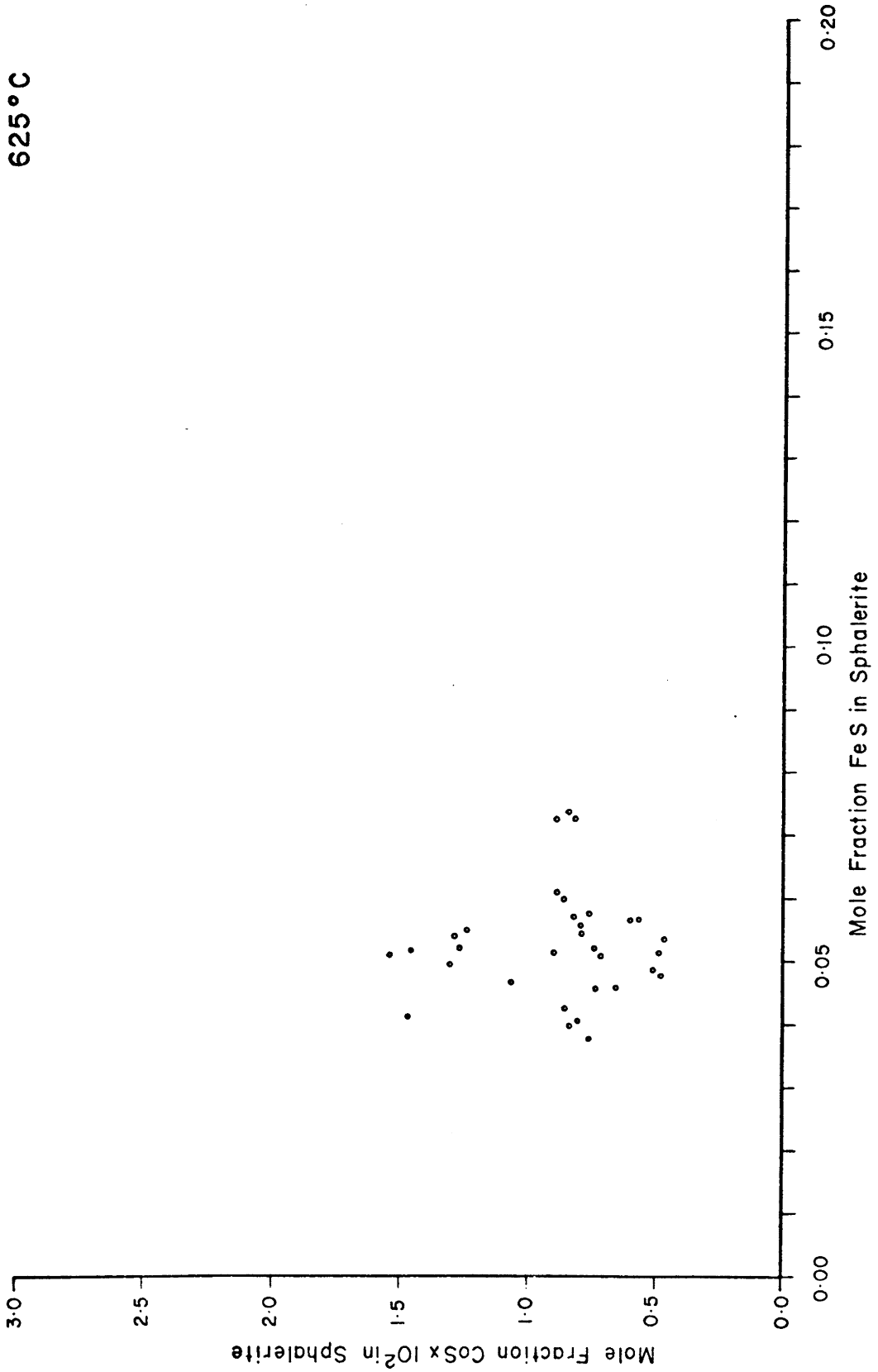
Figure 28: Interaction of CoS and FeS in sphalerite ar 575°C.
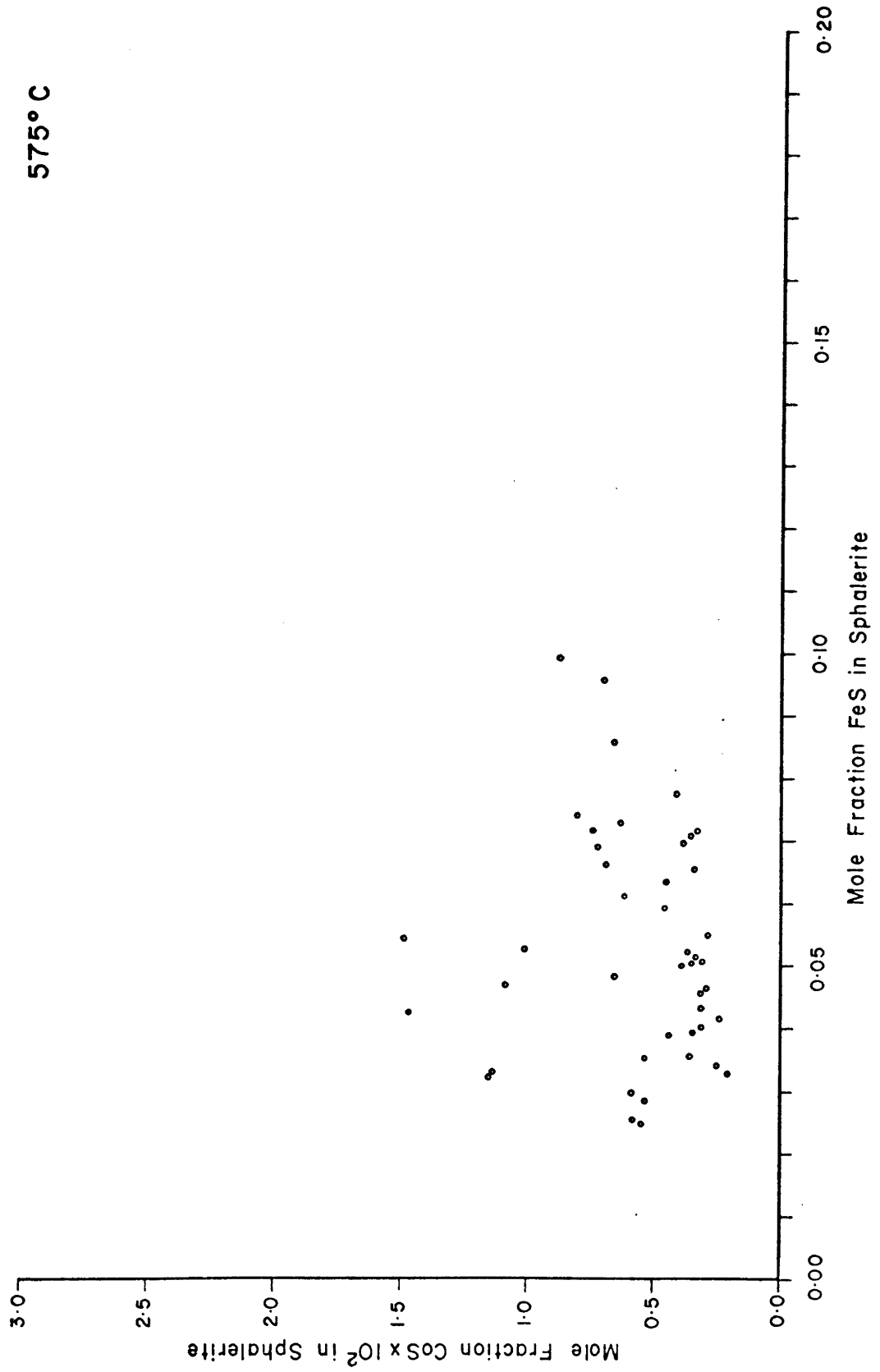
Figure 29: Interaction of CoS and FeS in sphalerite at 525°C.

525° C

$CoS = -0.0306 + 0.2277$ FeS (mole %)

$r = + 0.7190$

Mole Fraction FeS in Sphalerite

Mole Fraction CoS x 10^2 in Sphalerite
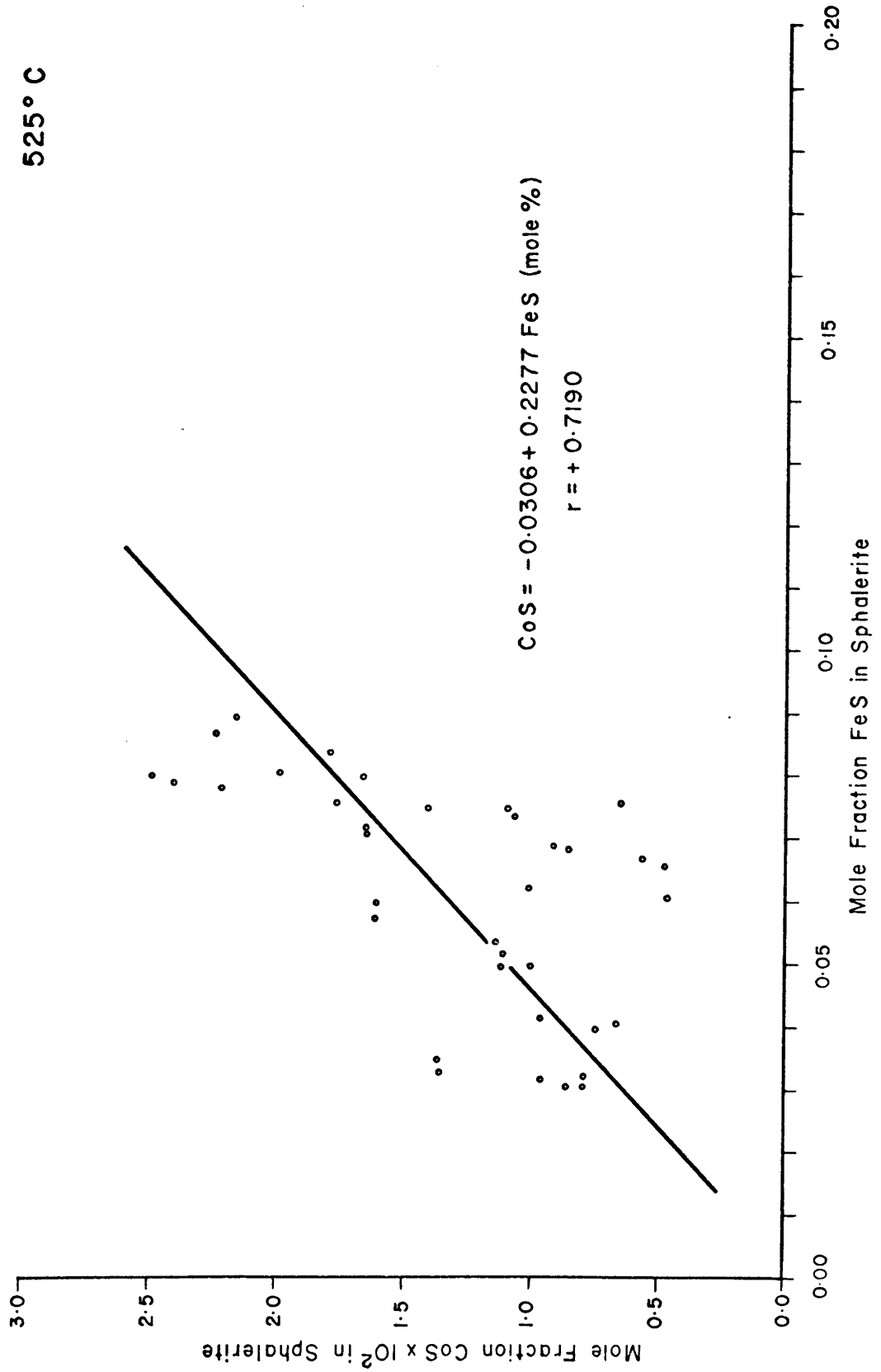
Figure 30: Interaction of CoS and FeS in sphalerite at 475°C.
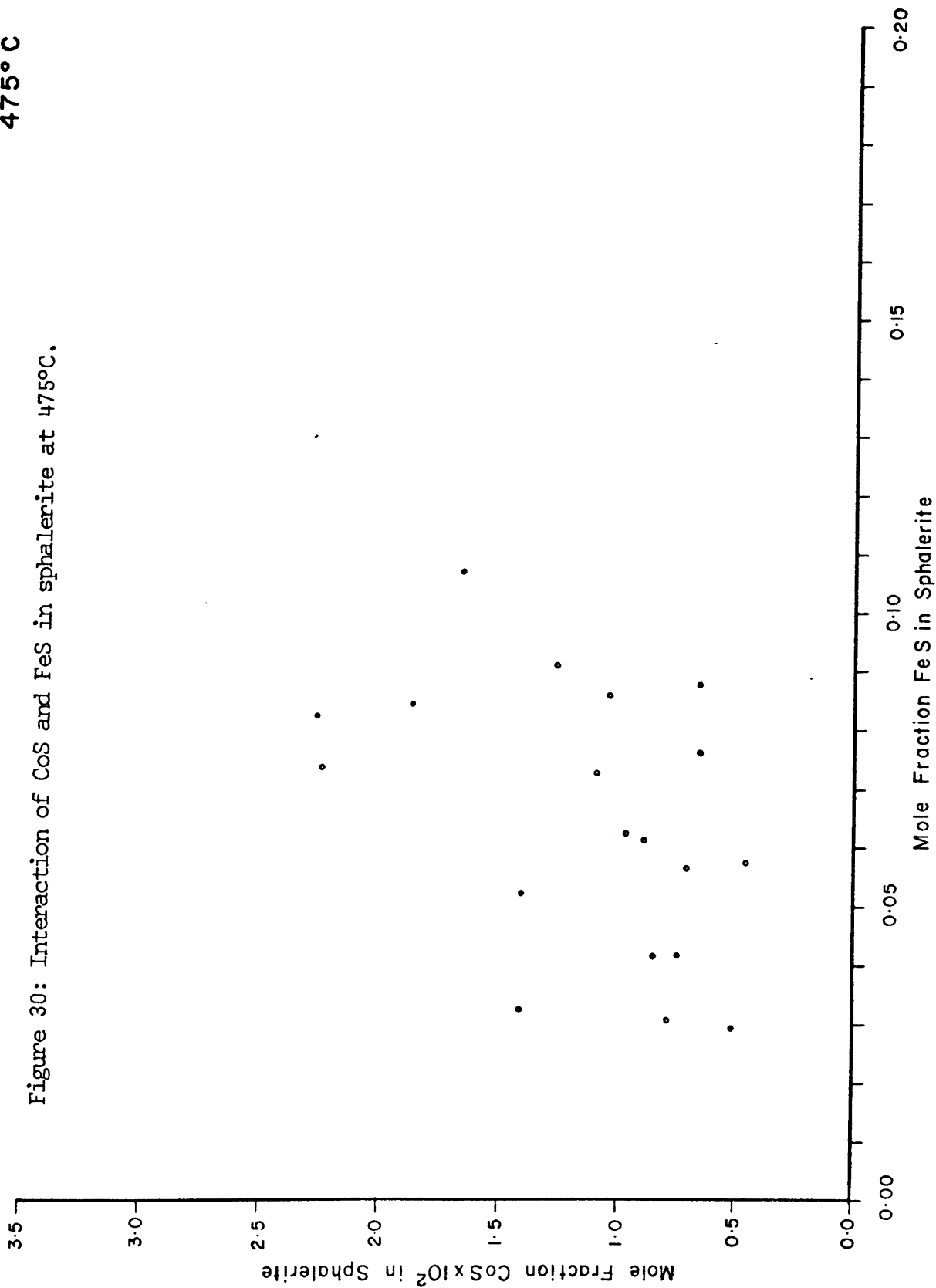
Figure 31: Interaction of CoS and FeS in sphalerite at 420°C.

420°C

$CoS = 0.2759 + 0.1272$ FeS (mole.%)

$r = +0.5770$

Mole Fraction FeS in Sphalerite

Mole Fraction CoS x 10^2 in Sphalerite
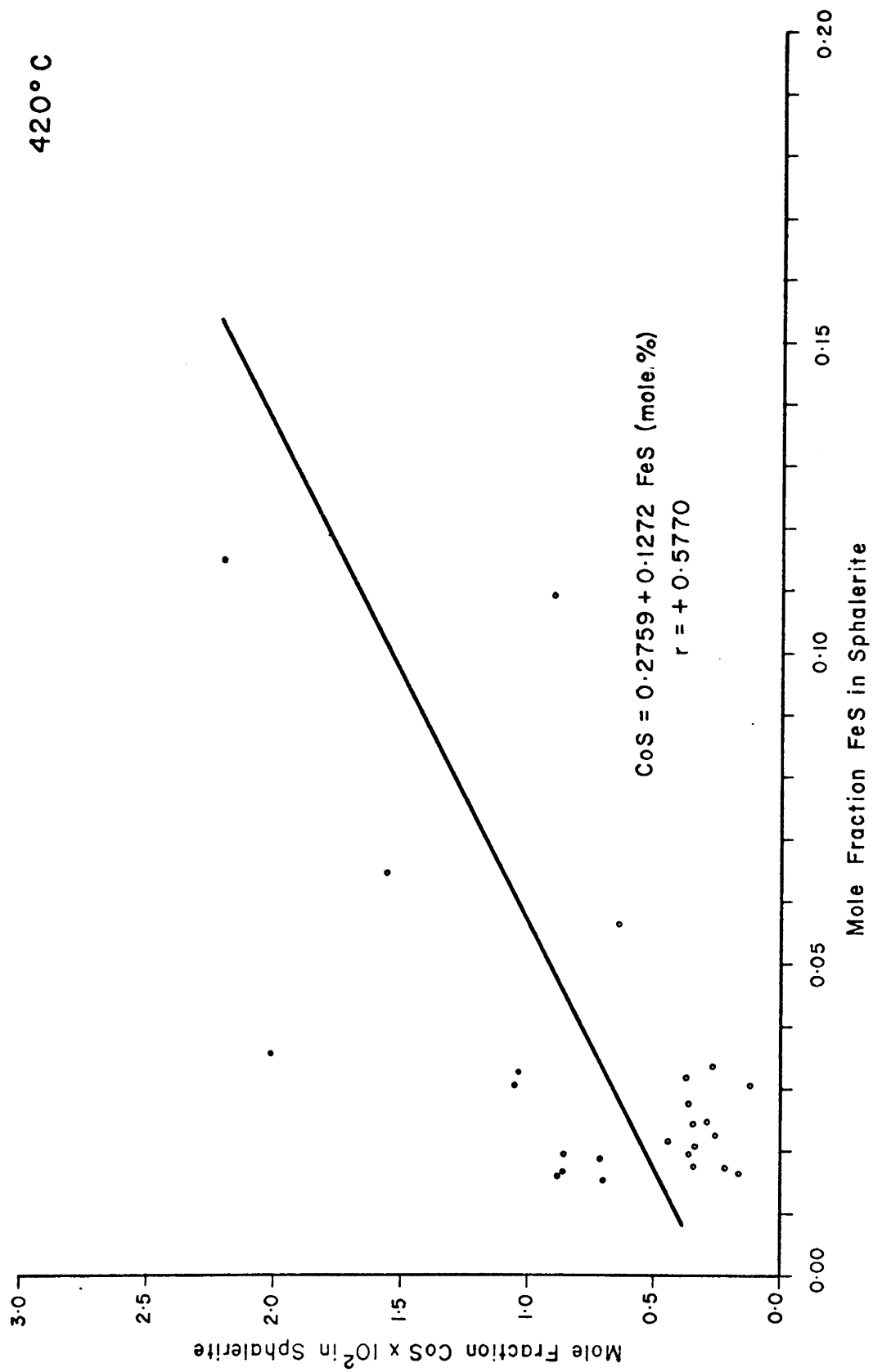
Figure 32: Interaction of CoS and FeS in sphalerite at 403°C.
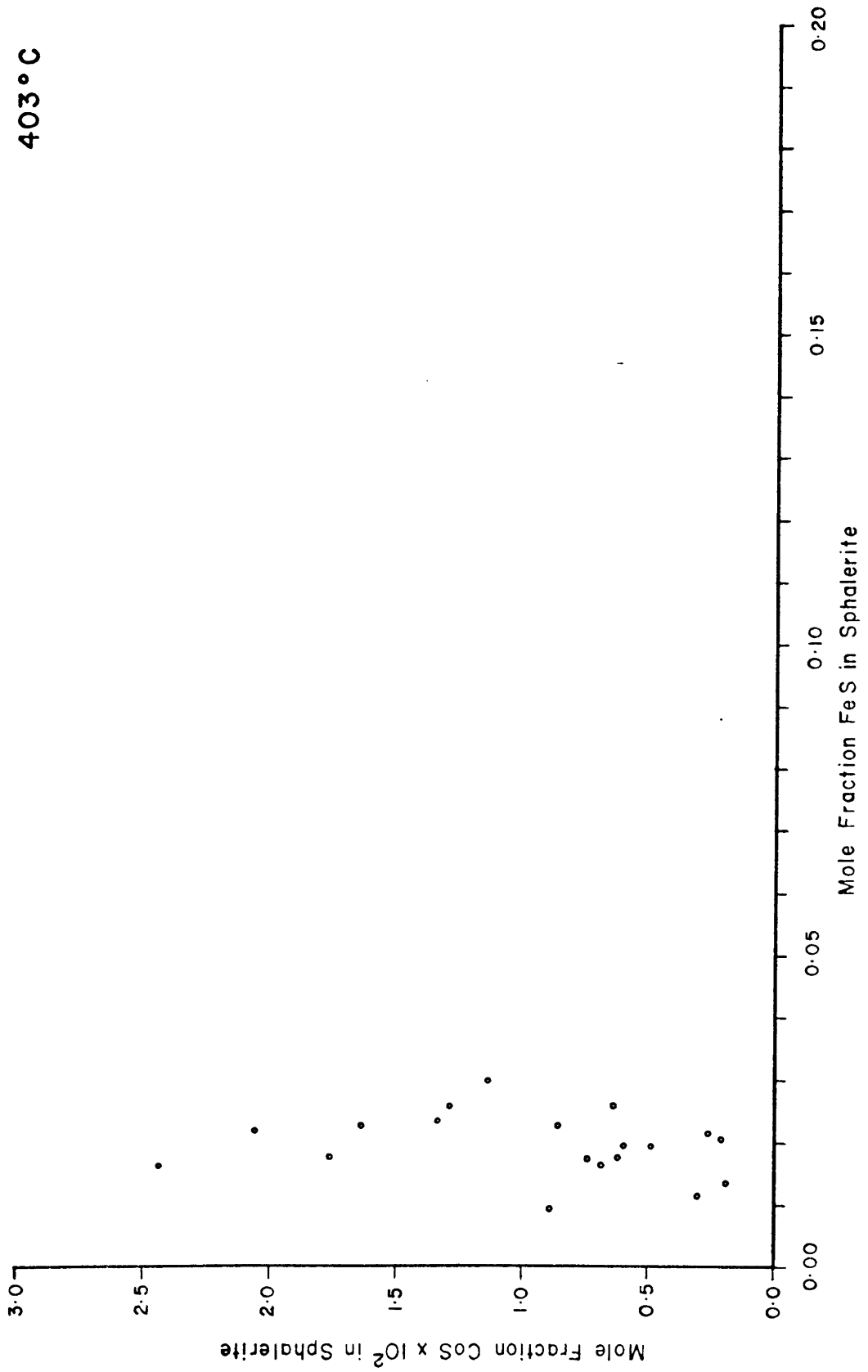
Figure 33: Interaction of CoS and FeS in sphalerite at 305°C.

305°C

CoS = 0.0283 + 0.3751 FeS (mole %)

r = + 0.8190
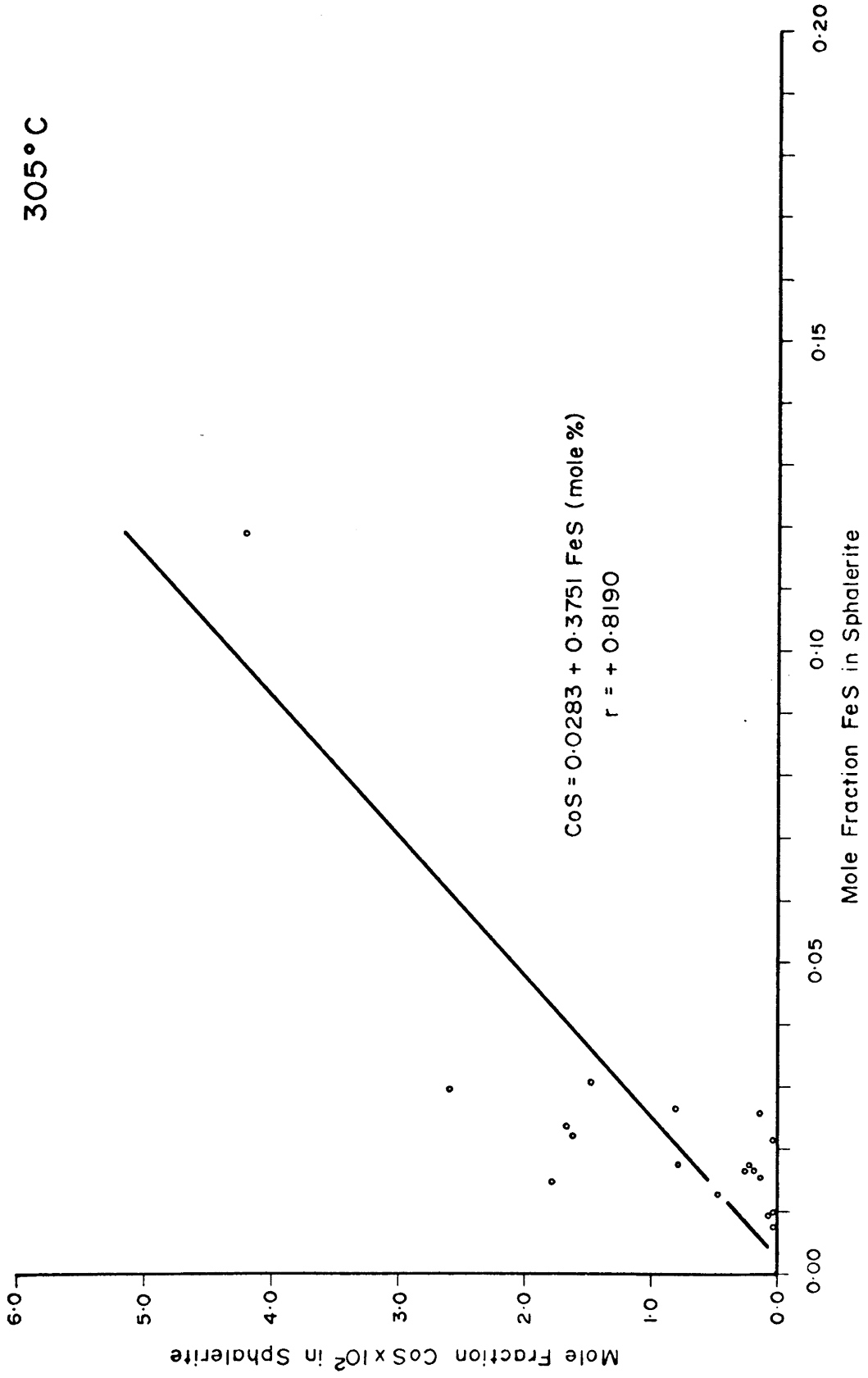
correlation between FeS and CoS in sphalerite is evident at 625°C. The absence of this interaction with decreasing temperature is probably due to slight lowering in the concentration range of FeS and not to a reduction in the potential of such an interaction.

At 525, 420 and 305°C, the concentration of CoS and FeS in sphalerite are directly correlated. This curious reversal can be explained in two ways. The direct correlation may be due to the presence of microinclusions of $(Fe, Co)S_2$ in some of the sphalerite crystals. This would result in anomalously high analyses of both CoS and FeS. For example, in Figure 33, if the analysis at 4.2 mole percent CoS and 12 mole percent FeS is disregarded, the significant correlation between FeS and CoS disappears. This sort of effect is also possible for analyses at 420°C (Figure 31). The direct correlation between CoS and FeS at 525°C (Figure 29) may be due entirely to chance. On the other hand, it could reflect small but sympathetic variations of CoS and FeS in sphalerite in response to random fluctuations of relative vapour space in the reaction tubes. It should be noted that the concentration of FeS in sphalerite from runs at 525°C is less than 10 mole percent, a level probably too low to cause a significant inverse interaction between FeS and CoS of the type detected at 675°C.

The significant influence of changes of FeS in sphalerite on the concentration of CoS in sphalerite means that the partitioning of Co between sphalerite and pyrite cannot be used as a geothermometer without a thorough evaluation of this interaction, over a wide range of FeS concentrations in sphalerite.

Variation Of FeS In Sphalerite:

Figure 34 shows the variation of FeS in sphalerite with temperature. The error bars at each point on this diagram represent twice the pooled standard deviation of FeS for all runs at each temperature. If an error bar is not present, the error is too small to plot. The narrow range of FeS content in sphalerite below 675°C is again, due to uniform experimental conditions. The marked increase of FeS to 14 mole percent at 675°C is, as in the case of runs containing Mn, due to a large increase in the relative vapour space in the reaction tubes.
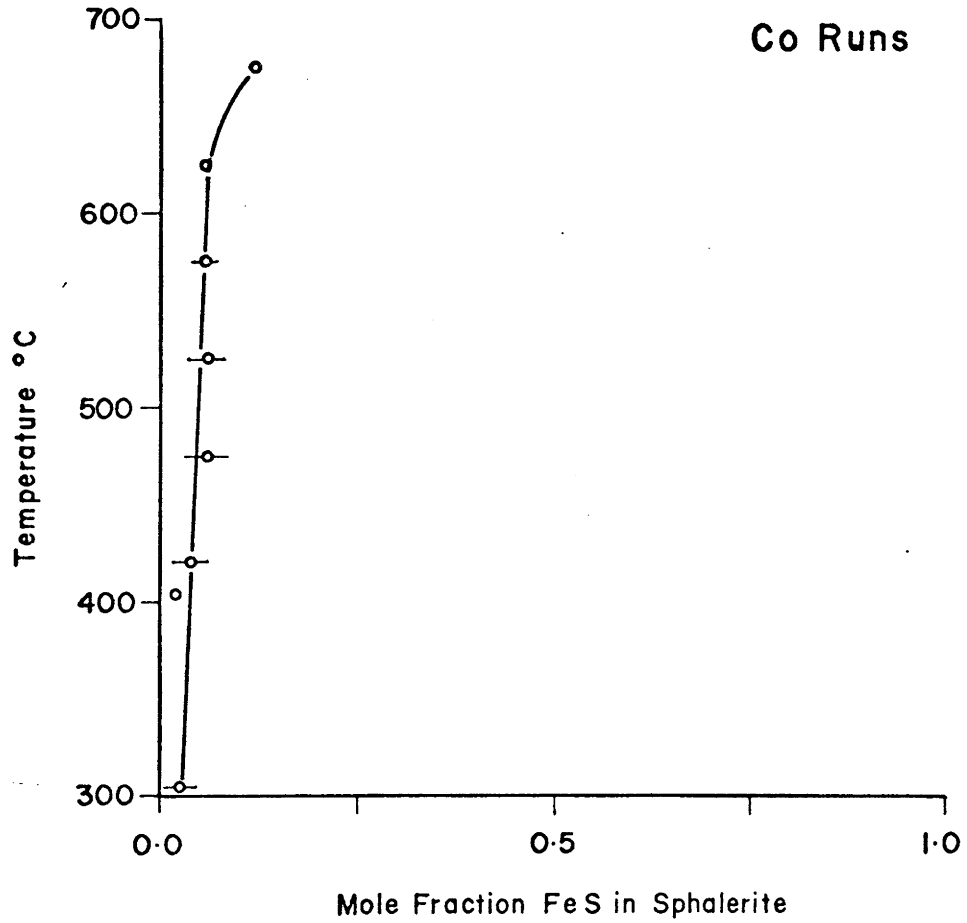
Figure 34: Variation of FeS and CoS-bearing sphalerite
with temperature.
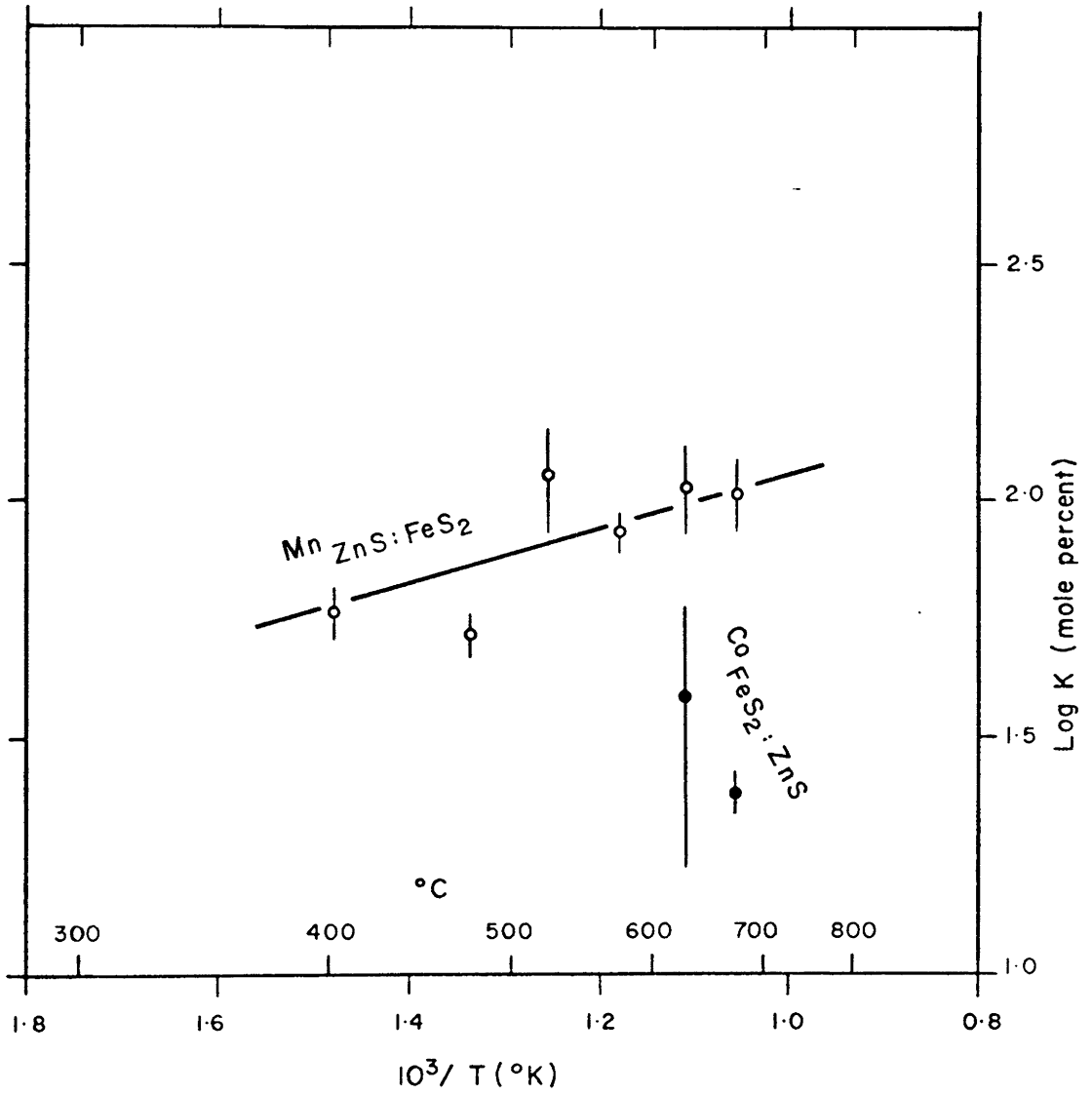
Figure 35: Variation of partition coefficients with temperature.

CONCLUSIONS

An attempt has been made to determine the partitioning of Mn and Co between sphalerite or wurtzite and pyrite as a function of temperature from 675 to 305°C. Microcrystalline wurtzite and pyrite were recrystallized in the presence of variable concentrations of MnS and CoS_2 in KCl - LiCl and NH_4Cl - LiCl eutectic fused salt mixtures for periods of time up to 47 days. The distribution of Mn and Co in the sphalerite or wurtzite and pyrite reaction products was determined by means of an electron probe microanalyzer.

Mn is selectively concentrated in sphalerite and wurtzite relative to pyrite by a factor of about 100. Both sphalerite and wurtzite as well as pyrite were found in the reaction products. Wurtzite is stabilized relative to sphalerite by concentrations of MnS in ZnS above 7 to 10 mole %. This transition is relatively insensitive to changes in temperature. Equilibrium conditions were apparently attained in most runs at temperatures down to 400°C. The partitioning of Mn obeys Henry's Law at concentration levels above those normally found in natural assemblages. No distinction could be drawn in the partitioning of Mn between sphalerite-pyrite and wurtzite-pyrite pairs. The amount of Mn in sphalerite or wurtzite relative to pyrite increases slightly with temperature. The partition coefficient (K) for Mn is a linear function of temperature (log K versus 1/T) within the range of temperatures considered. This variation in the partition coefficient can probably be used for the rough estimation of temperature of formation of natural sphalerite-

pyrite assemblages, although the magnitude of the partition coefficient would make the simultaneous chemical analysis of both phases by electron microprobe methods difficult if not impossible. No interaction of MnS and FeS in sphalerite and wurtzite is evident. Variations of FeS in sphalerite or wurtzite, up to a concentration of 16 mole % FeS in sphalerite or wurtzite should not affect the partitioning of Mn between sphalerite or wurtzite and pyrite.

Co is selectively concentrated in pyrite relative to sphalerite by a factor of 22 to 38. Only sphalerite and pyrite were present in the reaction products. Equilibrium conditions were probably attained only at temperatures of 675 and 625°C. Gross disequilibrium was evident at temperatures below 575°C, possibly due to differential rates of recrystallization of sphalerite and Co-rich pyrite. There may be a rapid decrease in the partitioning coefficient (K) for Co between pyrite-sphalerite pairs with increasing temperature. Sphalerite may become relatively more enriched with Co as temperature increases. A relationship between log K and 1/T was not established since partitioning coefficients could be calculated only at two temperatures (675 and 625°C). A marked inverse interaction of FeS and CoS in sphalerite was found to exist at 675°C. It may be due to the preferential inclusion of FeS in the tetrahedral sites of sphalerite. Significant direct correlations between CoS and FeS in sphalerite were found at 525, 420 and 305°C for lower concentration levels of FeS in sphalerite than at 675°C. These could be due to contamination effects of micro-inclusions of $(Co, Fe)S_2$ in sphalerite or to random fluctuations of

the relative vapour space in reaction tubes changing the concentrations of CoS and FeS sympathetically. These interactions between CoS and FeS invalidate the use of this system as a geothermometer until the character of this effect is fully investigated over a wide range of FeS concentrations in sphalerite.

The qualitative character of the partitioning of Co and Mn between sphalerite or wurtzite and pyrite can be adequately explained using crystal field theory. An analysis of this type should be carried out as a preliminary step in any experimental work on partitioning between sulphide phases.

Kinetic problems leading to lack of equilibrium in some of the runs, particularly those involving CoS_2, ZnS and FeS_2, point up the fact that thorough examination of reaction products by electron microprobe methods was absolutely necessary. The chemical analysis of mixtures of heterogeneous crystals by other techniques would give average values and would lead to highly erroneous conclusions. Kinetic difficulties of the type encountered here could probably be solved by: (1) considerably longer run times; (2) simultaneous precipitation of microcrystalline sulphide reagents to increase the homogeneity of the sulphide charges; (3) use of other eutectic fused salt mixtures.

The use of eutectic fused salt mixtures in the study of partitioning between sulphide minerals seems to hold promise, and it constitutes a viable alternative to methods of hydrothermal synthesis. For example, an extension of Bethke and Barton's (1971) investigation of the distribution of Cd, Mn and Se between galena

and sphalerite could be carried out down to 400°C by means of KCl - LiCl eutectic mixtures. In addition, partitioning between such sulphide pairs as pyrite-pyrrhotite and pyrite-chalcopyrite would be studied in this way.

The application of experimental data on partitioning between coexisting sulphides to ore deposits is fraught with numerous problems. The most important of these is the frequent inability to identify precisely equilibrated sulphides in natural assemblages. Even if a specific pair of coexisting sulphides were in chemical equilibrium at some time, it may be very difficult to determine whether partition coefficients reflect conditions of ore formation or some later metamorphic event. The apparently simple procedure of sampling can present severe obstacles due to the requirement of sample purity, when analyses are done by such methods as atomic absorption, and due to compositional inhomogeneities commonly present in natural sulphide crystals as a result of growth zonation and exsolution. It should be emphasized that the compositional homogeneity of sulphide crystals has usually not been considered in any detail either in experimental partitioning studies (e.g. Bethke and Barton, 1971) or in partitioning studies on natural sulphide assemblages (e.g. Ghosh-Dastidar, 1970) despite the fact that the occurrence of heterogeneous sulphides can lead to major errors in the calculation of partition coefficients. Finally, a strong selective concentration of trace elements in one phase of a specific mineral pair may be a common feature of sulphides, making the analysis of the depleted phase difficult.

Some of the problems outlined above may be solved by the use of ion probe techniques. This method provides greater analytical sensitivity than electron microprobe methods, chemical analysis on a micron scale and the potential of simultaneously measuring trace element concentrations and stable isotope ratios. Trace element distributions between coexisting sulphides in natural assemblages could be compared with fluid inclusion data and temperature estimates derived from sulphur isotope partitioning.

Appendix I

Analyses Of Mn In Sphalerite Or Wurtzite

Note - Appendix I

In the following tables, the numbered column headings refer to:

(1) Analysis identification number. For example, the identifier 14901 refers to an analysis of a single crystal of sphalerite or wurtzite from run 149. Repetition of the identifier indicates that analyses were carried out at two or more distinct spots on the crystal.

(2) Run temperature in °C

(3) Run time in days

(4) Weight per cent Mn in sulphide charge

(5) Mole per cent MnS in sphalerite or wurtzite

(6) Mole per cent FeS in sphalerite or wurtzite

(7) Mole per cent ZnS in sphalerite or wurtzite

(8) Deviation of original analytical total (in weight per cent) from 100%.

Lines started by "AV" give the averages for the preceding set of analyses. The presence of an asterisk (*) preceding the average value of MnS indicates that the distribution of MnS is heterogeneous and that the calculation and use of an average for the set of analyses is probably not justified.

	(1)	(2)	(3)	(4)	(5)	(6)	(7)	(8)
	14901				39.9900	14.2317	45.7783	-0.2442
	14901				39.5529	14.4533	45.9939	1.9657
	14902				40.5093	12.4335	47.0572	3.3312
	14902				40.3954	12.2804	47.3241	3.0115
	14903				41.0358	14.6072	44.3570	0.5299
	14903				41.6158	14.8567	43.5276	-0.8965
AV	149	675	10	25.30	40.5165	13.8105	45.6730	1.2829
	15001				37.2580	13.9839	48.7581	4.1390
	15001				37.3365	13.9879	48.6756	3.3065
	15002				37.3871	14.1607	48.4522	3.5825
	15002				37.1484	14.2552	48.5964	3.1454
	15003				36.8542	16.1723	46.9735	3.2619
	15003				36.8537	16.3678	46.7785	3.6415
AV	150	675	10	18.96	37.1396	14.8213	48.0390	3.5128
	15101				23.2557	13.7076	63.0367	0.9182
	15101				23.4453	14.4469	62.1079	1.9036
	15102				25.4548	16.4146	58.1305	-0.0767
	15102				24.2033	16.6964	59.1003	1.0864
	15103				22.4899	14.3199	63.1902	2.3976
	15103				22.5736	15.3513	62.0750	2.4173
AV	151	675	10	12.64	23.5704	15.1561	61.2734	1.4411
	15201				15.0879	17.1022	67.8099	-2.8378
	15201				15.9616	17.7918	66.2465	2.3211
	15202				16.2746	13.6273	70.0981	1.5624
	15202				15.8048	13.6618	70.5333	1.3576
	15203				16.2763	17.3842	66.3395	1.6362
	15203				16.2699	17.4470	66.2832	1.5548
AV	152	675	10	9.48	15.9459	16.1691	67.8850	0.9324
	15301				8.2361	14.9406	76.8233	-4.1060
	15301				8.2916	14.9570	76.7514	-4.1478
	15302				8.1336	14.9093	76.9571	-3.8545
	15302				8.2934	14.9518	76.7548	-4.0723
	15303				9.6971	16.2493	74.0536	-2.1258
	15303				10.3510	16.4889	73.1601	-3.0797
AV	153	675	10	6.32	8.8338	15.4161	75.7500	-3.5644

	(1)	(2)	(3)	(4)	(5)	(6)	(7)	(8)
	15401				3.1845	11.2732	85.5423	0.4063
	15401				3.3779	9.1081	87.5140	1.6609
	15402				.3.5974	11.9827	84.4199	2.7202
	15402				3.5007	11.6248	84.8744	3.1257
	15403				3.7920	14.1685	82.0395	0.7548
	15403				3.8779	14.3786	81.7434	1.2753
AV	154	675	10	3.16	3.5551	12.0893	84.3555	1.6572
	11301				42.6685	3.9726	53.3589	4.4735
	11301				42.9041	4.0218	.53.0741	3.7133
	11302				42.1199	3.7999	54.0802	4.0767
	11302				42.1532	3.8320	54.0148	4.0897
	11303				42.1431	7.2185	50.6384	3.0405
	11303				34.0741	7.8408	58.0851	1.7619
	11304				42.6854	5.0850	52.2297	3.8561
	11304				42.5200	4.1256	53.3545	3.0320
AV	113	625	14	25.30	*41.4085	4.9870	53.8545	3.5055
	11401				42.6284	4.1329	53.2388	3.1016
	11401				42.3173	4.2365	53.4462	3.6500
	11402				42.2409	5.0897	52.6694	3.2192
	11402				42.4641	4.3810	53.1548	2.5042
	11403				33.5571	7.9498	58.4931	2.2388
	11403				35.2549	7.6332	57.1119	1.2770
	11404				40.4029	3.9516	55.6455	1.6881
	11404				39.6035	3.9735	56.4229	2.1842
AV	114	625	14	18.96	39.8086	5.1685	55.0228	2.4829
	11501				28.2158	7.7105	64.0737	1.4203
	11501				26.8019	6.2577	66.9404	3.9822
	11502				26.4125	6.6461	66.9414	0.7879
	11502				25.1764	6.8297	67.9938	0.3478
	11503				25.3291	6.1622	68.5087	5.0514
	11503				22.9465	5.4308	71.6227	5.6965
AV	115	625	14	12.64	25.8137	6.5062	67.6801	2.8810
	11601				21.7001	8.1984	70.1015	1.2064
	11601				17.6098	5.4568	76.9335	3.0178
	11602				15.6011	7.7855	76.6134	1.3218
	11602				16.1045	7.1756	76.7198	1.6822
	11603				15.4815	5.1169	79.4016	3.2346
	11603				15.4028	5.0802	79.5171	3.8188
AV	116	625	14	9.48	16.9833	6.4689	76.5478	2.3803

	(1)	(2)	(3)	(4)	(5)	(6)	(7)	(8)
	11701				11.3123	7.2912	81.3965	1.0825
	11701				10.0662	6.7175	83.2163	2.1655
	11702				8.1840	5.6930	86.1230	0.4845
	11702				7.9691	5.8656	86.1653	0.6183
	11703				9.5956	6.5013	83.9013	2.2706
	11703				10.0368	6.6907	83.2726	2.4523
AV	117	625	14	6.32	9.5273	6.4599	84.0128	1.5138
	11801				3.4077	6.4804	90.1118	1.0193
	11801				4.7519	7.4350	87.8131	2.7687
	11802				4.8185	6.5298	88.6517	1.2461
	11802				4.7218	7.3092	87.9691	1.0550
	11803				1.3492	7.4645	91.1863	5.5413
	11803				5.1335	8.6412	86.2253	4.0462
AV	118	625	14	3.16	4.0304	7.3100	88.6595	2.6128
	8901				42.0030	3.8186	54.1785	2.4051
	8901				42.4377	3.4948	54.0675	4.0255
	8902				42.6386	3.5098	53.8516	4.2495
	8902				43.9509	4.7384	51.3108	3.4624
	8903				42.4454	2.9742	54.5808	2.7770
	8903				44.3491	5.6591	49.9918	2.1719
AV	89	575	14	25.30	42.9707	4.0325	52.0067	3.1819
	9001				33.6838	4.5310	61.7852	2.8288
	9001				34.4651	4.8427	60.6922	3.0724
	9002				42.7102	3.6557	53.6341	3.8641
	9002				42.8385	4.3195	52.8419	3.5494
	9003				39.0768	5.2469	55.6763	2.1881
	9003				32.8879	4.4995	62.6127	3.5038
	9004				33.5551	5.5237	60.9212	5.5820
	9004				36.0111	4.2108	59.7782	4.6783
AV	90	575	14	18.96	*36.9036	4.6037	58.4927	3.6584

	(1)	(2)	(3)	(4)	(5)	(6)	(7)	(8)
	12601				39.2464	7.6945	53.0591	3.4900
	12601				42.6313	3.8489	53.5199	1.8587
	12602				43.9020	5.0888	51.0092	0.7188
	12602				43.7050	4.7922	51.5029	0.7184
	12603				42.9003	3.5763	53.5234	1.1290
	12603				40.3145	7.3948	52.2907	1.2327
AV	126	575	27	18.96	42.1166	5.3992	52.4842	1.5246
	9101				24.8376	8.7288	66.4336	4.1151
	9101				25.4163	4.7613	69.8225	4.4816
	9102				25.5469	7.6801	66.7731	3.2412
	9102				25.3841	8.5997	66.0163	3.8688
	9103				23.0272	6.8082	70.1646	3.8048
	9103				25.1207	7.0797	67.7997	3.8965
AV	91	575	14	12.64	24.8888	7.2763	67.8349	3.9013
	12701				31.1049	12.5710	56.3241	4.0018
	12701				29.1993	8.6360	62.1647	3.8698
	12702				24.6509	7.5178	67.8313	4.7542
	12702				25.3948	6.8641	67.7411	3.1032
	12703				22.9845	7.1026	69.9130	1.3468
	12703				22.1373	4.8692	72.9936	0.7406
AV	127	575	27	12.64	25.9119	7.9268	66.1613	2.9694
	9201				9.5651	4.1111	86.3238	2.4729
	9201				9.8955	4.9736	85.1310	2.7817
	9202				9.4569	3.4532	87.0899	5.6456
	9202				6.3610	3.1657	90.4733	0.9233
	9203				8.8618	3.6911	87.4471	2.0421
	9203				10.6065	3.5697	85.8239	3.7392
	9204				8.8164	3.3449	87.8387	2.3517
	9204				7.2864	3.7301	88.9834	2.6452
AV	92	575	14	9.48	8.8562	3.7549	87.3888	2.8252
	12801				12.5593	3.9685	83.4722	1.3408
	12801				12.4654	3.7925	83.7421	0.9481
	12802				20.1149	6.3034	73.5818	0.5487
	12802				20.6051	8.7716	70.6233	0.4280
	12803				17.8476	5.2594	76.8930	1.0434
	12803				18.6345	4.9131	76.4525	1.4221
	12804				17.8840	5.4285	76.6875	0.2875
	12804				16.8379	8.7906	74.3715	-0.1773
AV	128	575	27	9.48	17.1186	5.9034	76.9779	0.7302

	(1)	(2)	(3)	(4)	(5)	(6)	(7)	(8)
	5101				15.1304	3.8593	81.0104	−1.3240
	5102				13.9516	4.8588	81.1897	−1.2097
	5103				17.2013	6.2264	76.5722	−2.1632
	5104				15.8875	3.8222	80.2903	−3.0200
AV	51	575	5	8.24	15.5427	4.6917	79.7656	−1.9292
	9301				8.8673	9.6213	81.5114	0.0344
	9301				7.8945	7.3887	84.7168	0.8222
	9302				4.9657	5.7956	89.2388	1.9689
	9302				4.6881	4.5143	90.7976	2.8093
	9303				11.2265	13.9203	74.8531	3.7525
	9303				7.6260	6.8218	85.5522	3.0476
	9304				6.2700	5.0627	88.6673	2.6286
	9304				6.2266	5.3100	88.4635	2.3817
AV	93	575	14	6.32	7.2206	7.3043	85.4750	2.1806
	12901				1.3873	10.9455	87.6673	0.1160
	12901				1.3360	10.3804	88.2836	−0.1536
	12902				1.4653	5.5744	92.9603	1.0704
	12902				1.2622	8.4107	90.3272	1.3961
	12903				11.8840	6.4547	81.6613	0.3272
	12903				11.6418	6.4195	81.9388	0.4917
	12904				15.2922	6.9288	77.7790	3.7313
	12904				14.5075	6.9116	78.5809	3.6238
	12905				15.3916	7.1199	77.4885	2.1035
	12905				15.0234	7.0255	77.9510	2.3667
AV	129	575	27	6.32	* 8.9191	7.6171	83.4637	1.5073
	9401				4.4202	7.7188	87.8609	0.8379
	9401				4.4151	8.9839	86.6010	−2.4489
	9402				3.1624	5.2167	91.6209	1.4520
	9402				4.3381	7.4861	88.1758	1.8462
	9406				2.7221	4.2822	92.9957	2.5522
	9406				4.8131	11.4332	83.7538	1.2071
	9404				2.6729	4.5587	92.7686	2.1719
	9404				3.2588	5.8511	90.8901	3.2884
AV	94	575	14	3.16	3.7253	6.9413	89.3333	1.3633
	13001				5.4351	6.8735	87.6914	0.1765
	13001				6.2688	6.8725	86.8587	−0.2638
	13002				4.2285	9.1694	86.6021	−1.1905
	13002				3.6242	6.4330	89.9428	1.2215
	13003				5.1469	7.3702	87.4829	0.5139
	13003				4.6427	6.4237	88.9337	1.7438
AV	130	575	27	3.16	4.8911	7.1904	87.9185	0.3669

	(1)	(2)	(3)	(4)	(5)	(6)	(7)	(8)
	6401				0.9305	4.7478	94.3217	−1.5094
	6402				0.8126	3.7739	95.4136	−2.9130
	6403				0.7984	3.0082	96.1935	0.3271
	6404				0.7639	3.0038	96.2324	−0.3259
	6405				0.8188	2.7125	96.4687	−0.2997
AV	64	575	21	2.42 *	0.8248	3.4492	95.7259	−0.9442
	6501				0.1681	3.2381	96.5983	3.3849
	6502				0.1819	1.9592	97.8590	1.2165
	6503				0.1858	2.1245	97.6897	1.4113
AV	65	575	21	1.24	0.1786	2.4406	97.3808	2.0042
	6801				0.0837	2.6455	97.2708	−0.6701
	6802				0.0782	3.2040	96.7178	−0.0719
	6803				0.0757	3.1505	96.7738	−0.2952
	6803				0.0757	3.1505	96.7738	−0.2952
	6804				0.0632	2.8885	97.0484	−1.4855
	6805				0.0653	2.8476	97.0870	−1.4797
	6806				0.0749	3.5299	96.3951	0.0216
	6807				0.0581	2.7588	97.1831	−2.2824
	6808				0.0475	3.6576	96.2949	0.8981
AV	68	575	21	0.13	0.0692	3.0926	96.8382	−0.6289
	10101				42.9482	2.1252	54.9267	0.8470
	10101				42.0216	5.5018	52.4765	1.9871
	10102				41.4747	6.9533	51.5720	2.6894
	10102				41.8104	5.2349	52.9547	3.4446
	10103				41.7562	3.1563	55.0876	2.4632
	10103				40.9211	7.6159	51.4630	2.5491
AV	101	525	30	25.30	41.8220	5.0979	53.0800	2.3301
	10201				42.6276	2.5192	54.8532	0.8019
	10201				41.8121	3.2062	54.9817	2.6123
	10202				41.9083	2.0084	56.0824	2.1966
	10202				41.1192	2.0559	56.8249	2.3005
	10203				41.8834	3.2548	54.8618	2.6579
	10203				42.0661	3.2858	54.6482	3.2589
AV	102	525	30	18.96	41.9028	2.7219	55.3753	2.3047
	2001				33.0228	2.2026	64.7746	−0.1163
	2002				34.8234	2.6426	62.5340	−1.9403
	2003				33.7112	2.6197	63.6690	−1.0926
	2004				33.7709	2.4375	63.7916	−1.5224
	2005				32.8287	2.9503	64.2210	−0.6486
	2006				31.8846	1.6880	66.4274	−1.2212

	(1)	(2)	(3)	(4)	(5)	(6)	(7)	(8)
AV	20	525	14	14.57	33.3403	2.4235	64.2362	−1.0902
	2601				36.0111	3.0332	60.9557	−2.1713
	2602				36.3269	2.5807	61.0923	−3.7920
	2603				34.1333	2.2634	63.6033	−0.9482
AV	26	525	28	14.57	35.4904	2.6258	61.8838	−2.3038
	10301				26.3314	5.1034	68.5652	2.2663
	10301				23.6296	6.5260	69.8444	1.3232
	10302				24.7662	3.1691	72.0648	2.7007
	10302				27.8051	8.3834	63.8115	2.6666
	10303				28.2214	7.5110	64.2677	2.5368
	10303				23.2415	7.7289	69.0296	1.6371
AV	103	525	30	12.64	25.6658	6.4036	67.9305	2.1884
	10401				10.9060	3.5635	85.5305	−2.1406
	10401				8.5979	2.4525	88.9496	−0.0838
	10402				8.4483	2.6223	88.9294	1.4670
	10402				9.3884	2.7863	87.8253	1.0539
	10403				10.7024	4.2537	85.0439	1.5297
	10403				9.2925	4.0462	86.6614	1.1527
AV	104	525	30	9.48	9.5559	3.2874	87.1566	0.4965
	2101				8.4770	1.9536	89.5694	−2.5400
	2102				9.4101	1.9812	88.6086	−1.7271
	2103				3.7236	6.1156	90.1609	−4.3210
	2104				8.0790	3.5505	88.3705	−1.5347
AV	21	525	14	8.24	* 7.4224	3.4002	89.1773	−2.5307
	2701				10.5297	1.7687	87.7015	−0.7459
	2702				10.3110	1.7080	87.9810	−3.2503
	2703				9.9558	1.8692	88.1750	−2.1037
	2704				15.0073	1.5161	83.4766	−1.8504
	2705				12.0515	2.3164	85.6321	−0.8053
	2706				10.0593	1.5007	88.4400	−0.5554
AV	27	525	28	8.24	*11.3191	1.7799	86.9010	−1.5518
	10501				1.3014	8.2564	90.4422	−4.3229
	10501				1.3015	8.3570	90.3415	−4.0277
	10502				0.9389	3.8243	95.2368	−3.2810
	10502				0.9394	3.6644	95.3962	−3.2060
	10503				1.0330	9.6474	89.3195	−3.9790
	10503				1.0612	9.6704	89.2684	−4.5962
AV	105	525	30	6.32	1.0959	7.2366	91.6673	−3.9021

	(1)	(2)	(3)	(4)	(5)	(6)	(7)	(8)
	2801				2.6313	2.7316	94.6372	−0.2458
	2802				2.7903	2.7495	94.4603	0.3413
	2803				2.3482	2.1427	95.5091	0.1198
AV	28	525	28	3.57	2.5899	2.5413	94.8688	0.0718
	10601				0.3302	8.2038	91.4660	−1.8206
	10601				0.3149	10.7164	88.9686	−3.5611
	10602				0.2695	3.4554	96.2751	2.6891
	10602				0.2707	3.1502	96.5791	2.5295
	10603				0.9200	10.1782	88.9019	−1.6595
	10603				0.5515	8.8401	90.6085	1.1756
	10604				0.5038	9.3673	90.1288	−0.2381
	10604				1.0395	11.0200	87.9406	−4.1567
AV	106	525	30	3.16 ✽	0.5250	8.1164	91.3585	−0.6302
	7401				0.4301	4.6580	94.9119	0.9770
	7402				0.3108	2.4237	97.2656	2.7468
	7403				0.3228	2.4730	97.2042	1.8733
AV	74	525	21	2.42	0.3546	3.1849	96.4605	1.8657
	13701				41.1525	1.1756	57.6719	0.5259
	13702				38.7301	1.6869	59.5830	1.3454
	13703				38.2374	4.5060	57.2566	−1.1628
	13704				36.8669	4.9459	58.1871	0.6956
AV	137	475	28	25.30	38.7467	3.0786	58.1747	0.3510
	13801				29.7823	5.5327	64.6851	−0.8730
	13802				34.1757	4.1246	61.6997	−0.5841
	13803				31.9195	4.3623	63.7182	−0.2678
AV	138	475	29	18.96	31.9592	4.6732	63.3676	−0.5750
	13901				24.0050	2.6619	73.3332	3.9396
	13902				25.7468	7.6054	66.6478	3.6935
	13903				24.4154	2.3575	73.2271	4.4204
	13904				22.3821	2.4272	75.1907	3.7349
AV	139	475	28	12.64	24.1373	3.7630	72.0997	3.9471
	14001				8.7461	2.3659	88.8880	3.0259
	14002				13.2147	7.0602	79.7252	2.6379
	14003				9.0776	2.6148	88.3076	0.9269
	14004				10.6816	6.6632	82.6552	3.7671
AV	140	475	28	9.48	10.4300	4.6760	84.8939	2.5894

	(1)	(2)	(3)	(4)	(5)	(6)	(7)	(8)
	14101				5.8463	10.0194	84.1344	1.4379
	14102				6.6937	10.1235	83.1828	-0.4942
	14103				2.2150	5.2912	92.4938	-1.0390
	14104				9.5171	12.3520	78.1309	2.4410
AV	141	475	28	6.32	6.0680	9.4465	84.4854	0.5864
	14201				4.2319	11.9215	83.8467	2.1015
	14202				3.5518	13.5028	82.9454	-4.9791
	14203				3.7110	11.6093	84.6797	-4.5107
AV	142	475	28	3.16	3.8316	12.3445	83.8249	-2.4628
	8401				2.0404	6.5326	91.4270	-0.8948
	8402				1.7301	3.8594	94.4105	-1.3810
	8403				2.3883	2.1713	95.4404	-1.2955
	8404				2.9466	2.7545	94.2990	-1.6531
	8405				2.8470	3.7611	93.3919	-1.8609
	8406				2.5277	5.4779	91.9944	-3.8873
AV	84	475	21	2.42	2.4134	4.0928	93.4938	-1.8288
	8501				0.0193	1.0844	98.8963	-0.8627
	8502				0.1338	3.8348	96.0314	2.2207
	8503				0.4176	5.3253	94.2570	0.9307
	8504				0.0206	1.7737	98.2057	1.1946
	8505				0.3602	8.2383	91.4015	3.1577
	8506				0.0315	2.5489	97.4197	1.2349
AV	85	475	21	1.24	* 0.1638	3.8009	96.0352	1.3126
	17301				34.5041	9.6427	55.8531	-1.5728
	17302				32.5071	3.7709	63.7221	-2.8151
	17303				36.4415	8.3263	55.2322	-1.3128
	17304				35.2045	9.1716	55.6240	-1.8887
	17305				35.9359	7.6498	56.4143	-0.2908
AV	173	420	47	25.30	34.9186	7.7123	57.3691	-1.5760
	17401				20.1591	2.2804	77.5605	1.2295
	17402				13.3019	6.3505	80.3476	-1.5377
	17403				15.8057	3.9984	80.1960	-2.1129
	17404				27.9570	2.0966	69.9464	-0.0239
	17405				6.8183	3.7588	89.4229	1.2843
AV	174	420	47	18.96	*16.8084	3.6970	79.4946	-0.2322

	(1)	(2)	(3)	(4)	(5)	(6)	(7)	(8)
	17501				11.2786	9.7610	78.9604	−2.2677
	17501				10.8714	9.5833	79.5455	−1.1823
	17502				9.3477	8.4295	82.2229	−0.6377
	17502				8.7625	7.7489	83.4887	0.0508
	17503				12.3089	9.7205	77.9707	−0.3019
	17503				13.4841	8.9256	77.5903	−0.5926
AV	175	420	47	12.64	11.0088	9.0281	79.9630	−0.8219
	17601				4.0177	8.3142	87.6682	0.7052
	17602				5.2789	12.2903	82.4307	−0.9125
	17603				8.0801	15.9840	75.9359	−0.0680
	17604				6.5428	11.7524	81.7048	−0.5456
	17605				7.2321	13.6324	79.1356	−0.9613
AV	176	420	47	9.48	6.2303	12.3947	81.3750	−0.3564
	17701				1.2878	13.7712	84.9411	−1.5431
	17702				0.8934	12.6885	86.4181	−2.3946
	17703				1.4454	13.6663	84.8883	−2.1291
	17704				2.6172	13.3704	84.0124	−0.9777
AV	177	420	47	6.32	1.5609	13.3741	85.0649	−1.7611
	17801				0.4551	7.3439	92.2010	−1.8432
	17802				0.3596	7.1394	92.5010	0.1663
	17803				0.3943	8.9153	90.6904	0.2012
AV	178	420	47	3.16	0.4030	7.7995	91.7974	−0.4919
	18501				36.8737	8.3786	54.7477	1.0581
	18502				31.5117	1.7199	66.7684	0.7379
	18503				49.5041	1.3697	49.1262	0.2601
	18504				34.3354	7.5872	58.0773	2.6113
AV	185	403	47	25.30	38.0521	3.9468	45.7439	2.0302
	18601				29.2834	7.4278	63.2888	0.1903
	18602				37.5460	1.5245	60.9295	1.7773
	18603				32.7363	7.1454	60.1182	1.3763
	18604				28.1551	9.1107	62.7677	1.0318
AV	186	403	47	18.96	31.9302	6.3021	61.7677	1.0319
	18701				7.8619	10.9434	81.1947	1.8703
	18702				10.4320	13.7995	75.7684	−0.3715
	18703				2.3785	9.0726	88.5489	−0.4890
	18704				7.8856	10.7708	81.3436	2.5325
	18705				8.2975	15.8458	75.8567	3.4070
AV	187	403	47	12.64	* 7.3711	12.0864	80.5424	1.3898

	(1)	(2)	(3)	(4)	(5)	(6)	(7)	(8)
	18801				4.3696	6.0925	89.5379	−3.2417
	18802				5.1999	7.3831	87.4171	−0.8458
	18803				5.3432	12.2794	82.3774	−1.3998
	18804				6.2538	12.3521	81.3941	−1.9430
AV	188	403	47	9.48	5.2917	9.5268	85.1816	−1.8576
	18901				4.5908	9.3826	86.0266	0.5905
	18902				1.6247	9.3752	89.0002	−0.4381
	18903				4.2316	7.2135	88.5549	0.4728
	18904				1.5903	7.5953	90.8144	0.1942
AV	189	403	47	6.32	* 3.0093	8.3917	88.5989	0.2048
	19001				0.3326	8.6783	90.9891	−3.0198
	19002				0.1349	4.2700	95.5952	−2.3078
	19003				0.1844	5.3103	94.5053	−0.3191
	19004				0.1939	5.2325	94.5737	1.6545
AV	190	403	47	3.16	0.2114	5.8728	93.9157	−0.9981
	19701				8.5618	1.2174	90.2207	0.1068
	19702				15.2488	1.0227	83.7286	1.9188
	19703				9.4624	0.8176	89.7201	1.5308
	19704				13.0690	8.8211	78.1099	−0.6659
	19705				7.5469	2.8090	89.6441	2.4799
AV	197	305	47	25.30	10.7778	2.9376	86.2847	1.0741
	19801				11.5170	3.5433	84.9498	−1.7609
	19802				8.9001	3.3686	87.7313	0.9746
	19803				7.1013	1.5221	91.3767	1.8025
	19804				5.7153	1.4406	92.8441	0.5736
AV	198	305	47	18.96	8.3084	2.4686	89.2229	0.3974
	19901				0.0729	1.7223	98.2048	−2.6221
	19902				0.0663	2.6955	97.2382	0.2795
	19903				0.1455	2.7361	97.1184	−1.3069
	19904				2.1073	9.1543	88.7384	1.5711
AV	199	305	47	12.64	* 0.5980	4.0771	95.3249	−0.5196
	20001				0.0180	1.6813	98.3008	−1.7497
	20002				16.2975	2.3055	81.3970	−2.5916
	20003				34.2782	2.4865	63.2353	−4.2060
	20004				0.0573	9.5681	90.3747	−3.1020
AV	200	305	47	9.48	*12.6627	4.0104	83.3269	−2.9123

	(1)	(2)	(3)	(4)	(5)	(6)	(7)	(8)
	20101				0.0856	7.3988	92.5157	−1.6698
	20102				0.0171	2.3591	97.6238	1.2923
	20103				0.1393	1.3314	98.5294	0.7139
AV	201	305	47	6.32	0.0807	3.6964	96.2229	0.1121
	20201				0.1645	13.7047	86.1308	−4.6031
	20202				0.4908	14.5936	84.9157	−2.0813
	20203				0.3187	12.8579	86.8234	−4.5102
AV	202	305	47	3.16	0.3246	13.7188	85.9565	−3.7315

Appendix II

Analyses Of Mn In Pyrite

Note - Appendix II

In the following tables, the numbered column headings refer to:

(1) Analysis identification number. For example, the identifier 14901
     refers to an analysis of a single crystal of pyrite from run 149.
     Repetition of the identifier indicates that analyses were carried
     out at two or more distinct spots on the crystal.

(2) Run temperature in °C

(3) Run time in days

(4) Weight per cent Mn in sulphide charge

(5) Mole per cent MnS_2 in pyrite

(6) Mole per cent FeS_2 in pyrite

(7) Mole per cent ZnS_2 in pyrite

(8) Deviation of original analytical total (in weight per cent)
     from 100%

Lines started by "AV" give the averages for the preceding set

of analyses. The presence of an asterisk (*) preceding the

average value of MnS indicates that the distribution of MnS_2

is heterogeneous and that the calculation and use of an average

for the set of analyses is probably not justified.

- = element not detected

	(1)	(2)	(3)	(4)	(5)	(6)	(7)	(8)
	14901				0.0413	99.9587	−	−1.0381
	14902				0.3910	99.6090	−	−2.3762
	14903				0.8509	99.1491	−	−3.6300
	14904				0.4596	99.5404	−	−1.9785
	14905				0.4662	99.5338	−	−3.9214
	14906				0.5649	99.4351	−	−3.1563
AV	149	675	10	25.30	*0.4623	99.5376	−	−.26834
	15001				0.3683	99.1491	0.4826	−0.4056
	15002				0.2494	99.6709	−	−0.9771
	15003				0.2533	99.4799	0.2668	−0.8129
	15004				0.6024	99.1944	0.2032	−0.9083
AV	150	675	10	18.96	0.3683	99.3735	0.2581	−0.7760
	15101				0.1231	99.5089	0.3680	−1.5372
	15102				0.0399	99.7264	0.2337	0.6308
	15103				0.0958	99.7977	0.1065	0.9711
	15104				0.0731	99.7312	0.1957	−2.0023
	15105				0.0977	99.6138	0.2885	−0.2966
	15106				0.2471	99.3590	0.3940	−0.8899
AV	151	675	10	12.64	*0.1128	99.6227	0.2644	−0.5207
	15201				0.0847	99.5441	0.3712	−2.2396
	15202				0.1316	99.1844	0.6840	−2.3727
	15203				0.0693	99.6969	0.2348	0.4530
	15204				0.2402	99.4379	0.3219	−2.8781
	15205				0.1475	99.5739	0.2786	−2.0992
AV	152	675	10	9.48	0.1345	99.4874	0.3781	−1.8273
	15301				0.0430	99.6065	0.3505	−0.2010
	15302				0.0556	99.4996	0.4448	−0.6629
	15303				0.0566	99.7454	0.1979	0.8315
AV	153	675	10	6.32	0.0517	99.6172	0.3311	−0.0108
	15401				0.0360	99.1010	0.8630	−2.2266
	15402				0.0507	99.2028	0.7465	−0.0831
	15403				0.0735	99.2826	0.6439	−1.2546
AV	154	675	10	3.16	0.0534	99.1954	0.7511	−1.1881
	11301				0.3180	99.3226	0.3594	−2.5923
	11302				0.1126	99.7543	0.1331	−2.3911
	11303				0.3960	99.1385	0.4655	−2.9101

	(1)	(2)	(3)	(4)	(5)	(6)	(7)	(8)
	11304				0.4622	99.3807	0.1571	-1.8924
	11305				0.6075	98.6269	0.7656	-1.8833
AV	113	625	14	25.30	0.3792	99.2445	0.3761	-2.3338
	11401				0.1947	99.2865	0.5188	1.5630
	11402				0.3703	98.8161	0.8136	1.1581
	11403				0.2564	99.0625	0.6810	0.8863
	11404				0.4575	98.9375	0.6050	0.6238
	11405				0.2421	99.1878	0.5701	0.6371
AV	114	625	14	18.96	0.3042	99.0580	0.6377	0.9737
	11501				0.3605	98.0151	1.6244	-1.9747
	11502				0.2565	98.4560	1.2875	-0.2680
	11503				0.3814	97.8834	1.7352	-3.3415
	11504				0.2573	98.2849	1.4579	-2.0949
AV	115	625	14	12.64	0.3139	98.1598	1.5262	-1.9198
	11601				0.1315	98.8578	1.0107	1.2486
	11602				0.1299	98.9837	0.9314	1.4834
	11603				0.1116	98.9666	0.9217	1.2137
AV	116	625	14	9.48	0.1243	98.9210	0.9546	1.3152
	11701				0.0568	99.1391	0.8040	-1.9528
	11702				0.0661	99.1011	0.8327	-1.5172
	11703				0.0699	99.0698	0.8602	-0.9463
AV	117	625	14	6.32	0.0643	99.1033	0.8323	-1.4721
	11801				0.0457	98.8450	1.1093	3.2750
	11802				0.0667	98.2909	1.6424	0.3427
	11803				0.0475	98.6883	1.2642	0.8434
	11804				0.0380	98.4065	1.5555	3.6379
AV	118	625	14	3.16	0.0495	98.5576	1.3929	2.0247
	8901				0.5008	98.9515	0.5477	-0.0088
	8902				0.5821	98.6620	0.7559	1.0550
	8903				0.6005	98.7092	0.6902	1.5081
	8904				0.6248	98.7438	0.6314	1.5474
	8905				0.4011	98.9270	0.6719	1.4386
	8906				0.5169	98.8878	0.5953	1.5627
AV	89	575	14	25.30	0.5377	98.8135	0.6487	1.1838

	(1)	(2)	(3)	(4)	(5)	(6)	(7)	(8)
	9001				0.3504	98.9491	0.7004	0.4495
	9002				0.3140	99.0843	0.6017	0.6301
	9003				0.4956	98.8855	0.6189	1.6060
	9004				0.3447	98.8916	0.7638	1.3124
AV	90	575	14	18.96	*0.3762	98.9525	0.6712	0.9995
	12601				0.2384	99.4087	0.3529	0.9704
	12602				0.1932	99.3990	0.4078	5.4783
	12603				0.2167	99.4987	0.2846	4.4195
	12604				0.4304	99.2132	0.3564	4.2489
AV	126	575	27	18.96	*0.2697	99.3799	0.3504	3.7793
	9101				0.3205	98.3156	1.3639	2.2481
	9102				0.3310	98.3069	1.3622	2.7124
	9103				0.3293	98.2811	1.3896	2.1152
	9104				0.1546	98.5256	1.3197	1.7947
	9105				0.2638	98.2650	1.4711	1.5961
	9106				0.3805	98.1362	1.4832	1.9299
AV	91	575	14	12.64	0.2966	98.3051	1.3983	2.0661
	12701				0.1288	99.4696	0.4016	1.2489
	12702				0.2100	99.3177	0.4722	3.0925
	12703				0.1235	99.7159	0.1606	3.7713
	12704				0.2857	99.4673	0.2470	0.6169
AV	127	575	27	12.64	0.1870	99.4926	0.3204	2.1824
	9201				0.0900	99.0085	0.9015	1.6940
	9202				0.1100	99.0756	0.8144	1.4718
	9203				0.1462	99.4109	0.4430	1.0363
	9204				0.1495	98.8707	0.9799	1.4562
AV	92	575	14	9.48	0.1239	99.0914	0.7847	1.4145
	12801				0.2117	98.8229	0.9654	−2.7674
	12802				0.2331	98.6836	1.0833	−2.1213
	12803				0.0999	99.2691	0.6311	−0.4389
	12804				0.1788	98.9107	0.9105	0.2063
AV	128	575	27	9.48	0.1809	98.9215	0.8975	−1.2803

	(1)	(2)	(3)	(4)	(5)	(6)	(7)	(8)
	5101				0.1377	99.6669	0.1954	-0.8964
	5102				0.2091	99.5840	0.2069	-0.3388
	5103				0.0910	99.7017	0.2073	-0.7377
	5104				0.1108	99.7195	0.1697	-1.1588
	5105				0.1279	99.6810	0.1911	-0.4998
AV	51	575	5	8.24	0.1353	99.6706	0.1941	-0.7263
	9301				0.0719	98.8362	1.0919	1.2331
	9302				0.0527	98.9851	0.9621	-0.5314
	9303				0.0893	98.9257	0.9850	-0.6374
	9304				0.0902	98.9079	1.0019	-0.3919
	9305				0.0707	99.0350	0.8943	-0.0991
AV	93	575	14	6.32	0.0750	98.9379	0.9870	-0.0853
	12901				0.0948	98.8250	1.0803	-2.2355
	12902				0.1023	98.9507	0.9470	-1.2901
	12903				0.2193	98.5624	1.2183	-1.4364
	12904				0.0923	98.5587	1.3490	-1.6639
AV	129	575	27	6.32	*0.1272	98.7241	1.1486	-1.6565
	9401				0.0263	99.0038	0.9699	0.6765
	9402				0.0174	98.7129	1.2696	1.5553
	9403				0.0338	98.7664	1.1998	1.0119
	9404				0.0342	98.8112	1.1546	1.6098
	9405				0.0323	98.7032	1.2644	1.4499
AV	94	575	14	3.16	0.0288	98.7994	1.1717	1.2607
	13001				0.0389	98.8208	1.1403	-0.5374
	13002				0.0442	98.9385	1.0173	0.5379
	13003				0.0280	98.9578	1.0142	-1.3388
	13004				0.0872	98.9579	0.9549	0.9347
AV	130	575	27	3.16	0.0496	98.9187	1.0317	-0.1009
	6401				0.0694	99.8953	–	0.0132
	6402				0.1124	99.8876	–	-0.1525
	6403				0.0732	99.8416	–	0.0012
	6404				0.0283	99.9717	–	-0.5501
	6405				0.0508	99.9492	–	-0.6717
AV	64	575	21	2.42	0.0666	99.9089	–	-0.2720

	(1)	(2)	(3)	(4)	(5)	(6)	(7)	(8)
	6501				–	99.7448	0.2513	0.2180
	6502				–	99.7529	0.2462	0.4765
	6503				–	99.7500	0.2408	0.1323
AV	65	575	21	1.24	–	99.7492	0.2461	0.2756
	6801				0.0325	99.9675	–	–1.2020
	6802				0.0335	99.9665	–	–1.0069
	6803				0.0292	99.9660	–	–1.3726
	6804				0.0340	99.9660	–	–1.1063
	6805				0.0254	99.9746	–	–0.9350
	6806				0.0210	99.9790	–	–1.1697
	6807				0.0313	99.9687	–	–1.0372
AV	68	575	21	0.13	0.0296	99.9704	–	–1.1185
	10101				0.4474	98.9514	0.6012	–0.5651
	10102				0.4785	98.6667	0.8547	–2.0951
	10103				0.4928	98.8872	0.6200	–1.2187
	10104				0.3596	99.0545	0.5860	–1.7454
AV	101	525	30	25.30	0.4446	98.8899	0.6655	–1.4061
	10201				0.1709	99.3683	0.4608	0.7454
	10202				0.4179	98.5452	1.0369	0.2506
	10203				0.4660	98.9501	0.5839	1.1216
	10204				0.5387	98.7230	0.7383	0.9167
AV	102	525	30	18.96	0.3984	98.8965	0.7050	0.7586
	2001				0.1535	99.7805	–	–0.7840
	2002				0.1645	99.7742	–	–1.2857
	2003				0.1898	99.7403	–	–0.6614
AV	20	525	14	14.57	0.1693	99.7650	–	–0.5770
	2601				0.1742	99.8258	–	–0.3065
	2602				0.1048	99.8952	–	–0.8224
	2603				0.0983	99.9017	–	–0.2625
AV	26	525	28	14.57	0.1258	99.8742	–	–0.4638
	10301				0.0949	99.3457	0.5594	1.5491
	10302				0.2332	99.1985	0.5683	1.2757
	10303				0.1508	99.0656	0.7835	1.5679
	10304				0.2421	99.0764	0.6815	1.1695
	10305				0.1974	99.1917	0.6109	0.7145
AV	103	525	30	12.64	0.1837	99.1755	0.6407	1.2553

	(1)	(2)	(3)	(4)	(5)	(6)	(7)	(8)
	10401				0.1717	98.4619	1.3664	1.4964
	10402				0.1110	98.9198	0.9692	0.7717
	10403				0.1074	98.8950	0.9976	2.8014
	10404				0.0978	98.9236	0.9786	3.4255
AV	104	525	30	9.48	0.1220	98.8000	1.0779	2.1237
	2101				0.0101	99.8434	0.1465	−0.2127
	2102				0.0145	99.8274	0.1581	0.8672
	2103				0.0119	99.8323	0.1558	0.8260
AV	21	525	14	8.24	0.0122	99.8343	0.1535	0.4935
	2701				0.0602	99.9398	−	−0.6516
	2702				0.0621	99.8802	−	1.3837
	2703				0.0597	99.8651	−	1.3629
	2704				0.0486	99.9514	−	1.1520
	2705				0.0670	99.8249	0.1081	1.4066
	2706				0.0610	99.8345	0.1045	1.7524
AV	27	525	28	8.24	*0.0598	99.8826		1.0677
	10501				−	98.7361	1.2524	0.2115
	10502				−	98.5238	1.4682	0.3119
	10503				−	99.0695	0.9233	0.1092
	10504				−	99.0084	0.9894	0.0909
AV	105	525	30	6.32	−	98.8344	1.1583	0.2061
	2801				0.0207	99.8773	−	01.5938
	2802				0.0201	99.8450	0.1348	−1.2522
	2803				0.0139	99.8776	0.1084	−2.7923
AV	28	525	28	3.57	0.0182	99.8666	0.1216	−1.8794
	10601				−	98.6310	1.3690	−0.2278
	10602				−	98.9859	1.0141	0.2838
	10603				−	98.8481	1.1517	0.5889
AV	106	525	30	3.16	−	98.8216	1.1783	0.2150
	7401				−	99.9414	−	−0.1062
	7402				−	99.9693	−	−0.1519
	7403				−	99.9551	−	0.1295
AV	74	525	21	2.42	−	99.9552	−	−0.0429

	(1)	(2)	(3)	(4)	(5)	(6)	(7)	(8)
	13701				0.6350	98.9928	0.3723	−2.0248
	13702				0.5975	98.7159	0.6866	−1.1634
	13703				1.1544	98.2849	0.5607	−2.3145
	13704				0.8234	98.7736	0.4030	−0.0035
AV	137	475	28	25.30	0.8026	98.6917	0.5056	−1.3766
	13801				2.7493	92.1526	5.0981	−0.9327
	13802				1.0228	97.2918	1.6854	−1.4001
	13802				1.0824	96.7922	2.1254	−0.1734
	13804				0.4991	98.0941	1.4067	0.3887
AV	138	475	28	18.96	* 1.3384	96.0826	2.25789	−0.5294
	13901				0.4009	98.3882	1.2109	−0.8685
	13902				0.2417	98.0685	1.6899	2.1626
	13903				0.4881	97.9217	1.5902	0.8902
AV	139	475	28	12.64	0.3769	98.1261	1.4970	0.7281
	14001				0.1806	98.5843	1.2351	0.0805
	14002				0.2480	98.6088	1.1432	−0.3072
	14003				0.1187	98.6305	1.2508	−0.7200
AV	140	475	28	9.48	0.1824	98.6078	1.2097	−0.3156
	14101				0.0936	98.3979	1.5085	−2.3883
	14102				0.0765	98.6605	1.2629	−0.8749
	14103				0.0642	98.8356	1.1002	0.0341
AV	141	475	28	6.32	0.0781	98.6313	1.2905	−1.0764
	14201				−	99.0228	0.9692	−0.9345
	14202				0.0222	98.8620	1.1158	−0.4600
	14203				0.0190	99.0663	0.9147	0.2267
	14204				0.0298	98.8570	1.1132	−1.0320
AV	142	475	28	3.16	0.0237	98.9520	1.0282	−0.5500
	8401				0.0651	98.9561	0.9788	−2.1223
	8402				−	99.9414	−	−2.2231
	8403				−	99.9536	−	−1.7681
	8404				−	99.9243	−	−1.7728
AV	84	475	21	2.42	−	99.6938	−	−1.9716
	8501				−	99.9706	−	−0.9408
	8502				−	99.9425	−	−0.2963
	8503				−	99.9376	−	−0.3932
AV	85	475	21	1.24	−	99.9502	−	−0.5434

	(1)	(2)	(3)	(4)	(5)	(6)	(7)	(8)
	17301				1.0383	97.8378	1.1239	-0.6822
	17302				1.0364	97.9057	1.0578	-0.1546
	17303				0.8734	98.2504	0.8762	0.2577
	17304				3.4306	95.2450	1.3244	-0.7474
	17305				1.5264	97.5093	0.9643	-2.7506
AV	173	420	47	25.30	*1.5810	97.3495	1.0693	-0.8154
	17401				0.6772	96.0201	3.3027	-0.3168
	17402				0.9380	95.4004	3.6616	0.3293
	17403				0.7330	96.0839	3.1831	1.7599
	17404				0.7226	99.2774	—	-1.0818
AV	174	420	47	18.96	*0.7677	96.6954	2.5369	0.1726
	17501				0.0270	99.7667	0.2062	-3.8843
	17502				0.0671	99.7049	0.2280	-2.3459
	17503				0.0905	99.3557	0.5538	-1.5013
AV	175	420	47	12.64	0.0615	99.6090	0.3293	-2.5772
	17601				0.0488	98.8885	1.0627	-0.3296
	17602				0.0713	98.5542	1.3746	-0.2819
	17603				0.1035	97.8129	2.0835	-0.2719
	17604				0.0745	98.1641	1.7613	0.6411
AV	176	420	47	9.48	0.0745	98.3549	1.5705	-0.0606
	·17701				0.0464	97.9253	2.0283	-1.9281
	17702				0.0734	97.9153	2.0114	0.1480
	17703				0.0412	97.9054	2.0534	-0.6739
AV	177	420	47	6.32	0.0537	97.9153	2.0310	-0.8180
	17801				0.0175	98.9668	1.0158	-1.2399
	17802				—	98.3505	1.6382	-0.8347
	17803				—	99.1069	0.8907	-1.2370
	17804				—	98.7110	1.2793	1.4325
AV	178	420	47	3.16	—	98.7837	1.2060	-0.4698
	18501				0.8397	98.2995	0.8606	-2.9797
	18502				0.9168	98.1632	0.9200	-0.2984
	18503				0.7339	98.4259	0.8402	-0.8469
	18504				0.5488	98.7192	0.7320	0.7356
	18505				0.4470	98.9258	0.6273	-1.6527
AV	185	403	47	25.30	0.6972	98.5066	0.7960	-1.0084

	(1)	(2)	(3)	(4)	(5)	(6)	(7)	(8)
	18601				0.5147	98.6087	0.8766	5.3293
	18602				0.5306	98.5642	0.9052	4.5795
	18603				0.4581	98.6569	0.8850	4.4730
	18604				0.4798	98.7259	0.7943	3.7539
AV	186	403	47	18.96	0.4958	98.6389	0.8653	4.5339
	18701				0.1034	98.1027	1.7939	-4.6445
	18702				0.1024	98.4297	1.4679	0.7335
	18703				0.0914	98.3363	1.5723	0.2682
	18704				0.0644	99.5007	0.4350	-2.9281
AV	187	403	47	12.64	0.0904	98.5923	1.3172	-1.6427
	18801				0.0603	98.7098	1.2299	-0.3481
	18802				0.0588	99.0265	0.9147	2.2298
	18803				0.0419	98.9568	1.0012	2.1911
AV	188	403	47	9.48	0.0537	98.8977	1.0486	1.3576
	18901				0.0862	98.5556	1.3581	0.6533
	18902				0.0414	98.6116	1.3470	0.4168
	18903					98.9743	1.0133	1.9763
AV	189	403	47	6.32	0.0638	98.7138	1.2395	1.0155
	19001				-	98.8145	1.1752	-0.2177
	19002				-	98.7525	1.2397	1.7796
	19003				-	98.7217	1.2782	1.7342
AV	190	403	47	3.16	-	98.7628	1.2311	1.0987
	19701				0.7604	97.4814	1.7582	2.1145
	19702				0.7145	97.4384	1.8471	1.9801
	19703				0.8684	97.6706	1.4609	0.0975
AV	197	305	46	25.30	0.7811	97.5301	1.6887	1.3974
	19801				0.4424	98.0870	1.4706	-1.9440
	19802				0.4613	96.6275	2.9111	-0.5518
	19803				0.5840	98.0405	1.3755	-1.6232
AV	198	305	47	18.96	0.4959	97.5850	1.9191	-1.3730
	19901				0.0194	98.5340	1.4466	2.6704
	19902				-	98.8837	1.1060	1.3535
	19903				0.0186	98.8110	1.1704	1.1671
AV	199	305	47	12.64	0.0190	98.7428	1.2410	1.7303

	(1)	(2)	(3)	(4)	(5)	(6)	(7)	(8)
	20001				–	98.5490	1.4394	1.2324
	20002				–	98.2995	1.6862	–4.1081
	20003				0.0179	98.3948	1.5873	–0.0386
AV	200	305	47	9.48	–	98.4144	1.5709	–0.9714
	20101				–	99.4002	0.5998	–0.0909
	20102				–	99.4137	0.5822	0.4101
	20103				–	99.3646	0.6227	1.9555
AV	201	305	47	6.32	–	99.3928	0.6016	0.7582
	20201				–	98.8429	1.1571	–2.3229
	20202				–	98.8044	1.1956	–1.7943
	20203				–	99.0323	0.9437	–0.5737
AV	202	305	47	3.16	–	98.8931	1.0988	–1.5636

Appendix III

Analyses Of Co In Sphalerite

Note - Appendix III

In the following tables, the numbered column headings refer to:

(1) Analysis identification number. For example, the identifier 15501 refers to an analysis of a single crystal of sphalerite from run 155. Repetition of the identifier indicates that analyses were carried out at two or more distinct spots on the crystal.

(2) Run temperature in °C

(3) Run time in days

(4) Weight per cent Co in sulphide charge

(5) Mole per cent CoS in sphalerite

(6) Mole per cent FeS in sphalerite

(7) Mole per cent ZnS in sphalerite

(8) Deviation of original analytical total (in weight per cent)
from 100%

Lines started by "AV" give the averages for the preceding set of analyses. The presence of an asterisk (*) preceding the average value of CoS indicates that the distribution of CoS is heterogeneous and that the calculation and use of an average for the set of analyses is probably not justified.

	(1)	(2)	(3)	(4)	(5)	(6)	(7)	(8)
	15501				2.6127	9.0903	88.2966	0.2520
	15501				2.6573	9.9682	87.3745	0.3723
	15502				2.1327	8.5504	89.3170	0.9036
	15502			:	2.1624	8.6162	89.2214	0.6735
	15503				2.0662	8.4014	89.5324	0.8800
	15503				2.3709	9.3120	88.3171	0.9604
AV	155	675	10	19.10	2.3337	8.9898	88.6764	0.6736
	15601				1.7496	10.2778	87.9726	1.8099
	15601				1.9640	11.6831	86.4529	-2.0785
	15602				1.5884	9.7562	88.6554	1.1032
	15602				1.6616	9.8920	88.4464	1.4221
	15603				1.7319	10.2825	87.9856	1.7198
	15603				1.6806	10.0359	88.2835	1.7196
AV	156	675	10	14.35	1.7294	10.3046	87.9660	0.9493
	15701				1.1637	10.2175	88.6188	0.5896
	15701				1.0846	10.5616	88.3538	1.4851
	15702				0.9014	10.3479	88.7507	1.0865
	15702				0.9852	10.1399	88.8749	1.7506
	15703				1.1422	10.7285	88.1294	1.4894
	15703				1.0492	10.6583	88.2926	1.3359
AV	157	675	10	9.57	1.0544	10.4423	88.5033	1.2895
	15801				1.5195	12.5227	85.9577	0.0433
	15801				1.2603	12.8207	85.9191	0.1811
	15802				0.7812	11.2853	87.9335	1.1020
	15802				0.7982	11.9423	87.2596	0.8517
	15803				0.7058	11.0350	88.2593	1.8426
	15803				0.7771	11.2556	87.9673	1.3634
AV	158	675	10	7.17	0.9737	11.8103	87.2160	0.8973
	15901				0.6605	12.3386	87.0009	0.3089
	15901				0.6222	12.2648	87.1130	0.2785
	15902				0.7661	12.6455	86.5884	0.1080
	15902				0.7412	12.6735	86.5853	-0.0149
	15903				0.6772	11.8230	87.4998	0.9260
	15903				0.6154	12.2520	87.1326	0.7399
AV	159	675	10	4.78	0.6804	12.3329	86.9866	0.3911
	16001				0.4091	14.2564	85.3345	-0.0435
	16001				0.4097	14.3421	85.2483	0.1728
	16002				0.3016	13.4762	86.2223	0.6633
	16002				0.3531	13.1594	86.4876	0.6061
	16003				0.4646	13.6961	85.8393	1.6408
	16003				0.5073	13.9684	85.5243	0.7679
AV	160	675	10	2.39	0.4076	13.8164	85.7760	0.6346

	(1)	(2)	(3)	(4)	(5)	(6)	(7)	(8)
	19001				0.8039	4.0437	95.1524	0.9967
	11901				0.8453	3.9897	95.1650	2.1113
	11902				1.3076	4.9275	93.7649	1.4431
	11902				1.4726	4.0992	94.4283	0.8817
	11903				0.7861	5.5826	93.6313	0.8584
	11903				0.8622	4.2458	94.8920	1.4224
	11904				0.8916	5.1156	93.9928	−1.6778
	11904				0.7533	3.7890	95.4577	−1.4766
AV	119	625	14	19.10	0.9653	4.4741	94.5605	0.5699
	12001				1.2424	5.4844	93.2732	1.6785
	12001				1.2834	5.3922	93.3244	2.0856
	12002				1.4694	5.1756	93.3550	2.8575
	12002				1.5343	5.1026	93.3632	2.4653
	12003				1.2725	5.2077	93.5197	2.0188
	12003				1.0709	4.6723	94.2569	2.9898
AV	120	625	14	14.35	1.3121	5.1725	93.5153	2.3492
	12101				0.7878	5.4329	93.7794	1.5686
	12101				0.8258	5.6979	93.4763	1.5275
	12102				0.7432	4.5757	94.6809	1.0298
	12102				0.6664	4.5759	94.7577	1.4947
	12103				0.7692	5.7381	93.4927	−0.2509
	12103				0.7205	5.0791	94.2004	0.5516
AV	121	625	14	9.57	0.7521	5.1833	94.0645	0.9869
	12201				0.8865	7.2499	91.8636	0.6818
	12201				0.8202	7.2556	91.9241	0.9741
	12202				0.8174	7.3360	91.8467	0.7012
	12202				0.7376	5.2016	94.0608	0.4142
	12203				0.8882	6.0703	93.0415	1.0829
	12203				0.8727	5.9828	93.1445	0.9663
AV	122	625	14	7.17	0.8371	6.5160	92.6468	0.8034
	12301				0.4969	5.3299	94.1732	−0.7270
	12301				0.4918	5.1482	94.3600	0.4874
	12302				0.4840	4.7833	94.7327	1.3648
	12302				0.5193	4.8389	94.6418	1.6138
	12303				0.5739	5.6543	93.7718	1.2977
	12303				0.5925	5.6319	93.7757	1.1178
AV	123	625	14	4.78	0.5264	5.2311	94.2425	0.8591

	(1)	(2)	(3)	(4)	(5)	(6)	(7)	(8)
	13101				0.5846	2.9898	96.4347	1.8188
	13101				0.5304	2.8539	96.6158	3.8219
	13102				0.5305	3.5137	95.9557	4.8786
	13102				0.6959	6.5147	92.7895	3.9163
	13103				0.4386	3.8870	95.6745	4.9753
	13101				0.6270	7.2828	92.0901	3.9149
AV	131	575	27	19.10	0.5678	4.5055	94.9266	3.8876
	9601				1.4718	4.2497	94.2785	-3.9233
	9601				1.1350	3.2969	95.5682	-0.8297
	9602				0.5766	2.5107	96.9128	0.9348
	9602				0.5443	2.4844	96.9714	0.8662
	9603				1.0862	4.7054	94.2084	-0.3611
	9603				1.0216	5.2571	93.7214	0.2440
	9604				1.1482	3.2104	95.6413	0.4571
	9604				1.4884	5.4108	93.1008	0.1844
AV	96	575	14	14.35	1.0590	3.8907	95.0502	-0.3035
	13201				0.7414	7.1752	92.9835	-0.3730
	13201				0.8027	7.3903	91.8070	3.6348
	13202				0.6126	6.1144	93.2731	3.1927
	13002				0.8727	9.9274	89.2000	1.9320
	13203				0.6609	4.8385	94.5007	4.1529
	13203				0.7250	6.9044	92.3706	3.1760
AV	132	575	27	14.35	0.7359	7.0583	92.2058	2.6192
	9701				0.2858	3.5745	96.1398	0.3014
	9701				0.2422	4.1334	95.6244	2.7800
	9702				0.3469	5.0473	94.6058	2.1716
	9702				0.3427	3.9457	95.7115	2.7187
	9703				0.3276	4.0469	95.6255	3.0316
	9703				0.3175	4.3274	95.3551	3.5291
AV	97	575	14	9.57	0.3105	4.1792	95.5103	2.4221
	13301				0.4632	5.9557	93.5810	-2.5946
	13301				0.4511	6.3551	93.1938	-0.6363
	13302				0.2085	3.3044	96.4871	4.3133
	13302				0.2466	3.3905	96.3629	3.8064

	(1)	(2)	(3)	(4)	(5)	(6)	(7)	(8)
	13303				0.3959	5.0110	94.5931	3.5255
	13303				0.6335	8.5710	90.7955	3.0542
AV	133	575	27	9.57	0.3998	5.4313	94.1689	1.9114
	13401				0.3142	5.0926	94.5933	−1.4655
	13401				0.3640	7.0964	92.5396	−1.2039
	13402				0.3736	5.2055	94.4210	−1.8866
	13402				0.3782	6.9862	92.6356	−1.5599
	13406				0.3318	6.5505	93.1176	−1.0633
	13406				0.3396	7.1375	92.5230	−0.8573
AV	134	575	27	7.17	0.3502	6.3448	93.3049	−1.3394
	13501				0.2863	4.6594	95.0544	−1.6483
	13501				0.7006	9.5447	89.7547	−0.8225
	13502				0.4242	7.7565	91.8193	−1.6242
	13502				0.2844	5.5016	94.2139	−1.1532
	13503				0.3054	4.5945	95.1002	−2.1963
	13503				0.3171	5.1089	94.5740	−2.4954
AV	135	575	27	4.78	0.3863	6.1943	93.4193	−1.6567
	10701				2.2381	7.6934	90.0686	1.7459
	10701				2.2481	8.6439	89.1081	2.1877
	10702				2.1749	8.8981	88.9270	2.7440
	10702				1.9945	8.0171	89.9884	2.8901
	10703				1.3606	3.2711	95.3683	3.6044
	10703				1.3796	3.4350	95.1854	4.2012
	10704				2.4969	7.9187	89.5845	0.2728
	10704				2.4232	7.8739	89.7029	0.2374
AV	107	525	30	19.10	2.0395	6.9689	90.9916	2.2354
	10801				1.7707	7.5527	90.6766	−1.7130
	10801				1.0186	4.1955	94.7859	−0.3464
	10802				1.6523	7.0366	91.3111	−2.0256
	10802				1.6562	7.0824	91.2615	−1.5346
	10803				1.6295	5.7027	92.6678	−2.9406
	10803				1.6151	5.9648	92.4202	−2.7082
AV	108	525	30	14.35	1.5571	6.2558	92.1870	−1.8781
	10901				1.1218	4.9215	93.9567	0.5444
	10901				1.0081	4.9929	93.9991	0.7129
	10902				0.7771	3.1103	96.1226	1.3593
	10902				0.7728	3.2017	96.0255	1.0213
	10903				0.9656	3.1286	95.9058	0.5774
	10903				0.8688	3.0376	96.0936	1.3604
AV	109	525	30	9.57	0.9190	3.7304	95.3505	0.9293

	(1)	(2)	(3)	(4)	(5)	(6)	(7)	(8)
	11001		.		1.7945	8.3187	89.8868	−1.2406
	11001				1.6720	7.9615	90.3666	−0.7574
	11002				0.8698	4.1181	95.0120	2.5850
	11002				1.1115	5.1712	93.7174	1.9266
	11003				0.6722	4.0471	95.2808	4.9610
	11003				0.7311	3.9387	95.3303	4.0062
	11004				1.1489	5.3598	93.4912	1.1590
	11004				1.4920	7.4945	91.0136	0.4893
AV	110	525	30	7.17	1.1865	5.8012	93.0123	1.6399
	11101				1.0944	6.4226	92.4830	4.9548
	11101				1.0707	6.3490	92.5803	3.8204
	11102				0.4703	5.0327	94.4971	4.5630
	11102				0.6530	6.5705	92.7765	4.1965
	11103				0.5626	5.7049	93.7325	0.9579
	11103				0.4974	4.5660	94.9366	0.7586
	11104				0.9218	6.8491	92.2290	1.4341
	11104				0.8664	6.7982	92.3354	1.1105
AV	111	525	30	4.78	0.7671	6.0366	93.1963	2.7245
	14301				1.4155	3.2224	95.3622	−0.6912
	14302				2.2466	7.3215	90.4320	−0.2884
	14303				3.6909	4.4686	91.8406	−1.0080
	14304				2.2562	8.2021	89.5418	0.6082
AV	143	475	28	19.10	2.4023	5.8036	91.7941	−0.3449
	14401				0.8831	6.1063	93.0107	−0.0311
	14402				1.0388	8.5869	90.3743	0.1659
	14403				1.0956	7.2629	91.6415	−1.9134
AV	144	475	28	14.35	1.0058	7.3187	91.6754	−0.9262
	14501				0.5197	2.9178	96.5625	1.2794
	14502				0.7379	4.1700	95.0921	−0.0161
	14503				0.6525	7.6016	91.7459	1.1894
AV	145	475	28	9.57	0.6367	4.8965	94.4668	0.8176
	14601				0.8388	4.1747	94.9865	1.8484
	14602				0.7883	3.0644	96.1473	1.9974
	14603				1.8713	8.4073	89.7214	0.3467
	14604				1.4173	5.2018	93.3809	−1.1615
AV	146	475	28	7.17	1.2289	5.2121	93.5590	0.7577

	(1)	(2)	(3)	(4)	(5)	(6)	(7)	(8)
	14701				0.6525	8.7352	90.6123	-1.0884
	14702				0.9740	6.2301	92.7959	2.9359
	14703				0.4511	5.7437	93.8052	2.7435
AV	147	475	28	4.78	0.6925	6.9030	92.4044	1.5303
	14801				1.2604	9.1024	89.6372	-3.4470
	14802				0.7199	5.6719	93.6082	1.0398
	14803				1.6618	10.6715	87.6667	-1.9513
AV	148	475	28	2.39	1.2140	8.4819	90.3040	-1.4528
	17901				2.2202	10.4660	87.3139	-0.3629
	17902				2.0104	3.5582	94.4314	2.5597
	17903				0.7043	1.5378	97.7580	-0.1913
	17904				0.8770	1.6009	97.5221	-0.1842
	17905				0.7149	1.8794	97.4057	0.8129
	17906				0.8778	1.6209	97.5013	0.1534
AV	179	420	47	19.10	*1.2341	3.4439	95.3220	0.4646
	18001				1.0372	3.2726	95.6903	-1.4709
	18002				0.8696	1.9639	97.1666	-0.7936
	18003				1.5727	6.4203	92.0071	-2.3619
	18004				1.0549	3.0742	95.8709	-4.4853
AV	180	420	47	14.35	1.1336	3.6827	95.1837	-2.2779
	18101				0.3678	1.9864	97.6459	-1.0447
	18102				0.3485	2.0932	97.5584	0.1243
	18103				0.3394	1.7431	97.9176	-0.3722
	18104				0.4482	2.1532	97.3987	-0.2260
AV	181	420	47	9.57	0.3759	1.9940	97.6301	-0.3797
	18201				0.9036	10.8028	88.2936	-2.6929
	18201				0.6388	5.6648	93.6964	0.9739
	18203				0.3411	2.4287	97.2302	1.5653
	18204				0.3696	2.7565	96.8739	1.7310
AV	182	420	47	7.17	0.5633	5.4132	94.0236	0.3943
	18301				0.2913	2.4938	97.2149	-1.2781
	18302				0.2526	2.2393	97.5081	-0.0411
	18303				0.2223	1.7319	98.0458	1.7179
	18304				0.1775	1.6486	98.1740	-0.1434
AV	183	420	47	4.78	0.2359	2.0284	97.7356	0.0638

	(1)	(2)	(3)	(4)	(5)	(6)	(7)	(8)
	18401				0.2771	3.3901	96.3329	0.8949
	18402				0.3794	3.1497	96.4709	1.5357
	18403				0.1222	3.0499	96.8278	1.5591
AV	184	420	47	2.39	0.2596	3.1966	96.5439	1.3299
	19101				2.0666	2.1937	95.7397	-4.4146
	19102				2.4313	1.5990	95.9697	-4.2162
	19103				1.7637	1.7380	96.4984	-2.6167
AV	191	403	47	19.10	2.0872	1.8436	96.0692	-3.7492
	19201				1.6281	2.2762	96.0957	-3.5494
	19202				1.3333	2.2351	96.4316	-0.8051
	19203				0.8799	0.9726	98.1475	-1.8585
AV	192	403	47	14.35	1.2804	1.8280	96.8916	-2.0710
	19301				1.1371	3.0139	95.8490	-2.9559
	19302				0.8624	2.2921	96.8456	-3.8363
	19303				1.2852	2.5851	96.1297	0.5524
AV	193	403	47	9.57	1.0949	2.6304	96.2747	-2.0799
	19401				0.6876	1.6145	97.6979	-1.1411
	19402				0.6083	1.7822	97.6095	1.9448
	19403				0.7328	1.7436	97.5237	1.4815
	19404				0.5989	1.9167	97.4844	2.0984
AV	194	403	47	7.17	0.6569	1.7642	97.5788	1.0959
	19501				0.6305	2.5962	96.7733	1.0476
	19502				0.4962	1.9270	97.5769	0.5389
	15903				0.3022	1.1215	98.5763	0.0016
AV	195	403	47	4.78	0.4763	1.8816	97.6421	0.5294
	19601				0.2218	2.0712	97.7071	0.7892
	19602				0.2627	2.1589	97.5784	3.1504
	19603				0.1853	1.3818	98.4329	2.3584
AV	196	403	47	2.39	0.2233	1.8706	97.9061	2.0993
	20301				1.6763	2.3255	95.9982	-1.8701
	20302				1.7921	1.4922	96.7157	-3.3680
	20303				2.6017	2.9766	94.4217	-4.4570
AV	203	305	47	19.10	2.0234	2.2648	95.7118	-3.2317

	(1)	(2)	(3)	(4)	(5)	(6)	(7)	(8)
	20401				4.2131	11.8462	83.9408	-0.7869
	20402				1.6206	2.2487	96.1307	2.5831
	20403				1.4983	3.0809	95.4208	1.2341
AV	204	305	47	14.35	*2.4440	5.7253	91.8307	1.0101
	20501				0.8076	2.6629	96.5295	2.1442
	20502				0.7820	1.7310	97.4870	3.8128
	20503				0.4653	1.2960	98.2386	3.6891
AV	205	305	47	9.57	0.6850	1.8967	97.4183	3.2154
	20601				0.2515	1.6529	98.0957	-1.8851
	20602				0.2124	1.7185	98.0690	-0.4872
	20603				0.2084	1.7302	98.0615	-1.3295
AV	206	305	47	7.17	0.2241	1.7005	98.0753	-1.2339
	20701				0.1403	2.5942	97.2655	-0.1896
	20702			.	0.1316	1.5341	98.3344	4.3383
	20703				0.3660	2.1264	97.5077	-0.0764
AV	207	305	47	4.78	*0.2127	2.0849	97.7025	1.3574
	20801				0.0359	0.7426	99.2215	-3.8060
	20802				0.0615	0.9447	98.9939	-1.0039
	20803				0.0295	0.9782	98.9924	-1.8698
AV	208	305	47	2.39	0.0423	0.8885	99.0692	-2.2266

Appendix IV

Analyses of Co In Pyrite

Note - Appendix IV

In the following tables, the numbered column headings refer to:

(1) Analysis identification number. For example, the identifier 15501 refers to an analysis of a single crystal of pyrite from run 155. Repetition of the identifier indicates that analyses were carried out at two or more distinct spots on the crystal.

(2) Run temperature in °C

(3) Run time in days

(4) Weight per cent Co in sulphide charge

(5) Mole per cent CoS_2 in pyrite

(6) Mole per cent FeS_2 in pyrite

(7) Mole per cent ZnS_2 in pyrite

(8) Deviation of original analytical total (in weight per cent) from 100%.

Lines started by "AV" give the averages for the preceding set of analyses. The presence of an asterisk (*) preceding the average value of CoS_2 indicates that the distribution of CoS_2 is heterogeneous and that the calculation and use of an average for the set of analyses is probably not justified.

- = element not detected.

	(1)	(2)	(3)	(4)	(5)	(6)	(7)	(8)
	15501				50.4332	48.0282	1.5386	1.2149
	15502				56.1073	43.0879	0.8047	0.4183
	15503				56.8135	42.6240	0.5625	−0.0130
	15504				56.9815	42.3696	0.6488	−1.3059
	15505				50.5431	48.6969	0.7599	1.4640
	15506				47.3895	51.9897	0.6207	−0.6296
AV	155	675	10	19.10	53.0446	46.1327	0.8225	0.1914
	15601				39.0248	60.3000	0.6752	1.3848
	15601				40.5347	58.8652	0.6001	1.9623
	15602				44.9007	54.3676	0.7317	0.8519
	15602				46.4224	52.9251	0.6525	1.4043
	15603				39.2727	60.1235	0.6038	−0.4470
	15603				39.8251	59.5329	0.6420	0.7216
	15604				52.6449	46.5640	0.7910	1.0809
	15604				49.2840	49.8349	0.8811	0.1513
	15605				41.7848	57.6881	0.5271	1.5389
	15605				40.7334	58.6870	0.5796	0.6322
AV	156	675	10	14.35	43.4427	55.8887	0.6684	0.9281
					34.3730	65.6269	−	−0.6921
	15701							
	15702				35.6264	64.4123	−	0.3090
	15703				27.6273	72.1196	0.2530	0.3819
	15704				26.9467	71.8617	1.1915	−1.0871
	15705				36.0194	63.2333	0.7473	1.8312
	15706				36.5621	62.9464	0.4914	1.5171
	15707				33.9422	65.6026	0.4552	1.3826
	15708				30.8379	67.5853	1.5768	2.3381
	15709				33.1727	66.4635	0.3638	1.3842
AV	157	675	10	9.57	32.7786	66.6501	0.5711	0.8183
	15801				21.1122	77.0142	1.8735	−0.0673
	15802				19.9195	79.0850	0.9955	−3.0013
	15803				21.3797	77.6844	0.9359	0.6511
	15804				21.5107	77.4861	1.0031	0.5200
	15805				20.8875	78.1394	0.9731	0.1068
	15806				18.7640	80.2048	1.0313	−0.9644
	15807				18.8767	80.1363	0.9870	0.4478
AV	158	675	10	7.17	20.3500	78.5357	1.1142	−03296
	15901				14.2102	84.3508	1.4390	−0.5206
	15902				23.9060	75.4782	0.6157	1.7082
	15903				21.7195	77.3054	0.9750	2.0374
	15904				13.0482	86.0508	0.9010	1.2344
	15905				18.2217	80.7267	1.0516	1.7791
	15906				14.4340	84.8094	0.7566	1.8982

	(1)	(2)	(3)	(4)	(5)	(6)	(7)	(8)
	15907				15.5928	83.8462	0.5610	2.2466
	15908				14.6059	72.7050	1.6891	0.6404
AV	159	675	10	4.78	16.9673	82.0340	0.9986	1.3780
	16001				11.7941	87.2349	0.9710	-3.6063
	16002				8.8882	90.1664	0.9454	-0.0170
	16003				9.2438	89.8321	0.9241	-0.5000
	16004				10.1623	88.9613	0.8764	-0.4409
	16005				8.2677	90.7808	0.9515	0.5463
AV	160	675	10	2.39	9.6712	89.3950	0.9337	-0.8036
	11901				55.8182	44.1818	-	1.7819
	11902				51.1988	48.8011	-	3.1230
	11903				57.2606	42.6878	-	3.6020
	11904				45.8176	54.1180	-	2.0461
	11905				55.6102	44.2491	0.1407	3.7586
AV	119	625	14	19.19	53.1411	46.8076	-	2.8623
	12001				29.7614	68.7889	1.4497	2.3324
	12002				35.2007	63.2523	1.5471	4.6780
	12003				40.8264	58.4719	0.7017	0.4613
	12004				29.7109	69.6528	0.6363	2.4604
	12005				42.5824	56.6995	0.7181	4.5149
	12006				30.5007	68.8808	0.6185	2.6834
AV	120	625	14	14.35	34.7637	64.2910	0.9452	2.8551
	12101				26.4075	73.0851	0.5074	0.5493
	12102				25.2450	74.0590	0.6960	1.3011
	12103				32.7334	66.5086	0.7579	1.8790
	12104				29.3302	70.1077	0.5621	-1.1016
	12105				25.0316	74.4595	0.5089	0.7852
	12106				26.8377	71.9538	1.2085	2.2380
AV	121	625	14	9.57	27.5976	71.6956	0.7068	0.9418
	12201				21.0075	77.7205	1.2719	1.7165
	12202				24.3255	74.7377	0.9368	1.6554
	12203				46.6083	52.2274	1.1643	3.5240
	12204				28.7267	70.4840	0.7893	2.6102
	12205				33.7448	65.4348	0.8204	3.3234
	12206				22.0018	76.9328	1.0654	2.9120
	12207				45.0017	54.4167	0.5816	3.5976
AV	122	625	14	7.17	31.6309	67.4219	0.9471	2.7627

	(1)	(2)	(3)	(4)	(5)	(6)	(7)	(8)
	12301				25.3899	73.7165	0.8936	-0.7457
	12302				28.7032	69.7132	1.5835	-1.0433
	12303				24.0267	74.9916	0.9818	-1.2178
	12304				37.7181	61.4493	0.8326	0.4605
	12305				26.9988	72.1301	0.8712	-0.8509
	12306				38.3716	60.5210	1.1074	-1.6137
AV	123	625	14	4.78	30.2014	68.7535	1.0450	-0.8352
	13101				45.6787	52.8912	1.4301	0.7422
	13102				43.1504	56.1972	0.6524	1.8282
	13103				15.9687	81.8890	2.1423	-1.9235
	13104				15.5833	83.3702	1.0465	-1.8431
	13105				42.0978	57.3032	0.5989	-0.6424
	13106				20.0386	77.6703	2.2911	-0.7918
AV	131	575	27	19.10	*30.4196	68.2201	1.3602	-0.4384
	9601				47.4945	51.1006	1.4048	-3.4588
	9602				46.7747	52.2041	1.0212	4.0749
	9603				55.4903	42.9031	1.6066	4.5655
	9604				44.1769	54.2412	1.5818	4.4052
AV	96	575	14	14.35	48.4841	50.1123	1.4036	2.3967
	13201				54.4406	44.4218	1.1376	-0.2668
	13202				45.8715	53.1434	0.9850	-0.0707
	13203				49.9203	48.7450	1.3347	-0.2518
	13204				28.4329	69.5283	2.0388	-2.9850
	13205				45.3377	52.8518	1.8105	-0.4859
	13206				46.9203	50.9402	2.1395	-0.9689
AV	132	575	27	14.35	*45.1538	53.2717	1.5744	-0.8382
	9701				18.0738	80.2928	1.6334	-0.7320
	9702				37.9213	60.3036	1.7751	-1.3212
	9703				32.5846	65.7287	1.6867	-0.9502
	9704				34.7365	63.3878	1.8756	1.0003
	9705				38.4949	58.7931	2.7120	-1.1446
AV	97	575	14	9.57	*32.3622	65.7012	1.9365	-0.6296

	(1)	(2)	(3)	(4)	(5)	(6)	(7)	(8)
	13301				26.3241	72.1499	1.5259	0.9190
	13302				38.5934	59.0078	2.3988	−0.5388
	13303				45.6258	52.5997	1.8745	−1.2817
	13304				42.4125	55.5658	2.0217	−0.0074
	13305				36.1944	62.1093	1.6963	−1.0708
	13306				39.4306	59.1097	1.4596	−0.4705
AV	133	575	27	9.57	38.0968	60.0736	1.8295	−0.4084
	13401				19.6756	78.4042	1.9202	0.2486
	13402				19.3460	78.4570	2.1970	0.3867
	13403				22.0303	76.9634	1.0062	−1.2902
	13404				24.5880	73.4400	1.9720	−1.0092
AV	134	575	27	7.17	21.4100	76.8161	1.7739	−0.4160
	13501				40.4859	58.1871	1.3279	−0.9174
	13502				25.6645	72.6107	1.7248	−1.4985
	13503				7.1903	91.0512	1.7585	−0.2161
	13504				36.8527	60.8621	2.2852	−1.9882
	13505				50.6036	47.0269	2.3695	−2.0240
	13506				43.4402	54.6221	1.9377	−1.6522
	13507				43.2813	55.6371	1.0816	−1.1134
	13508				37.2299	61.4267	1.3434	−1.4427
AV	135	575	27	4.78	*35.5934	62.6779	1.7286	−1.3566
	10701				76.3958	23.0095	0.5947	4.1084
	10702				65.8809	33.5027	0.6163	5.2745
	10703				64.5607	33.7815	1.6578	4.8929
AV	107	525	30	19.10	68.9458	30.0979	0.9563	4.7586
	10801				64.7878	34.0065	1.2056	4.1426
	10802				58.3623	40.2536	1.3841	4.1573
	10803				70.8998	27.4464	1.6538	4.8017
	10804				65.1389	33.3015	1.5597	3.5416
AV	108	525	30	14.35	64.7972	33.7520	1.4508	4.1608
	10901				68.6086	29.3425	2.0488	3.0869
	10902				66.6675	31.1509	2.1815	4.0988
	10903				52.4743	45.3061	2.2195	4.1513
	10904				54.8665	43.0877	2.0458	5.3053
AV	109	525	30	9.57	60.6542	37.2218	2.1239	4.1606

	(1)	(2)	(3)	(4)	(5)	(6)	(7)	(8)
	11001				70.8250	27.7350	1.4400	5.3731
	11002				53.8350	44.5982	1.5668	3.2180
	11003				65.1024	33.3800	1.5176	3.9813
	11004				65.5100	32.9399	1.5501	4.0596
	11005				69.6257	29.3343	1.0400	4.2500
AV	110	525	30	7.17	*64.9796	33.5975	1.4229	4.1764
	11101				59.6182	38.4364	1.9454	2.9218
	11102				44.9509	53.3616	1.6874	2.3054
	11103				64.6486	33.3534	1.9980	4.7034
	11104				74.2071	23.6863	2.1065	4.9122
AV	111	525	30	4.78	60.8562	37.2094	1.9343	3.7107
	14301				59.7908	36.3127	3.8965	-1.5379
	14302				64.4613	31.2079	4.3308	-0.6699
	14303				0.6752	95.1455	4.1793	1.6552
	14304				54.9986	40.3255	4.6759	0.0594
AV	143	475	28	19.10	*49.2945	46.4808	4.2247	-0.4724
	14401				46.2540	52.9779	0.7681	-2.2850
AV	144	475	28	14.35	46.2540	52.9779	0.7681	-2.2850
	14501				58.7464	40.2385	1.0151	-0.8218
	14502				49.2495	49.6031	1.1474	-2.3132
	14503				66.1609	32.9186	0.9205	-1.2498
	14504				67.2644	31.6705	1.0651	-0.2384
	14505				58.7599	40.3451	0.8950	0.2661
	14506				47.5503	51.2309	1.2188	1.1490
AV	145	475	28	9.57	57.9552	41.0011	1.0436	-0.5347
	14601				2.2451	97.6198	0.1351	-3.7426
	14602				1.4989	98.2881	0.2129	-0.0584
	14603				·2.5400	97.0308	0.4292	-1.4698
	14604				1.2033	98.6446	0.1522	0.6348
AV	146	475	28	7.17	1.8718	97.8958	0.2323	-1.1590
	14701				1.2117	98.2314	0.5569	-1.8300
	14702				1.0547	98.4997	0.4456	-0.9508
	14703				0.8309	98.6531	0.5160	0.8438
	14704				2.5582	96.5597	0.8821	-1.4576
	14705				0.8462	98.5036	0.6502	-0.7623
AV	147	475	28	4.78	* 1.3003	98.0894	0.6102	-0.8314

	(1)	(2)	(3)	(4)	(5)	(6)	(7)	(8)
	14801				1.7670	97.1702	1.0628	-2.2838
	14802				0.1879	98.7541	1.0580	0.3072
	14803				0.2139	98.5542	1.2319	-1.2204
	14804				0.7388	98.0813	1.1799	-2.9281
	14805				0.1678	98.3684	1.4638	0.8030
AV	148	475	28	2.39	* 0.6151	98.1855	1.1993	-1.0644
	17901				73.9917	25.2601	0.7482	-0.5201
	17902				69.7212	29.5802	0.6985	-3.4751
	17903				62.9494	36.1540	0.8969	-0.6696
	17904				62.4685	36.6725	0.8590	-0.4444
	17905				59.9349	38.7966	1.2685	-0.3685
	17906				64.4473	34.6369	0.9158	0.5128
AV	179	420	47	19.10	65.5854	33.5167	0.8978	-0.8275
	18001				1.7181	97.7415	0.5404	-1.0898
	18002				1.0521	98.3734	0.5745	-0.0344
	18003				44.9924	54.4177	0.5899	-2.4909
	18004				53.5986	45.7455	0.6559	-2.1224
	18005				57.7516	41.6653	0.5831	-2.2346
	18006				58.0028	41.3943	0.6029	-1.6383
AV	180	420	47	14.35	*36.1859	63.2229	0.5911	-1.6017
	18101				58.1932	40.8629	0.9438	0.5437
	18102				46.6850	52.4842	0.8308	-3.4782
	18103				56.3109	42.8786	0.8105	-1.1340
	18104				56.8086	42.3378	0.8536	-0.5347
	18105				59.3689	39.8212	0.8098	-1.8665
AV	181	420	47	9.57	*55.4733	43.6770	0.8497	-1.2939
	18201				48.3459	51.6541	–	-0.2854
	18202				49.7970	50.2030	–	-1.4787
	18203				43.6420	56.3580	–	1.0526
	18204				52.8693	47.1306	–	-1.0417
	18205				49.5025	50.4974	–	-1.1392
AV	182	420	47	7.17	48.8314	51.1686	–	-0.5785
	18301				60.1302	38.2992	1.5706	-2.4477
	18302				0.3593	98.9099	0.7308	-2.0245
	18303				1.1582	97.7399	1.1019	-2.3561
	18304				62.1985	37.3653	0.4362	-1.5414
	18305				62.2466	37.2213	0.5321	-1.5564
	18306				65.0905	34.4335	0.4760	-2.3061
AV	183	420	47	4.78	*41.8639	57.3281	0.8079	-2.0387

	(1)	(2)	(3)	(4)	(5)	(6)	(7)	(8)
	18401				0.0693	98.3732	1.5575	−4.2910
	18402				50.7447	48.4562	0.7991	−2.0790
	18403				0.1307	99.1259	0.7434	−4.3081
	18404				0.2241	98.5825	1.1935	−2.3366
AV	184	420	47	2.39	*12.7922	86.1344	1.0734	−3.2537
	19101				72.6049	26.7425	0.6527	2.5707
	19102				84.6860	14.3792	0.9348	3.3620
	19103				83.9241	15.0900	0.9859	3.2057
	19104				83.5094	15.7695	0.7211	2.9220
	19105				78.1320	21.1570	0.7109	3.1238
	19106				78.9617	20.3737	0.6645	3.6642
AV	191	403	47	19.10	80.3029	18.9186	0.7783	3.1414
	19201				1.1580	98.6301	0.2119	0.9509
	19202				4.7594	94.8462	0.3944	2.5686
	19203				4.6223	95.1714	0.2063	3.2412
	19204				78.8034	20.8507	0.3459	4.4014
	19205				86.1136	13.6583	0.2281	3.9835
	19206				54.5082	45.2985	0.1933	2.5668
AV	192	403	47	14.35	*38.3275	61.4091	0.2633	2.9521
	19301				0.6238	98.9253	0.4509	−1.4988
	19302				1.3976	98.0007	0.6016	−0.5986
	19303				83.6758	15.4070	0.9173	3.8815
	19304				83.6562	15.9921	0.3517	3.1193
	19305				74.1612	25.4147	0.4241	3.0587
AV	193	403	47	9.57	*48.7029	50.7479	0.5491	1.5924
	19401				0.2549	99.6117	0.1334	0.1562
	19402				88.5854	9.2963	2.1183	3.9698
	19403				84.7651	14.5224	0.7125	1.9064
	19404				0.3774	99.1156	0.5070	0.7475
	19405				89.8378	9.7648	0.3975	1.7900
AV	194	403	47	7.17	*52.7641	46.4621	0.7737	1.7140
	19501				0.4904	99.3063	0.2033	−2.2992
	19502				24.5393	74.4768	0.9838	−0.3622
	19503				82.5320	15.9302	1.5378	2.7436
	19504				22.8820	76.0945	1.0234	0.5672
AV	195	403	47	4.78	*32.6109	66.4520	0.9371	0.1623

	(1)	(2)	(3)	(4)	(5)	(6)	(7)	(8)
	19601				2.1409	97.1376	0.7215	1.0379
	19602				1.2948	97.9236	0.7815	1.8632
	19603				1.9013	97.3544	0.7443	2.2411
AV	196	403	47	2.39	1.7790	97.4718	0.7491	1.7141
	20301				0.6896	98.9398	0.3706	-0.9686
	20302				6.4459	92.7885	0.7656	-1.0425
	20303				74.7010	24.7350	0.5639	1.9735
	20304				8.6881	91.2579	0.0540	-1.9839
AV	203	305	47	19.10	*22.6311	76.9303	0.4385	-0.5054
	20401				7.8546	91.6052	0.5403	-0.5951
	20402				83.4362	15.0448	1.5189	0.5052
	20403				72.0727	27.1453	0.7819	-0.3843
AV	204	306	47	14.35	*54.4545	44.5984	0.9470	-0.1581
	20501				4.3781	95.0617	0.5603	0.6513
	20502				3.5350	95.8482	0.6167	-0.1159
	20503				8.5568	87.6547	3.7885	1.4116
	20504				2,5938	97.3730	—	-0.9411
AV	205	305	47	9.57	4.7659	93.9844	1.6552	0.2515
	20601				0.1877	99.8123	—	-1.8708
	20602				1.9367	97.8439	0.2194	-0.5966
	20603				6.6887	93.2983	—	1.2847
	20604				0.8912	98.9389	0.1700	-2.9064
	20605				1.2438	98.6501	0.1061	-0.2093
	20606				4.1146	95.8854	—	0.0952
AV	206	305	47	7.17	*2.5104	97.4047	—	-0.7005
	20701				0.8724	98.8526	0.2750	-0.8527
	20702				1.2825	97.8663	0.8512	-3.1910
	20703				0.3803	99.3004	0.3194	-.29665
AV	207	305	47	4.78	0.8450	98.6731	0.4819	-2.3367
	20801				1.1417	98.3974	0.4609	-4.8167
	20802				1.8315	97.9754	0.1932	-1.7949
	20803				5.8512	93.6521	0.4966	-0.3743
	20804				2.2089	97.4642	0.3269	-4.3639
	20805				2.0320	97.4548	0.5131	-1.6820
AV	208	305	47	2.39	*2.6131	96.9887	0.3981	-2.6064

REFERENCES

Arnold, R. G., Coleman, R. G. and Fryklund, V. C. (1962) Temperature of crystallization of pyrrhotite and sphalerite from the Highland-Surprise mine, Coeur D'Alene district, Idaho: Econ. Geol., vol. 57, p.1163-1174.

Barnard, M. M. (1965) Solubilities of selected chalcophile elements in hydrothermally synthesized β-ZnS (Sphalerite): Ph.D. Thesis, The Pennsylvania State University.

Barton, P. B. Jr., Bethke, P. M. and Toulmin, P. III (1963) Equilibrium in ore deposits: Min. Soc. Am., Special Paper 1, p.171-185.

Barton, P. B. Jr. and Toulmin, P. III (1966) Phase relations involving sphalerite in the Fe-Zn-S system: Econ. Geol., vol. 61, no. 5, p.815-849.

Bethke, P. M. (1967) Personal communication.

Bethke, P. M. and Barton, P. B. (1959) Trace-element distribution as an indicator of pressure and temperature of ore deposition (Abstract): Bull. Geol. Soc. Am., vol. 70, p.1569-1570.

Bethke, P. M. and Barton, P. B. (1971) Distribution of some minor elements between coexisting sulfide minerals: Econ. Geol., vol. 66, p.140-163.

Bethke, P. M., Barton, P. B. and Page, N. J. (1958) Preliminary experiments on the distribution of selenium between coexisting sulfides (Abstract): Bull. Geol. Soc. Am., vol. 69, p.1759-1760.

Boorman, R. S. (1966) Subsolidus studies in the system FeS-ZnS (303-714°C): Ph.D. Thesis, Dept. Geology, University of Toronto.

Boorman, R. S. (1967) Subsolidus studies in the ZnS-FeS-FeS$_2$ system: Econ. Geol., vol. 62, p.614-631.

Boyd, F. R. (1968) Quantitative electron-probe analysis of pyroxenes: Annual Rpt. Div. Geophys. Lab., Carnegie Inst. Wash Year Book 66, p.327-334.

Burns, R. G. (1970) Mineralogical applications of crystal field theory: Cambridge University Press.

Cabri, L. J. (1969) Density determinations: Accuracy and application to sphalerite stoichiometry: Am. Mineral., vol. 54, p.539-548.

147

Czamanske, G. K. and Goff, F. E. (1973) The character of Ni^{+2} as demonstrated by solid solutions in the Ni-Fe-Zn-S system: Econ. Geol., vol. 68, p.258-268.

Delarue, G. (1960) Propriétés chemiques dans l'eutectique LiCl-KCl fondu II. - Soufre, sulfures, sulfites, sulfates: Bull. Soc. Chim. France, 1960, p.906-910.

Delarue, G. (1962) Comportement des oxydes et des sulfures métalliques dans l'eutectiques LiCl-KCl fondu - Reactions chimiques mettant en jeu les ions O^{2-} et S^{2-}: Chimie Analytique, vol. 44, no. 3, p.91-101.

Denbigh, K. (1971) The principles of chemical equilibrium: Cambridge Univeristy Press, Third Edition.

Dixon, W. J. and Massey, F. J. (1957) Introduction to statistical analysis: McGraw-Hill Book Co., Inc., New York.

Doe, B. R. (1962) Distribution and composition of sulfide minerals at Balmat, New York: Bull. Geol. Soc. Am., vol. 73, p.833-854.

Duncumb, P. and Reed, S. J. B. (1968) The calculation of stopping power and backscatter effects in electron probe microanalysis: in Quantitative Electron Probe Microanalysis, ed. Heinrich, K. F. J., National Bureau of Standards Special Publication no. 298, p. 133-154.

Fleischer, M. (1955) Minor elements in some sulfide minerals: Econ. Geol., 50th Ann. Vol., p.970-1024.

Frazer, J. Z., Fitzgerald, R. W. and Reid, A. M. (1966) Computer programs EMX and EMX2 for electronmicroprobe data processing: SIO Reference 66-14, June 20, 1966, Scripps Institution of Oceanography, University of California, La Jolla, California, 67 p.

Frazer, J. Z. (1967) A computer fit to mass absorption coefficient data: SIO Reference 67-29, Institute for the Study of Matter, University of California, La Jolla, California, 19 p.

Fyfe, W. S. (1964) Geochemistry of solids, an introduction: McGraw-Hill Co., Ltd.

Ghosh-Dastidar, P. (1969) A study of trace elements in selected Appalachian sulfide deposits: Ph.D. Thesis, University of New Brunswick.

Ghosh-Dastidar, P., Pajari, G. E. Jr. and Trembath, L. T. (1970) Factors affecting the trace element partition coefficients between coexisting sulfides: Econ. Geol., vol. 65, p.815-837.

Goldstein, J. I. and Comella, P. A. (1969) A computer program for electron probe microanalysis in the field of metallurgy and geology: Report X-642-69-115, Goddard Space Flight Center, Greenbelt, Maryland, 82 p.

Halbig, J. B. (1965) Solubility of selected chalcophile elements in hydrothermally synthesized galena: unpublished MSc. Thesis, The Pennsylvania State University, 111 p.

Halbig, J. B. (1969) Trace element studies in sythetic sulfide systems: The solubility of thallium in sphalerite and the partition of selenium between sphalerite and galena: Ph. D. Dissertation, College of Earth and Mineral Sciences, The Pennsylvania State University.

Halbig, J. B. and Wright, H. D. (1969) Distribution of selenium between hydrothermally synthesized sphalerite and galena at trace-level concentrations (Abstract): Trans. Am. Geophys. Union, vol. 50, no. 4, p.339.

Hall, W. E. (1961) Unit-cell edges of cobalt-iron bearing sphalerites: U. S. Geol. Survey Prof. Paper 424-B, p.271-273.

Hall, W. E., Rose, H. J. and Simon, F. (1971) Fractionation of minor elements between galena and sphalerite, Darwin lead-zinc-silver mine, Ingo County, California and its significance in geothermometry: Econ. Geol., vol. 66, p.602-606.

Heinrich, K. F. J. (1966) X-ray absorption uncertainty: in Electron Microprobe, Proc. Symp. Electron Microprobe, Washington, D. C., 1964, ed. T. D. McKinley, K. F. J. Heinrich and D. B. Wittry, John Wiley and Sons, Inc., p.269-377.

Holland, H. D. (1956) The chemical composition of vein minerals and the nature of ore forming fluids: Econ. Geol., vol. 51, p.781-797.

Hulliger, F. (1968) Crystal chemistry of chalcogenides and pnictides of the transition elements: in Structure and Bonding, vol. 4, p.83-229.

Hutta, J. J. and Wright, H. D. (1964) The incorporation of U and Ag by hydrothermally synthesized galena: Econ. Geol., vol. 59, p.1003-1024.

Keil, K. (1967) The electron microprobe X-ray analyzer and its applications in mineralogy: Fortschr. Miner., vol. 44, no. 1, p.4-66.

Kelly, Wm. C. and Turneaure, F. S. (1970) Mineralogy, paragenesis and geothermometry of the tin and tungsten deposits of the eastern Andes, Bolivia: Econ. Geol., vol. 65, p.609-680.

Klemm, D. D. (1962) Untersuchungen über die mischkristallbildung im dreieckdiagramm FeS_2-CoS_2-NiS_2 und ihre beziehungen zum aufbau der naturlichen bravoite: N. Jb. Miner. Mh., vol. 100, p.76-91.

Klemm, D. D. (1965) Synthesen und analysen in den dreiecksdiagramen FeAsS-CoAsS-NiAsS und FeS_2-CoS_2-NiS_2: N. Jr. Miner. Abh., vol. 103, p.205-255.

Kretz, R. (1959) Chemical study of garnet, biotite and hornblende from gneisses of southwestern Quebec, with emphasis on distribution of elements in coexisting minerals: Jour. Geol., vol. 67, p.371-402.

Kretz, R. (1960) The distribution of certain elements among coexisting calcic pyroxenes, calcic amphiboles and biotites in skarns: Geochim. et Cosmochim. Acta, vol. 20, p.161-191.

Kretz, R. (1961) Some applications of thermodynamics to coexisting minerals of variable composition. Examples: Orthopyroxene-Clinopyroxene and Orthopyroxene-Garnet: Jour. Geol., vol. 69, p.361-387.

Kroger, F. A. (1938) Formation of solid solutions in the system zinc sulfide-manganese sulfide: Zeit. Krist., A100, p.543-545.

Kroger, F. A. (1939) Solid solutions in the ternary system ZnS-CdS-MnS: Zeit. Krist., A102, p.132-135.

Krumbein, W. C. and Graybill, F. A. (1965) An introduction to statistical models in geology: McGraw-Hill Book Co., New York.

Manning, P. G. (1967) Absorption spectra of Fe(III) in octahedral sites in sphalerite: Canadian Mineralogist, vol. 9, p.57-64.

Marfunin, A. S. and Mkrtchyan, A. R. (1967) Mössbauer spectra of Fe^{57} in sulfides: Geochemistry International, vol. 4, p.980-989.

McIntire, W. L. (1963) Trace element partition coefficients - a review of theory and applications to geology: Geochim et Cosmochim. Acta, vol. 27, p.1209-1264.

Nickel, E. H. (1968) Structural stability of minerals with the pyrite marcasite arsenopyrite, and lollingite structures: Canadian Mineralogist, vol. 9, p.311-321.

Nickel, E. H. (1970) The application of ligand-field concepts to an understanding of the structural stabilities and solid-solution limits of sulphides and related minerals: Chem. Geol., vol. 5, p.233-241.

Nickel, E. H., Webster, A. H. and Ripley, L. G. (1971) Bond strengths in the disulphides of iron, cobalt and nickel: Canadian Mineralogist, vol. 10, p.773-780.

Norrish, K. and Chappell, B. W. (1967) X-ray Fluorescence spectrography: in Zussman, J. ed., Physical Methods in Determinative Mineralogy, Academic Press, London and New York, Chapter 4.

Philibert, J. (1963) A method for calculating the absorption correction in electron probe microanalysis: in Proc. Third Intern. Symp. X-Ray Optics and X-Ray Microanalysis., Stanford, 1962, Academic Press, ed. H. H. Pattee, N. E. Cosslett and A. Engstrom, p.379-392.

Ramberg, H. (1952) The origins of metamorphic and metasomatic rocks: University of Chicago Press.

Reed, S. J. B. (1965) Characteristic fluorescence corrections in electron-probe microanalysis: Brit. Journ. Appl. Phys., vol. 16, p.913-926.

Riley, J. F. (1965) An intermediate member of the binary system FeS_2(pyrite)-CoS_2 (cattierite): Amer. Min., vol. 50, p.1083-1086.

Riley, J. F. (1968) The cobaltiferous pyrite series: Amer. Min., vol. 53, p.293-295.

Roedder, E. (1967) Fluid inclusions as samples of ore fluids: in Geochemistry and Hydrothermal Ore deposits, H. L. Barnes, ed., Holt, Rinehart and Winston, Inc., p.515-574.

Schröke, H. (1958) The determination of exsolution equilibrium: Neues. Jahr. Mineral. Monatsh, 1958, p.67-69.

Scott, S. D. (1968) Stoichiometry and phase changes in zinc sulphide: Ph.D. Thesis, Dept. of Geochemistry and Mineralogy, The Pennsylvania State University.

Scott, S. D. (1971) Mössbauer spectra of synthetic iron-bearing sphalerite: Canadian Mineralogist, vol. 10, p.882-885.

Scott, S. D. and Barnes, H. L. (1972) Sphalerite-wurtzite equilibria and stoichiometry: Geochim. et Cosmochim. Acta, vol. 36, p.1275-1295.

Skinner, B. J. (1961) Unit-cell of natural and synthetic sphalerites: Am. Min., vol. 46, p.1399-1411.

Snedecor, G. W. and Cochran, W. G. (1967) Statistical Methods: Iowa State University Press, 6th edition.

Springer, G. (1967) Die Berechnung von Korrekturen für die quantitative Elektronenstrahl-Mikoanalyse: Fortschr. Miner., vol. 45, no. 1, p.103-124.

Springer, G., Schachner-Korn, D. and Long, J. V. P. (1964) Metastable solid solution reactions in the system FeS_2-CoS_2-NiS_2: Econ. Geol., vol. 59, p.475-491.

Straumanis, M. E., Amstutz, G. C., Chan, S. (1964) Synthesis and X-ray investigation within the system FeS_2-CoS_2: N. Jb. Miner. Abh., vol. 101, p.127-141.

Title, R. S. (1965) Electron paramagnetic resonance spectra of Cr^+, Mn^{+2} and Fe^{+2} in cubic ZnS: Phys. Rev., vol. 131, p.623.

Troshin, Y. P. (1965) The distribution of trace elements of different valences among hydrothermal minerals as an index of the oxidation-reduction regime within the system: Geochemistry International, vol. 2, p.937-946.

Whittaker, E. J. W. and Muntus, R. (1970) Ionic radii for use in geochemistry: Geochim. et Cosmochim. Acta, vol. 34, p.945-956.

Williams, K. L. (1967) Electron probe microanalysis of sphalerite: Am. Min., vol. 52, p.475-492.

Wright, H. D., Hutta, J. J. and Barnard, W. M. (1963) Incorporation of some trace elements by hydrothermally synthesized galena and sphalerite (Abstract): Econ. Geol., vol. 58, no. 7, p.1192-1193.

Wright, H. D., Barnard, W. M. and Halbig, J. B. (1965) Solid solution in the system ZnS-ZnSe and PbS-PbSe at 300°C and above: Am. Min., vol. 50, p.1802-1815.

Yund, R. A. and Giletti, B. J. (1964) Partition of Zn between pyrite and galena: Geol. Soc. Am. Abstracts, 1964, p.231-232.